

**CREATING A SIMPLIFIED MODEL OF THE  
ALKALI-SILICA REACTION IN CONCRETE BY UTILISING FINITE ELEMENT  
MODELLING TECHNIQUES**

**A DISSERTATION SUBMITTED BY:**

**ROBERT MURDOCH**

In Fulfilment of the requirements of

ENG 4111/2 Research Project

Towards Degree of

Bachelor of Engineering (Civil)

October 2015



## Abstract

The Alkali-Silica Reaction (ASR) in concrete was first discovered in the 1940s and has since become a well documented problem in structures in Australia and around the world. The result of ASR can result in unexpected and premature deterioration of large and expensive buildings and pieces of infrastructure such as bridges and dams. The nature of ASR means that not only does it reduce the capacity of the concrete but also expose it to further deterioration. It is for this reason that it has become a serious concern for the owners of these structures and engineers alike. There have been many studies into the mechanisms that drive ASR, many of which have involved complex numerical and mathematical modelling as part of the study. Due to the complex nature of the reaction there are no models that are simple but effective enough to use on a practical basis. This thesis was designed to produce a macroscopic model of the alkali silica reaction using Finite Element Analysis (F.E.A.) software in order for engineers to use on a practical basis.

A simplified model operates by idealizing a scenario and focusing on producing fairly accurate results for a given set of parameters rather than try to model the process in its entirety. These models can be very useful when conducting preliminary assessments because they can model the behaviour of a system on a macro scale. Having a simplified model would potentially save a large number of man-hours and material costs when trying to repair these structures by giving the engineers a greater understanding of the current structural state and the extent to which they need to either repair or demolish and rebuild.

Last year, Tracy Knight simulated the growth of ASR in physical specimens, demonstrated the reduction in compressive strength of a sample and then showed that the compressive strength could be restored by using composite materials to create a confining pressure around the column. I intended to construct a simplified model of the ASR by using the Finite Element Modelling (FEM) software Strand7 and then check my model by replicating her compression test results. A test such as this where the model has to replicate certain known characteristics is a good method of validation, otherwise the model might predict erroneous behaviour.

Strand7 does not have the capability to model the crack initiation and propagation which is integral in the ASR process therefore an alternate way of replicating the reduction in compressive strength needed to be found. The tensile forces associated with the alkali silica reaction will be replicated by way of elevated temperatures at the nodes. By encouraging expansion in the localised as a function of temperature it recreates the expansion characteristic of the ASR gel along with the tensile forces within the surrounding concrete matrix.

The development of this model started by reproducing the results of a simple compression test on a concrete cylinder to achieve a baseline for my results to be reflected against. Next the nature of the ASR would be replicated by way of a temperature being applied at various nodes to induce thermal expansion in the concrete and the patterns of cracking investigated. This is then refined in the next stage which involved applying both the temperature and compressive loading simultaneously to confirm that this process replicated the reduction in strength associated with ASR and this was verified using a three dimensional model. The modelling process had been planned to include a stage at the end where the three dimensional model would be confined with fibre composites in

order to replicate Tracy Knight's thesis and restore the original strength to the concrete but the work load and time constraints did not allow for this to happen.

Many opportunities exist to extend the work I have begun. Not enough time has been devoted to refining the method of determining how many temperature nodes are required and what type of loading conditions various patterns will give. The ultimate goal of being able to replicate the results in Tracy Knight's thesis is yet to be achieved. The results of the compressive testing will continue to be used to validate the models created.

**University of Southern Queensland**  
**Faculty of Health, Engineering and Sciences**  
**ENG4111/ENG4112 Research Project**

## **Limitations of Use**

The Council of the University of Southern Queensland, its Faculty of Health, Engineering & Sciences, and the staff of the University of Southern Queensland, do not accept any responsibility for the truth, accuracy or completeness of material contained within or associated with this dissertation.

Persons using all or any part of this material do so at their own risk, and not at the risk of the Council of the University of Southern Queensland, its Faculty of Health, Engineering & Sciences or the staff of the University of Southern Queensland.

This dissertation reports an educational exercise and has no purpose or validity beyond this exercise. The sole purpose of the course pair entitled “Research Project” is to contribute to the overall education within the student’s chosen degree program. This document, the associated hardware, software, drawings, and other material set out in the associated appendices should not be used for any other purpose: if they are so used, it is entirely at the risk of the user.

**University of Southern Queensland**  
**Faculty of Health, Engineering and Sciences**  
**ENG4111/ENG4112 Research Project**

## **Certification of Dissertation**

I certify that the ideas, designs and experimental work, results, analyses and conclusions set out in this dissertation are entirely my own effort, except where otherwise indicated and acknowledged.

I further certify that the work is original and has not been previously submitted for assessment in any other course or institution, except where specifically stated.

Robert Murdoch

Student Number: U1017280

Signature

Date

## **Acknowledgements**

This dissertation was produced under the principle supervision of Associate Professor Yan Zhuge (University of Southern Queensland).

Acknowledgements are extended to Tracey Knight for the use of the results from her dissertation carried out during the previous year.

# Table of Contents

Abstract .....	iv
Limitations of Use.....	vi
Certification of Dissertation .....	vii
Acknowledgements.....	viii
List Of Figures.....	xii
List Of Tables .....	xiv
Nomenclature .....	xv
1. Introduction .....	1
1.1. Project background .....	2
1.2. Project aims.....	3
1.3. Project objectives.....	3
1.4. Constraints .....	4
1.5. Consequential Effects and Ethics .....	4
2. Literature Review .....	5
2.1. Concrete.....	5
2.1.1. Material Properties .....	5
2.1.2. Fracture Mechanics.....	7
2.2. Alkali-Silica Reaction (ASR).....	8
2.2.1. The Mechanism of ASR.....	9
2.2.2. Environment.....	12
2.2.3. Pessimum Effects .....	12
2.2.4. Effects.....	13
2.3. Composite Materials .....	15
2.3.1. Fibre-Reinforced Polymer (FRP).....	15
2.3.2. Fibres.....	15
2.3.3. Matrix .....	17
2.3.4. Fibre Volume Fraction .....	17
2.3.5. Geometry and Orientation of Fibres.....	17
2.3.6. Mechanical Properties .....	18
2.3.7. Fabrics and Preforms.....	18
2.4. Finite Element Model.....	19
2.4.1. Modelling ASR Affected Concrete using Finite Element Method .....	19
2.4.2. Microscopic Models .....	19

2.4.3.	Mesoscopic Models .....	21
2.4.4.	Macroscopic Models.....	22
3.	Finite Element Modelling .....	24
3.1.	Element Types .....	25
3.2.	Boundary Conditions .....	25
3.3.	Meshing .....	25
3.4.	Aspect Ratio.....	26
3.5.	Use of Symmetry .....	26
3.6.	Natural Subdivisions at Discontinuities: .....	27
3.7.	Sizing of Elements – The h and p methods:.....	27
3.8.	Linear Static Vs Non-Linear Static Solver:.....	28
4.	Preliminary Finite Element Modelling .....	30
4.1.	Modelling of Concrete Cylinder Compression Test .....	31
4.2.	Linear Static Model.....	32
4.2.1.	Axisymmetric Model.....	32
4.2.2.	Plates and Meshing .....	33
4.3.	Convergence Study .....	35
4.4.	Nonlinear Static Model.....	36
4.4.1.	Yield Criterion .....	36
4.4.2.	Stress Strain Table .....	38
4.4.3.	Results .....	39
5.	Refined Model .....	45
5.1.	Results From Previous Thesis Concrete Cylinder Compression Test.....	45
5.2.	How to simulate the ASR Testing .....	46
5.3.	Application of Temperature Nodes in Models .....	48
5.3.1.	Linear Analysis of Temp Load .....	48
5.3.2.	Nonlinear Analysis of Temp Load .....	51
5.4.	Combined Temperature and External Loading .....	51
5.4.1.	Linear Analysis .....	51
5.4.2.	Nonlinear Analysis .....	53
6.	Three Dimensional Model .....	55
6.1.	Linear Static Analysis .....	56
6.2.	Nonlinear Static Analysis .....	58
6.3.	Addition of Temp Nodes.....	60

7. Discussion.....	63
7.1. Order of Loadings.....	63
7.2. Conclusions .....	65
7.3. Recommendations .....	65
References:.....	66
Appendix A: Project Specification.....	70
Appendix B: Risk Assessment .....	71
Appendix C: Gantt Chart .....	73
Appendix D: Stress Strain Table .....	75
Appendix E: Graphs and Data .....	76

## List Of Figures

Figure 2.1 - Concrete Response to Monotonic and Cyclic Compression Load (Lowes 2000) .....	5
Figure 2.2 - Brazil Test ( <a href="http://i.ytimg.com/vi/6lkZlrLp_mE/hqdefault.jpg">http://i.ytimg.com/vi/6lkZlrLp_mE/hqdefault.jpg</a> ) .....	6
Figure 2.3 - Stress Strain Tensile Curve (Lowe 2000) .....	6
Figure 2.4 – Stress-Strain Failure Curves for Different Failure Modes ( <a href="http://www.theconcreteportal.com/cons_rel.html">http://www.theconcreteportal.com/cons_rel.html</a> ) .....	7
Figure 2.5 - ASR in a Bridge in Quebec (Fernandes & Broekmans 2013). .....	8
Figure 2.6 - Well Crystallised Silicate and Poorly Crystallised Silicates (Ferraris 1995).....	10
Figure 2.7 - Types of Silicates and their Characteristic Patterns of Cracking from ASR (Ferraris 1995) .....	11
Figure 2.8 - Influence of Temperature on ASR Expansion (Richardson 2002) .....	12
Figure 2.9 - Pessimism Effect in Concrete (Richardson 2002) .....	13
Figure 2.10 – Map Cracking (Swamy 1995) .....	14
Figure 2.11 - Cracking With Reinforcement (Swamy 1995) .....	14
Figure 2.12 - Spool of Glass Fibre .....	15
Figure 2.13 - Typical Stress-Strain Failure .....	18
Figure 2.14 - Representative Volume Element. The grey zone is the unreacted part while $\delta_c$ is the thickness of layer with capillary pores and cracks (Pan et. al. 2012) .....	19
Figure 2.15 Optical photograph of damaged aggregate (Schlangen & Copuroglu 2010) .....	20
Figure 2.16 - (left) Finite element mesh, (right) Microstructural image (Pan et. al. 2012).....	21
Figure 2.18 - Graphic Representation of Model (Herrador et. al. 2009).....	22
Figure 2.17 - Expansion strain rate in terms of compression stress (Pan et. al. 2012) .....	22
Figure 3.1 - Use of Symmetry ( <a href="http://www.ansys.stuba.sk/html/guide_55/graphics/GBAS21.gif">http://www.ansys.stuba.sk/html/guide_55/graphics/GBAS21.gif</a> ) .....	26
Figure 3.2 - Subdivisions at Continuities .....	27
Figure 4.1 - Stiffness as the reaction progresses (Pan et. al. 2012).....	30
Figure 4.2 - Concrete Fracture Patterns (ASTM 39) .....	31
Figure 4.3 - Failure modes determined by boundary conditions (Murray et. al. 2007).....	32
Figure 4.4 - Transform a 3D image to 2D.....	32
Figure 4.5 - Constraints for Solid Axisymmetric Structure ( <a href="http://mostreal.sk/html/guide_55/g-bas/GBAS2.htm">http://mostreal.sk/html/guide_55/g-bas/GBAS2.htm</a> ) .....	33
Figure 4.6 - Standard Compression Test, (Left) Stress in 11, (Right) Displacement in X Direction .....	34
Figure 4.7 - Convergence study on the linear model .....	35
Figure 4.8 - Tensile and Compressive Stress-strain Curve of Concrete (Bajracharya 2010) .....	36
Figure 4.9 - Von Mises Failure Criterion .....	37
Figure 4.10 - Max Strain Failure Criterion .....	37
Figure 4.12 - Initial Nonlinear Results .....	39
Figure 4.11 - Stress-Strain Curves.....	39
Figure 4.13 - Table Extended By Maintaining Gradient (Strand7).....	40
Figure 4.14 - Revised Table With Zero Gradient Ends.....	41
Figure 4.16 - Model Results at 37MPa (Stress 11, Stress 33, Disp. DX).....	42
Figure 4.15 - Graph Showing Model Converging.....	42
Figure 4.17 - Stress 11 Results at 38 - 41 MPa .....	43
Figure 4.18 - Stress 22 at 38 to 41 MPa.....	43

Figure 4.19 - Stress 33 at 38 to 41 MPa .....	43
Figure 4.20 - Comparison of Linear to Nonlinear Model .....	44
Figure 5.1 - Results From Tracy Knight's Experiments (Knight 2014) .....	45
Figure 5.2 - ASR effect on characteristic strength (Knight 2014) .....	46
Figure 5.3 - Cracking in Cylinders (Knight 2014) .....	47
Figure 5.4 - Linear Analysis Horizontal Temp Nodes @ 40 Degrees .....	48
Figure 5.5 - Linear Analysis Horizontal Temp Nodes Yielding @ 46 Degrees.....	49
Figure 5.6 - Stress on Nodes.....	49
Figure 5.7 - Results Increasing Distance From Surface .....	49
Figure 5.8 - Vertical Nodes at 40 Degrees.....	50
Figure 5.9 - Vertical Nodes at 46 Degrees.....	50
Figure 5.10 - Deformation of Nonlinear Model .....	51
Figure 5.11 - Effect of Temperatures at Nodes.....	52
Figure 5.12 – 50 Deg. Nodes Step 20, 22 & 37.....	53
Figure 5.13 - 30 Deg. Nodes Step 20, 22 & 37.....	53
Figure 5.14 - Stress-Strain Graph with Temperature Nodes.....	54
Figure 5.15 - 50MPa Concrete Subjected to 30MPa Load With Temp Nodes .....	54
Figure 6.1- Single Radian Sector Symmetric Model .....	55
Figure 6.2 - 90 Symmetric Model.....	55
Figure 6.3 - Complete Cylinder (Sector Meshing) .....	55
Figure 6.4 - Complete Cylinder (US Dept Roads Mesh).....	55
Figure 6.5 - Linear Results 3D Cylinder (US Dept. Transport Mesh) .....	56
Figure 6.6 - Linear Results 3D Sector Symmetric Model .....	56
Figure 6.7 - Linear Results 3D Cylinder (Radial Mesh) .....	57
Figure 6.8 - Convergence Study for 3 Dimensional Model .....	57
Figure 6.9 - 7.5mm Axisymmetric Model.....	58
Figure 6.10 - 7.5mm Full 3D Cylinder Model.....	58
Figure 6.11 - 7.5mm One Radian Sector Symmetric Model.....	59
Figure 6.12 - Comparison of Three 7.5mm Models in DX.....	59
Figure 6.13 - Comparison of Three Models in DY .....	60
Figure 6.14 - Stress Development in Axisymmetric Model.....	61
Figure 6.15 - Stress Development in Sector Symmetric Model .....	61
Figure 6.16 - Comparison of Stress Development Between Two Models .....	62
Figure 7.1 - External Load Applied Followed By Node Temperatures .....	63
Figure 7.2 - Node Temperatures Applied Followed By External Load .....	63
Figure 7.3 - Comparison of Load Deflection Curve For Both Combinations .....	64

**List Of Tables**

Table 2.1 - Strength and Modulus Properties of Carbon Fibres..... 16  
Table 2.2 - Strength and stiffness of components used in lattice simulation (Schlangen & Copuroglu 2010)..... 20  
Table 4.1 - Mesh Sizes and Results..... 35  
Table 6.1 - Brick Size and Displacement..... 57

## Nomenclature

ASR – Alkalai-silica Reaction

AAR – Alkalai-aggregate Reaction

CFRP – Carbon Fibre Reinforced Polymer

FEA – Finite Element Analysis

FEM – Finite Element Modelling

FRP – Fibre Reinforced Polymer

$\text{OH}^-$  – Hydroxide Ion

$\text{Na}^+$  – Sodium Ion

$\text{K}^+$  - Potassium Ion



# 1. Introduction

The term alkali-silica reaction (ASR) refers to an expansive reaction between naturally occurring alkalis in the concrete and particular alkali-reactive aggregates that were used in the manufacture of the concrete. This reaction creates a potentially expansive gel in the concrete which is activated when exposed to water. The expansive force of this gel causes cracking in the concrete which can greatly reduce its physical properties and lead to a situation where the structure needs to be repaired or replaced.

This process has become a significant problem in Australia as more and more structures are diagnosed as being affected. Since the 1980s there have been procedures used to minimise the number of new cases but the structures which were built previously using the reactive aggregates are showing signs of distress. In order to preserve their intended life spans they need to be assessed for damage and strengthened via retrofitting.

The use of finite element analysis as part of the design procedure for concrete structures is becoming standard practice in Australia. The use of FEM of concrete structures extends from slabs, shear walls, beams, columns and shell shapes and any complicated combination of these as well as issues such as fire ratings, shrinkage and creep. The ability to incorporate ASR into these models to be able to model the strength of an existing structure would be of great use.

To date there have been several models which have attempted to explain the behaviour of the concrete affected by ASR. Some have focussed on the microscopic behaviour within the structure of the concrete while others have addressed the interaction between the aggregate, cement and the expansive gel. These are generally done via the use of complex mathematical models which are generally out of the scope of many engineers in the field.

To develop an accurate model of a structure is not an easy task as concrete exhibits a strong nonlinear response to many factors such as bond slipping, cracking, strain softening, and biaxial stiffening. Therefore it is the aim of this study to develop a simple and effective means of incorporating a characteristic loss of compressive strength without adding undue constraints and complexity.

## **1.1. Project background**

Previous work in 2014 by Tracy Knight was done on strengthening ASR affected piles by wrapping with FRPs. She showed a positive correlation between wrapping with the FRPs and increased compressive strength. This dissertation focuses on using her empirical results to verify a finite element model of an ASR affected concrete column subjected to the confining forces of carbon fibre reinforcements.

FRPs are used to 'retrofit' a structure when, over the time the structure has been in service, the requirements and/or usage of the structure have changed and higher load tolerances are required of it. These materials are also used to repair a structure to return its load bearing capacity to that which it was designed for originally.

There are many benefits to using FRP in repair and retrofit applications such as high strength and stiffness to weight ratios, and the repair can be tailored to the structural and operational needs of the damaged infrastructure. However, the most important aspect of FRPs is the speed and relative ease of installation. This has added implications considering the scope of this report deals with bridges which are vital components of the State's transport infrastructure. In this type of situation the cost of the FRP is often offset by the reduction in labour, shut-down times and site constraints (Transportation Research Board 2003).

There exists here an opportunity to understand and predict this behaviour in ASR affected structures so that greater planning and specific solutions can be tailored for each occurrence. To date the modelling has been restricted to complex mathematical models which are out of the scope of many engineers. Finite element modelling software however is widely used in industry for design purposes and very accessible to engineers in the field. Analysis using FEM can vary from simple linear analysis which seeks to estimate strength and deflection in conservative adherence with design codes to highly nonlinear scenarios where strength and damage from static or dynamic loading is predicted. The application of FEM for detailed scenarios where the objective is to understand the behaviour of the concrete itself is growing in popularity when assessing existing structures.

## 1.2. Project aims

This project attempts to add to the pool of knowledge about how ASR degrades the strength of the concrete and how it can be incorporated into finite element models in a simple and practical manner. Ultimately it will result in the development of a functioning simplified mechanical model of the ASR reaction that can be easily replicated in industry.

The complex nature of the reaction and its subsequent effects in the concrete structure is not a typical application of FEM software and thus requires careful consideration. Once the process is refined it should provide structural engineers with a valuable tool in creating preliminary assessments of structures which have been identified as being affected by the ASR. Simplified models are useful as they can create a basic understanding of the problems that will most likely be encountered, in assessing and designing for the maintenance and retrofit of ASR affected structures.

## 1.3. Project objectives

The objectives of this project will be in accordance to the project specification (Appendix A) :

1. Research the alkali-silica reaction in concrete structures, the causes and processes involved in its development.
2. Research FEM theory. How the models are developed and what is necessary in creating an accurate model. What types of models are generally developed using computer programs such as Strand7.
3. Learning the fundamentals of the computer package. How to implement the ideas and theories in order to create a functional model.
4. Using Strand7 to create a two dimensional model to represent the outer layer of the concrete column. Once this is created we will use the temperature load functions of the software to simulate the ASR pressure in the unconfined concrete.
5. Reuse this model from Part 1 and generate discrete cracks by creating a line of nodes which allow for small spaces between the cracking.
6. Create a three dimensional model, assume that the cracking is symmetrical, use one quarter of the model and apply the temperature load function.
7. Retrofit the three dimensional model with a layer of adhesive and a layer of carbon fibre composite material. Apply the temperature loading cases again.

## **1.4.Constraints**

- The amount of data and the accuracy of the data from the previous year's thesis.
- The practicality of using FEM for this application where it is usually a mathematical modelling exercise.
- Licensing conditions restrict the use of the Strand7 program to the student package. All functionality is accessible but the availability of instructional material for the program is restricted.
- Ability of the programmer to utilise the tools in the package

## **1.5.Consequential Effects and Ethics**

The aim of this project is to extend the life of existing, damaged structures rather than demolish and rebuild them. This approach is designed to save money by accurately predicting the speed and severity of the degradation of a structure and allow for the planning of maintenance and retrofitting schedules. This will allow other projects to progress, reduce the energy consumption that materials such as concrete require and reduce the amount of waste associated with replacing a structure.

The FRP are a petroleum based, non-recyclable product which brings into question their appropriateness as a proposed building material. They present a health hazard to the user by producing toxic fumes in their manufacture and usage.

## 2. Literature Review

### 2.1. Concrete

When developing a model about concrete it is important to understand how it behaves in various situations and under various loadings. Standardised testing can give us various material properties such as compressive strength, tensile strength and the Young's modulus through uniaxial cyclic compressive or tensile loading as well as reversed-cyclic loading.

#### 2.1.1. Material Properties

Concrete is a non homogenous material that consists of various grades of aggregate and sand and hydrated cement paste (hcp) which is the product of a chemical reaction between Portland cement and water. The area between the hcp and coarse aggregate particles is referred to as the transition zone, this is slightly higher in water to cement ratio and thus weaker than the surrounding material.

When the concrete is subject to loading the failure is seen by a series of crack propagations. This is initiated in the transition zone and begins as a series of microcracks which slowly grow and join together ultimately resulting in the loss of strength characteristics

##### 2.1.1.1. Uniaxial Compression Testing

Compressive strength is the quality of the concrete to resist crushing loads (Standards Australia 2002). The uniaxial compressive strength test conducted in Australia, according to AS1012.8, is either a 150x300mm or 100x200mm cylinder, the latter being more common. Figure 2.1 shows a typical stress-strain curve which is divided into the following zones:

- Initially the response is linear-elastic, there is a minimal amount of cracks which form within the transition zone but do not increase in size while the loading is constant (stable).
  - Increased crack growth remains stable and the material stiffness is reduced.
  - Further crack growth begins to become unstable that continue to grow under a constant load. The cracks begin to form in the hcp.
  - Microcracks in the transition zone and hcp begin to join together and form continuous crack systems
  - Loading continues beyond compressive strength. This results in a softening stage as a result of multiple continuous crack systems.
- (Lowes 2000)

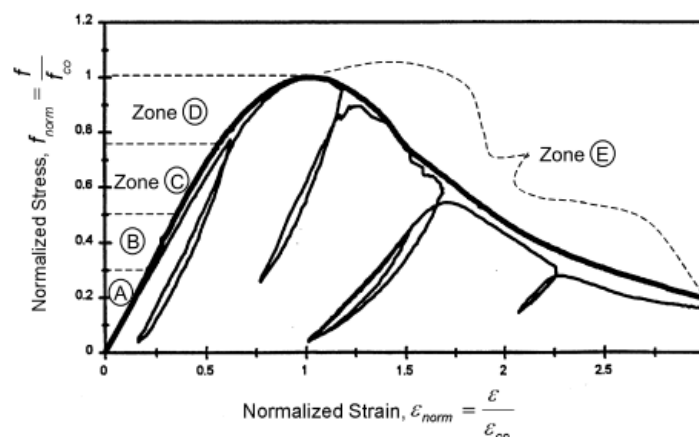


Figure 2.1 - Concrete Response to Monotonic and Cyclic Compression Load (Lowes 2000)

Figure 2.1 also shows the cyclical compression loading which follows the general stress-strain curve. The stiffness of the load-unload cycles is also roughly equivalent to the stiffness and deteriorates as the strain increases.

### 2.1.1.2. Uniaxial Tension Testing

The tensile strength of concrete refers to its ability to resist stretching or bending forces. Technically speaking, concrete is strong in tension but exhibits much greater strength in compression (Mor 2015). The primary cause of concern regarding the tensile strength of concrete relates to the need for steel reinforcing and the degree a member will have to be reinforced.

Testing concrete specimens in pure tension is difficult and not common practice. Modern methods in Australia utilize the Brazil method (Figure 2.2), or splitting test, where the cylinder is subject to compression along its vertical axis (Standards Australia 2002).

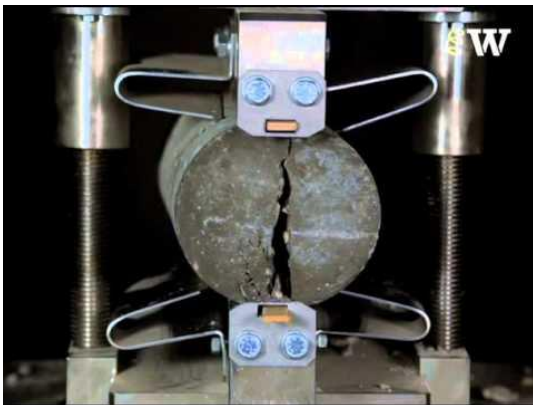


Figure 2.2 - Brazil Test  
([http://i.ytimg.com/vi/6lkZlrLp\\_mE/hqdefault.jpg](http://i.ytimg.com/vi/6lkZlrLp_mE/hqdefault.jpg))

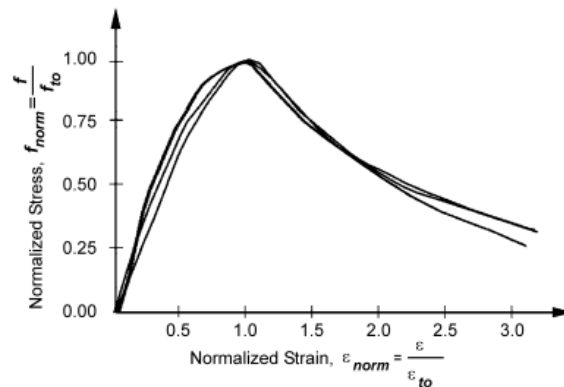


Figure 2.3 - Stress Strain Tensile Curve (Lowe 2000)

This process is described in AS1012.10 and the equation given as:

$$f_{ct} = \frac{2000P}{\pi LD}$$

Where  $f_{ct}$  = Indirect tensile strength  
 $P$  = Maximum compressive force applied  
 $L$  = Cylinder length  
 $D$  = Cylinder diameter

The important characteristics of the tensile response in Figure 2.3 are:

- i. A linear-elastic nature is observed until the tensile strength is achieved. At this point small microcracks appear in the transition zone.
- ii. Further loading results in a gradual loss of strength. This is due to the cracks developing into continuous systems in both the transition zone and hcp.

### 2.1.2. Fracture Mechanics

Fracture mechanics (Carpinteri A & Ingrassia AR 2012) is the study of the response and failure of structures due to crack initiation and propagation (Shah et. al. 1995).

The fracture mechanics of concrete are very complex and slowly becoming more understood. In fracture mechanics a material is described as brittle, ductile or quasi-ductile depending on how it behaves during failure. A brittle material fractures and all stresses drop to zero, a ductile material will yield while in a quasi-brittle material the stresses gradually decline after the peak stress is reached. The effect this has is that a brittle material will fail in a catastrophic fashion, a ductile material will twist and deform well before ultimate failure is reached whereas the quasi-brittle material will go through a softening zone as a load deformation response after peak stress is reached (Shah et. al. 1995)

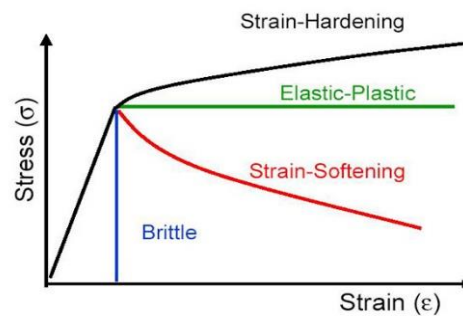


**Figure 2.4 – Stress-Strain Failure Curves for Different Failure Modes**  
([http://www.theconcreteportal.com/cons\\_rel.html](http://www.theconcreteportal.com/cons_rel.html))

The way that a structure fails is not only due to materials but geometry as well. For ductile materials the structure fails when stress on the entire section reaches the material yield strength, in which case a strength-based failure criterion can be used. However, when a brittle material is used the structure will fail when the stress in any area is equal to the tensile strength. In this case the maximum stress depends not only on the material but also the geometry and boundary conditions as well so a strength failure criterion is not suitable. In the case of both brittle and quasi-brittle materials an energy based equation is more commonly used rather than strength. In the quasi-brittle materials a second failure criterion is needed to completely describe the inelastic energy in the fracture process zone to completely describe the softening process.

The size and shape of the samples has an effect on the results, this is more so with cubes than cylinders (Del Viso et. al. 2007).

## 2.2. Alkali-Silica Reaction (ASR)

In the USA in the 1920s several large concrete structures were identified as having severe cracking, but there was limited understanding as to why and how this was happening. It wasn't until 1940 that Stanton noted that the hydroxide ions (OH<sup>-</sup>) and alkalis from the cement paste, notably sodium (Na) and potassium (K), were reacting with certain types of aggregate. A gel is formed by this reaction which then absorbs water and creates internal tensile forces which cause the concrete to crack. This became known as an alkali-aggregate reaction (AAR) of which there are three types:

1. **Alkali-Carbonate Reaction.** The alkalis in the cement paste react with aggregates such as dolomite, this is a type of AAR which is rarely seen in Australia;
  2. **Alkali-Silicate Reactions** which occur layered silicate rocks react with alkalis
  3. **Alkali-Silica Reaction occurs** between the alkalis and poorly formed silica aggregates
- (Fernandes & Broekmans 2013).



Figure 2.5 - ASR in a Bridge in Quebec (Fernandes & Broekmans 2013).

ASR was first recognised in Australia by Vivian in the 1950s (Standards Australia 1996). The ASR reaction is not completely understood and changes depending on the chemical and physical qualities of the elements used to create the concrete.

The presence of the gel from the alkali-silica reaction alone is not considered destructive. Some gel does not expand very much, others none at all. The ASR gel must be high swelling and create enough tensile force within the concrete to form cracks for the ASR to be considered destructive.

For ASR to occur there are three factors which are required to happen simultaneously:

- i. Presence of sufficient water to allow the reaction to take place and to expand the gel.
  - ii. Presence of sufficient alkalis to create the ASR gel
  - iii. The aggregate must be ASR-reactive
- (Swamy 1992)

### 2.2.1. The Mechanism of ASR

The cement used is mostly Portland cement which consists of calcium carbonate (in the form of limestone, coral or chalk), alumina, silica (sand) and iron oxide (normally in the form of clay or shale), which is sintered at high temperatures with gypsum added at the end of the process (Standards Australia 2002). Sodium (Na) and Potassium (K) are also present mainly due to geological processes forming the minerals used and the nature of how cement is manufactured. The reaction that takes place involves the calcium in the portland cement combining with silica and water to form a calcium-silica-hydrate (C-S-H) gel:

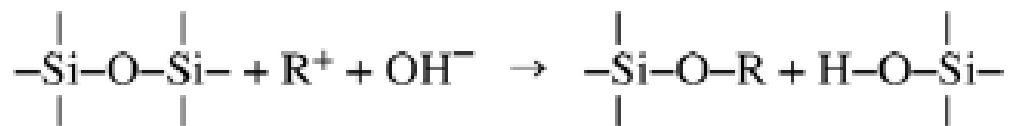


Equation 2.1 - The Calcium-Silica Hydrate Reaction (Shi et. al.2012)

The alkali-silica reaction can be simplified to a two-step process:

- 1) Alkali + Reactive Silica -> Alkali-Silica Gel

The OH<sup>-</sup> ions break apart the siloxane networks (SiO<sub>2</sub>) on the aggregate surface

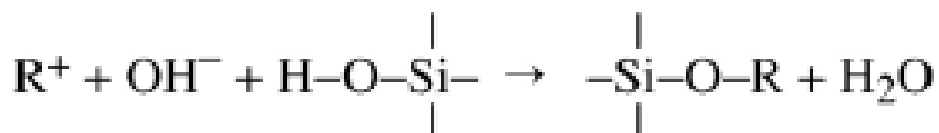


Equation 2.2 - Reaction for the Formation of Alkali-Silica Gel and Silicic Acid (Ichikawa & Miura 2007)

This generates the alkali silicate gel and silicic acid (SiOH).

(The R<sup>+</sup> denotes a Ca<sup>2+</sup>, Na<sup>+</sup> or K<sup>+</sup> ion.)

The silicic acid immediately reacts with OH<sup>-</sup> ions to convert to alkali silicate



Equation 2.3 - Formation of Alkali Silicate (Ichikawa & Miura 2007)

- 2) Alkali-Silica Gel + Moisture -> Expansion

The resultant oligomeric alkali silicate (alkali silicate gel) is hygroscopic and expands in the presence of water



Equation 2.4 - Expansion of Alkali Silicate (Ichikawa & Miura 2007)

### 2.2.1.1. Pore Water Solution

As the hydration phase of cement progresses there is less and less excess water available but even in well cured cement water still exists within this porous medium. Normally in the pores this is expressed as a Relative Humidity (RH) value. Water acts as a medium by which the alkali use to travel to the site, the water is also necessary for absorption by the ASR gel (Swamy 1992). Hydroxide ions are present in large quantities due to the hydration of the cement, it is usual for the concrete to have a pH level of 12.5. The pH is then raised to 13 and higher due to the varying levels of hydroxide ions associated with soluble alkalis such as Na<sup>+</sup> and K<sup>+</sup>. Due to the way that cement is manufactured, some of the Na<sup>+</sup> and K<sup>+</sup> will be immediately present in the pore water and more is released later on as the hydration of the cement continues (Standards Australia 2002).

### 2.2.1.2. Reactive Silica

Not all aggregates are created equal. In well-formed aggregate there is a limited amount of surface area for any reaction with the hydroxide ions to take place whereas in poorly crystallised aggregate the opportunity is much greater.

The quartz (SiO<sub>2</sub>) in the aggregate is a three dimensional structure similar to ice, in poorly crystallised structures the dissolved hydroxyl ions (OH<sup>-</sup>) can attach to the Si-O-Si bonds and form Si-OH (Fernandes & Broekmans 2013). The Na and K ions diffuse toward the OH<sup>-</sup> ions and the gel like ASR material is formed. There is no single composition of the ASR gel and each type will have a different ability to swell, varying viscosities and flow rates. The cracking is then formed due to the hygroscopic nature of the gel and the internal tensile forces that the absorption of water creates when the gel expands.

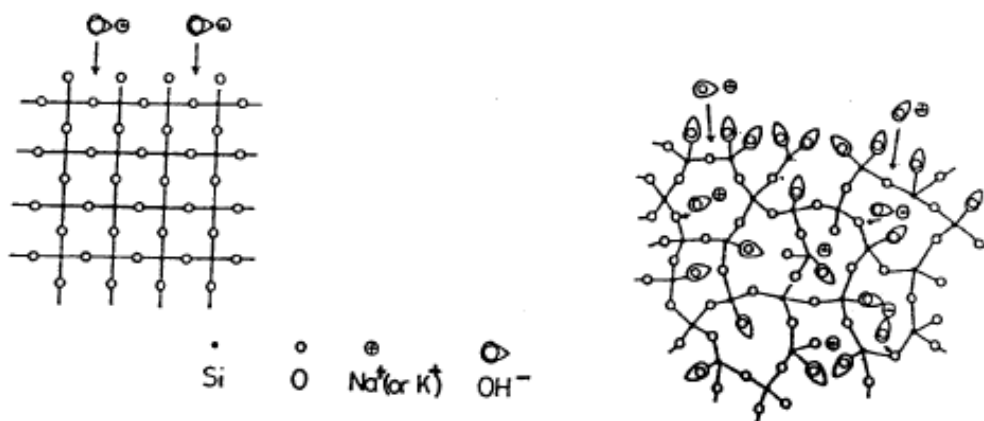


Figure 2.6 - Well Crystallised Silicate and Poorly Crystallised Silicates (Ferraris 1995)

Different aggregates have differing reaction patterns depending on the composition and the way the mineral has crystallised (Giaccio 2008). The following diagram shows the different ways that ASR presents itself in various minerals

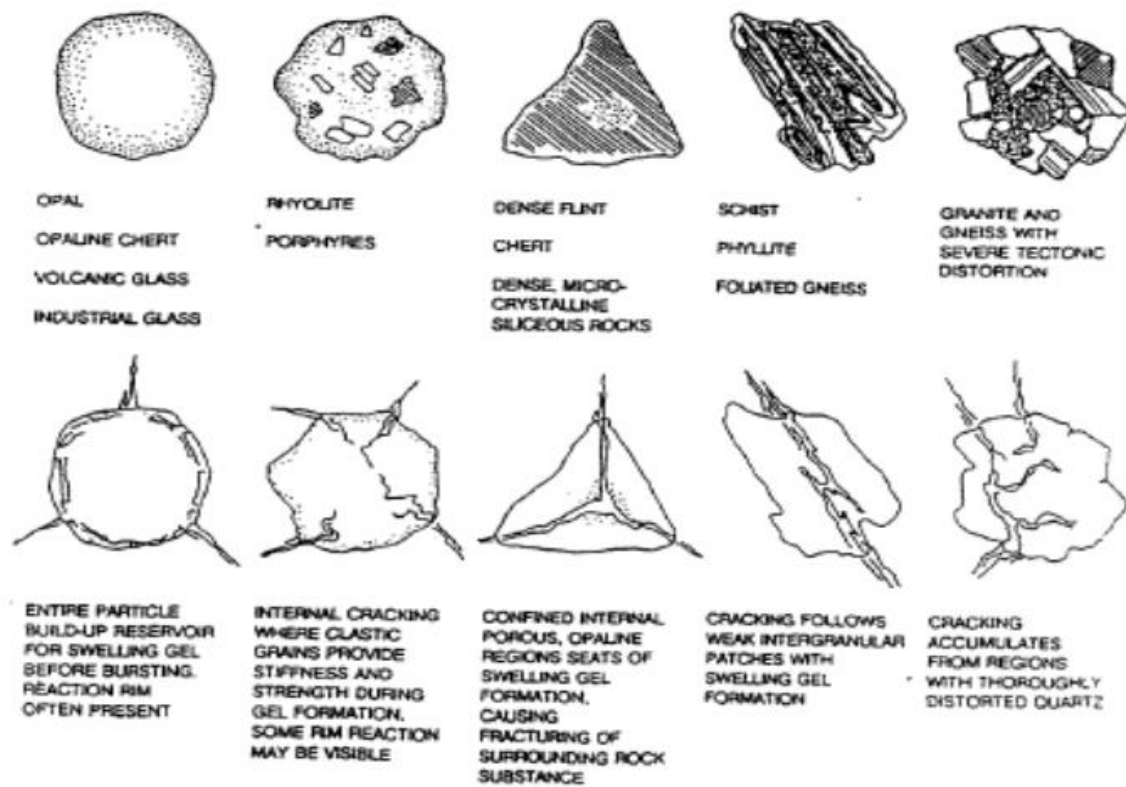


Figure 2.7 - Types of Silicates and their Characteristic Patterns of Cracking from ASR (Ferraris 1995)

Amorphous silica (opal), chalcedony, cristobalite, tridymite and volcanic glass are all highly reactive and can produce an ASR reaction as little as one year. Whereas granitic and metamorphic rocks need a longer induction period and usually take more than 10 years (Giaccio et. al. 2008)

The size of the aggregate also affects the speed and scope of the reaction. Smaller aggregates (ie sands) that are considered poorly crystallised will react quicker than larger aggregate made from the same material due to the smaller aggregate having a larger surface area which gives more scope for the reaction to take place

### 2.2.2. Environment

While the mineral structure is one of the main causes of ASR, the environmental conditions the concrete is exposed to can have a significant effect on the reaction (Giaccio et. al. 2008). One study showed that the difference in ambient temperature can speed up the reaction by up to four or five times (Fournier et. al. 2009). This effect declines with time, eventually the colder temperatures may reach, and even exceed the higher temperature effects (Richardson 2002).

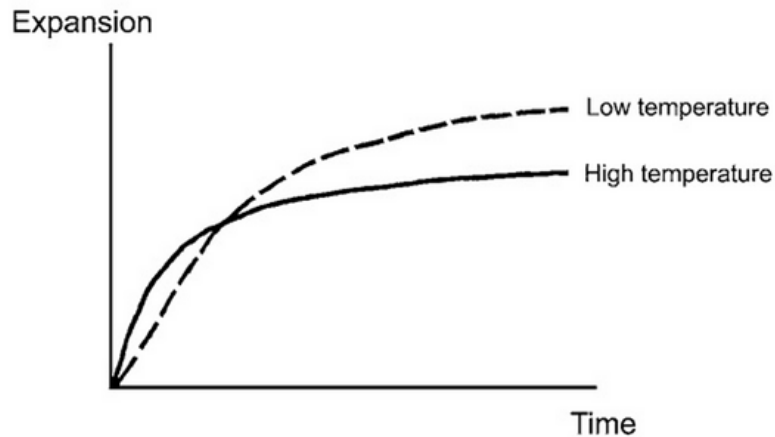


Figure 2.8 - Influence of Temperature on ASR Expansion (Richardson 2002)

Environments where there is an abundance of external alkalis such as deicing salts, coastal areas, saline groundwater and water from industrial processes, will increase the expansion, especially when cracking is already present (Farny & Kerkhoff 2007) and the exposure to water creates greater swelling. Finally exposure to cycles of wetting and drying, freezing and thawing will increase the extent of deterioration due to ASR (Standards Australia 1996).

### 2.2.3. Pessimum Effects

There have been studies to show that there is a ratio of the amount of reactive aggregates to inert aggregates that will give the maximum expansion, above or below which the reaction will not take place. The process is proportional to the interaction between the amount of reactants and the amount of alkalis left after the reaction. The level of reactants that give the maximum expansion is called the 'pessimum proportion' (Helmuth 1993).

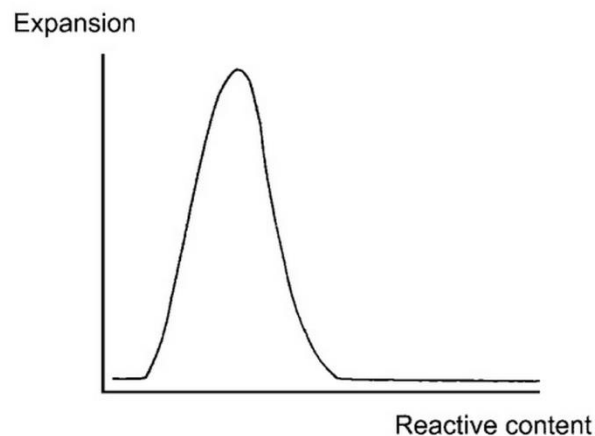


Figure 2.9 - Pessimum Effect in Concrete (Richardson 2002)

A 'pessimum size effect' also exists where a reaction will find a maximum with a particular size of reactive aggregate. As the aggregates get smaller or larger than this size the levels of expansion will diminish (Helmuth 1993).

#### 2.2.4. Effects

Experimental studies have shown that there are two conflicting effects of ASR when dealing with strength. The first is the reduction in compressive strength, tensile strength and e-modulus, while the second is a beneficial pre-stressing effect due to the restraining action of the steel against the expansion of the ASR. The literature often states the reduction in the tensile strength which, during design for concrete beams in bending is usually ignored, is important for such things as the bond and anchorage of rebars and bolts, shear and punching without shear reinforcement.

The effect of ASR on the integrity of concrete depends firstly on the rate of the reaction and the chemical processes that drove it, then on the type of micro-cracking pattern that the reaction causes. (Giaccio et. al. 2008). Damage from ASR is less common than the ASR itself and generally takes the form of cracking or differential movement (Richardson 2002). Studies have reported losses in compressive, tensile and ductile strength associated with ASR from 10% of up to 30%. The effect of expansion from the ASR reaction can reduce the elastic modulus from 20 – 50% (Hobbs 1988).

Often the reaction appears but will exhausts itself leaving the structure in a reduced, but still serviceable, capacity. It is suggested that cracks that develop due to ASR can affect the steel reinforcement. There are also concerns with the cracks providing sites for freeze/thaw damage to occur (Richardson 2002). If the damage is extensive enough the structure will have to be demolished and replaced, as happened to the overpass in Quebec (Figure 2.5).

The type of cracking induced by ASR depends on the loading and type/orientation of the reinforcement in the concrete. Depth of cracking can vary from 25-50mm but can extend even more (Richardson 2002). In unreinforced sections of concrete takes the shape of map cracking, this is usually associated with differential movement between the outside and inside of the concrete.

The confinement of columns using a carbon fibre wrap has been shown to be effective however the benefits are not observed until the concrete begins to dilate and fail, this is when the confining strength of the carbon fibre adds to the concrete. ASR affected RC beams are subject to greater reductions in shear than in bending, however if there is shear reinforcement there is a pre-stressing effect. It is the degree of expansion at this point that is the issue which is often related to the degree of confinement by the rebars (1, 2 or 3 directions).

Whereas reinforced sections tend to crack in line with the direction of the reinforcement (Hobbs 1988).

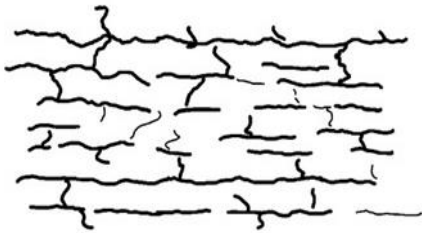


Figure 2.11 - Cracking With Reinforcement (Swamy 1995)

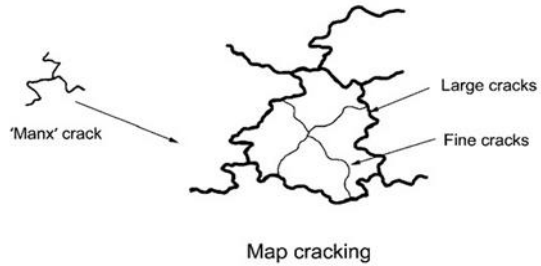


Figure 2.10 – Map Cracking (Swamy 1995)

## 2.3.Composite Materials

A composite material is a multiphase material formed from a combination of two or more materials. They typically consist of a strength component and a matrix which binds them together. When bound they keep their individual identities and properties but the material as a whole takes on improved specific characteristics which the original materials are incapable of possessing if acting alone (Lee 1989).

The specific qualities of composite materials can be tailored to cater to specific activities by appropriately altering the proportions, distributions, morphologies, degrees of crystallinity, as well as the structure and interface between the components used in their formation (Chung 2010). This quality means it is possible to design an appropriate material which is also economically viable. As a result the modern development of these materials is application driven and process oriented as opposed to the conventional criteria based on purely mechanical and structural suitability (Chung 2010).

### 2.3.1.Fibre-Reinforced Polymer (FRP)

An FRP is produced using strong fibres bound in a matrix of resin. The resin is usually a viscous fluid which is applied to the fibres and sets as a hard solid when activated. These polymers are commonly known as plastics and have been around since the 19<sup>th</sup> century but most of the advancements have been made in the last 50 years. Most plastics fall into one of two broad categories:

1. Thermoplastic – can be formed and reformed using heat (eg. polyethylene, PVC etc)
2. Thermoset – are hardened by chemical reaction and cannot be reused. (eg. unsaturated polyesters, epoxies, vinyl esters)

(Scott Bader 2005)

### 2.3.2.Fibres

The three main types of reinforcement used in composite materials today are glass, aramid and carbon fibres. Reinforcements can contain more than one material. For instance it may contain a combination of glass/aramid, carbon/aramid or carbon/glass. These combinations take on the beneficial attributes of each material; a combination of aramid/glass will possess the impact resistance of aramid and the compressive strength of glass (Scott Bayer 2005).

#### Glass

Glass fibres are readily available, very strong (a single filament 9-15 microns in diameter is about 3.5 GPa), non-combustible and chemically resistant. The fibres themselves are made by melting products such as sand, kaolin, limestone and colemanite then drawing and rapidly cooling the molten glass (Scott Bader 2005). It is available in different forms and grades with the two most prominent being 'E' (electrical) and 'C' (chemical) types with others being R, S or T type. The fibres are arranged in either a uni-directional, bi-directional or randomly distributed weave all giving different structural properties to the composite. There are four main forms which are continuous



Figure 2.12 - Spool of Glass Fibre

rovings, yarn for fabrics or braiding, mats and chopped strand (US Dept. Defence 1997)

Tensile strength can be reduced by abrasion and these flaws tend to increase under cyclic loads. The tensile strength can also be reduced under sustained static loads and in the presence of water (Mahmoud 1997).

## Carbon and Graphite

High modulus, uni-directional carbon fibre composites often have a modulus stronger than steel. Both are based on hexagonal grapheme layer networks, while carbon fibres are well ordered on a two dimensional plane the bonding between planes is weak whereas graphite is well ordered three dimensional structure, making it stronger but a longer and more costly process (US Dept. Defence 1997).

These fibres are mostly produced by carbonising polyacrylonitrile (PAN) between 1000°C and 3500°C. Other, cheaper, precursors can be used but produce fibres of lower quality. The degree of carbonisation the precursor material undergoes will determine properties such as density and elastic modulus, hence a wide range of strength and stiffness requirements can be met (Scott Bader 2005)

Advantages of carbon fibres are the exceptional tensile-strength to weight and modulus to weight ratios, high resistance to corrosion, low coefficient of linear expansion and high fatigue strength. The drawbacks include the high cost, low impact resistance and high electrical conductivity (Mahmoud 1997).

**Table 2.1 - Strength and Modulus Properties of Carbon Fibres**

**Strength and Modulus Figures for Commercial PAN-based Carbon Fibres:**

Grade	Tensile Modulus (GPa)	Tensile Strength (GPa)	Country of Manufacture
<b>Standard Modulus (&lt;265GPa) (also known as 'High Strength')</b>			
T300	230	3.53	France/Japan
T700	235	5.3	Japan
HTA	238	3.95	Germany
UTS	240	4.8	Japan
34-700	234	4.5	Japan/USA
AS4	241	4.0	USA
T650-35	241	4.55	USA
Panex 33	228	3.6	USA/Hungary
F3C	228	3.8	USA
TR50S	235	4.83	Japan
TR30S	234	4.41	Japan
<b>Intermediate Modulus (265-320GPa)</b>			
T800	294	5.94	France/Japan
M30S	294	5.49	France
IMS	295	4.12/5.5	Japan
MR40/MR50	289	4.4/5.1	Japan
IM6/IM7	303	5.1/5.3	USA
IM9	310	5.3	USA
T650-42	290	4.82	USA
T40	290	5.65	USA
<b>High Modulus (320-440GPa)</b>			
M40	392	2.74	Japan
M40J	377	4.41	France/Japan
HMA	358	3.0	Japan
UMS2526	395	4.56	Japan
MS40	340	4.8	Japan
HR40	381	4.8	Japan
<b>Ultra High Modulus (~440GPa)</b>			
M46J	436	4.21	Japan
UMS3536	435	4.5	Japan
HS40	441	4.4	Japan
UHMS	441	3.45	USA

### **2.3.3. Matrix**

The matrix is formed from a resin which is a general term used to describe the polymer, polymer precursor material or mixture that sets in a similar manner to a hard lacquer or enamel. Polymers are composed of long chains of simple repeated units and are generally categorised as thermosetting or thermoplastic (Gurit 2015).

#### *Polyesters (Thermoset)*

Polyester resins, or simply polyesters, are unsaturated polyesters which have thermoset properties and are therefore able to be cured from a liquid or solid state. Generally speaking orthophthalic or isophthalic polyester resins and are the most widely used resin systems. They are robust, relatively fast and inexpensive solution for inexpensive applications.

#### *Vinyl Ester Resins*

These are similar in structure to polyesters but differ with some important characteristics. They have better ability to absorb shock loadings, and hence are tougher and more resilient than polyester resins. Ester groups are degraded by hydrolysis so a vinylester chain has better water resisting properties however this usually requires an elevated curing temperature (Gurit 2015).

#### *Epoxy Resins*

Epoxyes are polymerizable thermosetting resins containing one or more epoxide groups (US Dept. Defence 1997). Epoxyes are generally superior to most other resin types as far as mechanical properties and resistance to environmental factors is concerned. They have a high strength and modulus, low levels of volatiles, excellent adhesion, low shrinkage, good water and chemical resistance and are easily processed. (US Dept. Defence 1997)

The time taken to cure epoxyes is greater than polyesters and the basic cost is also higher.

### **2.3.4. Fibre Volume Fraction**

Since the mechanical properties of the fibres are greater than that of the resins it is logical to conclude that the higher the fraction of fibres in the composite the stronger it will be. There is a limit to this as the fibres have to be sufficiently coated and packed in the resin to be held in place. When being done by hand this ratio is about 30-40% while in very sophisticated and strictly controlled conditions it is closer to 70% FVF (Gurit 2015).

### **2.3.5. Geometry and Orientation of Fibres**

The orientation of the fibres is important as the main mechanical properties are directed along the longitudinal axis. If the magnitude and direction of the loads are known then these anisotropic qualities of the composite can be orientated in whichever way the stress at that point in the structure requires. This distinguishes composites from metals in the way that a composite material itself designed for the task it will be used for.

### 2.3.6. Mechanical Properties

The choice of fibre and resin used must be matched in order to utilise the full mechanical properties of the fibre. The graph shows the stress/strain properties of different fibres, if the S-glass fibre was used the full extent of its tensile strength would not be utilised if the resin did not yield to at least 5.6%. In this case the epoxy resin does so and the fibre's tensile strength will be fully utilised.

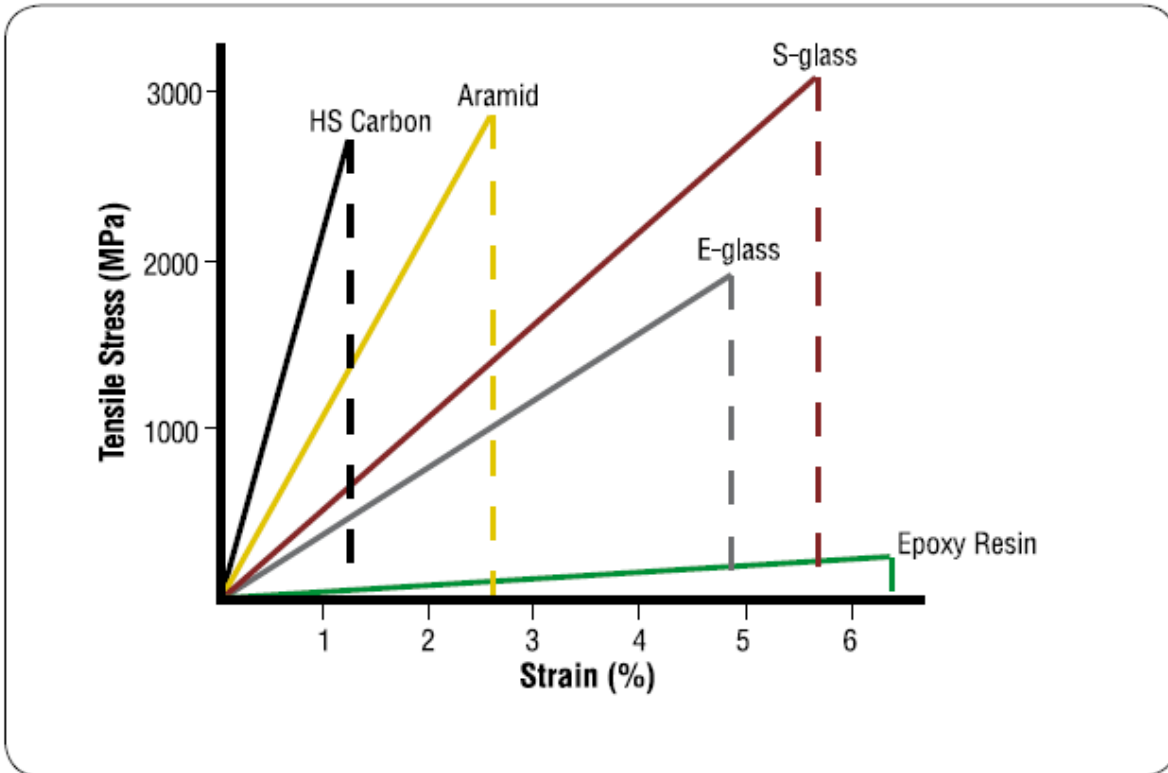


Figure 2.13 - Typical Stress-Strain Failure

### 2.3.7. Fabrics and Preforms

A fabric is an assortment of one or more layers of fibres either woven or held together by a secondary material. The types of fabrics are sorted according to the stand weight, tow (bundle of fibres) or strand count, complexity of weave pattern, and fabric finish. Generally the cost is related to the weight and thickness of the weave (US Dept. Defence 1997).

Drape refers to the ability of the material to conform to a complex surface and crimp refers to the degree of deformation involved in weaving the strand under and over other strands

## 2.4. Finite Element Model

The Finite Element Method is a very versatile numerical method which started off being used for stress analysis applications and has grown to be used on problems involving fluid mechanics, heat transfer, diffusion, vibration and electrical and magnetic fields. It is too difficult to simply define a relationship between a complex shape and applied loads, deflections and internal stresses. The complex shape is therefore broken up into a finite number of elements (discretised) that have a much simpler form. From this point the relationships between applied load, deflections and internal stresses at special known locations on these elements, called nodes, are set and then the forces and displacements at the unknown nodal locations determined through a system of algebraic equations (Service 2002).

This has become a very useful and practical tool due to the fact that it can be altered to suit the complex shape or unique loadings of the problems. While FEA is a powerful tool, its accuracy depends on the ability to create an accurate model before analysis can begin.

### 2.4.1. Modelling ASR Affected Concrete using Finite Element Method

ASR modelling tends to fall into two groups

- i. The formation and expansion processes involving the chemical reaction kinetics and diffusion
- ii. The mechanical fracturing from expansion and deterioration of the structure

The chemical reaction determines the degree of the ASR reaction whereas the second part describes the extent to which the ASR has structurally degraded the concrete. The model should, ideally, be able to do both of these things but the reality is that the chemical reaction is based on so many factors that it makes it nearly impossible to make one model to suit every case. Therefore there have been theoretical, semi-empirical and numerical models developed depending on the observed qualities of the ASR affected concrete in question.

### 2.4.2. Microscopic Models

Theoretical models are focussed on a representative volume element (RVE) where the interaction between the ASR gel and a single spherical piece of aggregate takes place. Several chemical reactions take place in this space, such as the diffusion process, kinetics of dissolution and gel formation and its swelling. The primary objective of this model is to describe the pessimum expansion effect (described in sect 2.1.3) between the ASR-affected concrete and the size of the aggregate.

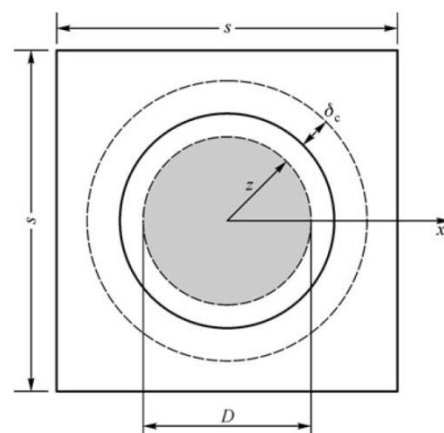


Figure 2.14 - Representative Volume Element. The grey zone is the unreacted part while  $\delta_c$  is the thickness of layer with capillary pores and cracks (Pan et. al. 2012)

One such model was the Delft Lattice Model (Schlangen & Copuroglu, 2007) was created where the aggregate structure is modelled using digitized images of a sample of ASR-affected concrete. Lattice models allow the use of linear elastic fracture mechanics to describe the formation of cracks in heterogeneous materials. The lattice is divided up into a 2D triangular mesh with each beam being able to transfer a bending moment, normal forces and shear forces. When a 3D square mesh was used 3D shear forces, bending and torsion moments in different directions were added. To begin with all stiffness and strength parameters are equal across the lattice but this can be varied to simulate heterogeneity.

The model is then defined as a lattice under an applied load where the load vector and stiffness matrix are known and the displacement vector is unknown. The normal stress in each element is then taken to represent the strength so when an element in the mesh exceeds a certain threshold it has to be removed.

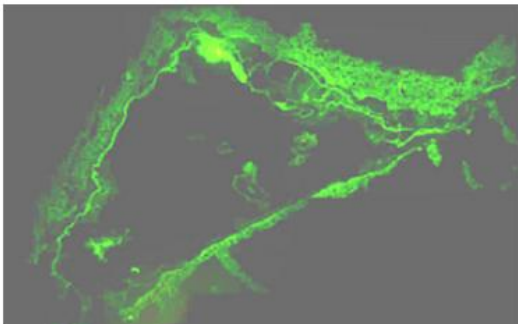


Figure 2.15 Optical photograph of damaged aggregate (Schlangen & Copuroglu 2010)

The mechanism of ASR is shown in the digitized image. It is then discretized as a lattice consisting of 42000 small beam elements, with three spots (shown as black dots) selected as the points where the ASR expansion takes place. The strength parameters of the beam elements in the three locations were taken from the range in Table 2.2 and the stiffness was multiplied by a factor of 10.

Table 2.2 - Strength and stiffness of components used in lattice simulation (Schlangen & Copuroglu 2010)

	Aggre- gate	Dissolved rim of aggregate	ITZ	Cement matrix	ASR gel
Strength	7.0-13.0	1.0-2.0	1.5-2.5	3.0-5.0	1.0

### 2.4.3. Mesoscopic Models

Meso scale models model the interaction of the aggregate and cement paste in the concrete. This scale model is often used to model the pessimum effect and how it defines the potential worst aggregate size.

Dunant and Scrivener chose to use FEM in 3D by modelling the two phases as discrete. They proposed that the damage was induced by gel pockets growing and cracking the aggregate. The gel pockets were modelled so that they were in perfect connection with their surroundings as they grew. The gel was given a linear elastic property while the aggregate was considered to be quasi-brittle and followed a damage law. The gel was grown with a given strain and the reaction was stopped when 3% of the aggregate had reacted. The stress created by the growing gel was enough to crack the aggregate and surrounding cement paste. Not only did this show that the cracking was similar to experimental observations but it also went toward explaining why there is a loss of stiffness due to the aggregate cracking while the cement remained in compression.

Shin and colleagues using finite element modelling to develop a microstructure-based method of investigating the mechanical fracture associated with ASR. Pictures from an electron microscope were used to identify the constituents of concrete and a FEM, including pores, aggregates, voids, gels, paste and cracks, was constructed using the images. The pressure of the gel was reconstructed by assigning the gel a fictitious thermal expansion coefficient and temperature change. Two dimensional linear elastic finite element modelling was used and the results were a very good match for the empirical data.

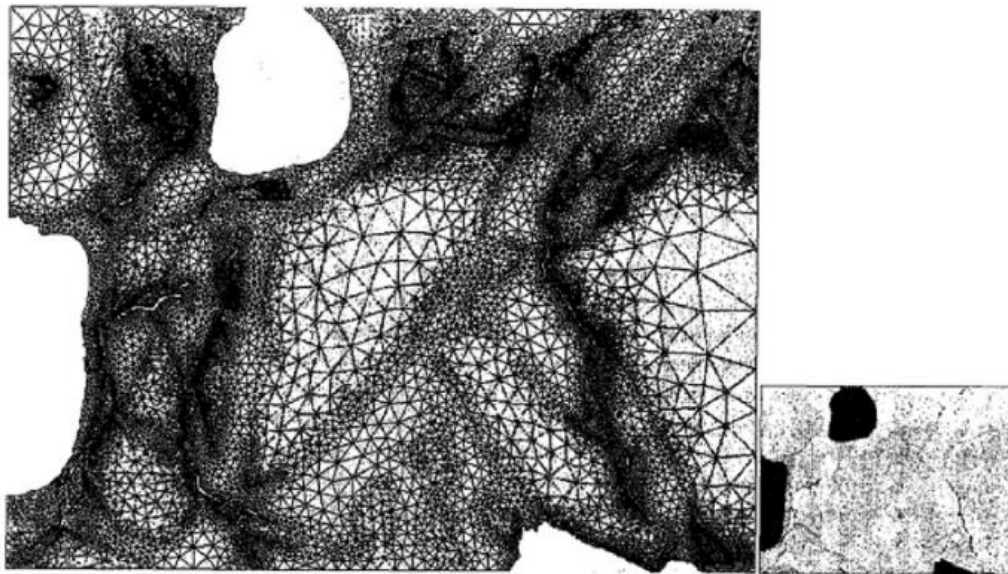


Figure 2.16 - (left) Finite element mesh, (right) Microstructural image (Pan et. al. 2012)

### 2.4.4. Macroscopic Models

Macroscopic models simulate effects of ASR on a local level and analyse the overall effect of the damage caused on a global/structural scale. These effects are such as the displacement field, stress field and damage cracking of the structure. They generally consist of the mechanical processes and the chemical kinetics. Depending on the model the material may be treated as linear elastic to isotropic/anisotropic damage models. These models are designed to predict deformation against loading, possibly involving time factors such as creep, shrinkage and cracking.

#### 2.4.4.1. The Parametric Model

This was simple and effective, but ignored the complex chemical reaction and treated the anisometric expansion as dependent on the stress state. The expansion in these models was modelled as an initial strain propagated by a temperature increase (Pan et. al. 2012).

The expansion rate was given as:

$$\epsilon_i^{asr} = \begin{cases} \epsilon^u & \text{for } 0 \leq \sigma_i \leq \sigma_L \\ \epsilon^u - K \log(\sigma_i/\sigma_L) & \text{for } \sigma_L \leq \sigma_i \leq \sigma_{max} \\ 0 & \text{for } \sigma_i > \sigma_{max} \end{cases}$$

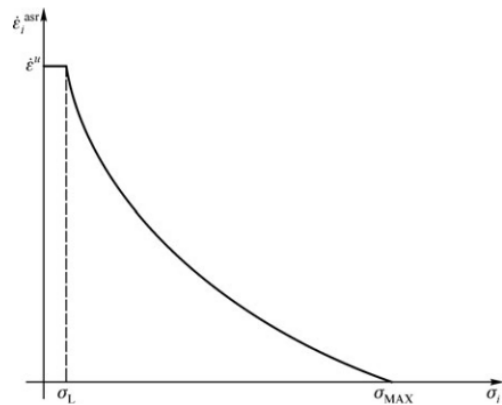


Figure 2.17 - Expansion strain rate in terms of compression stress (Pan et. al. 2012)

$\sigma_L$  was considered to be 0.25 MPa at which no restriction of the ASR expansion took place whereas  $\sigma_{max}$  is referred to as the inhibition pressure at which no expansion can take place (Herrador et. al. 2009). They then added a creep component ( $\epsilon_c$ ) to introduce the mechanic strains (Figure 2.18).

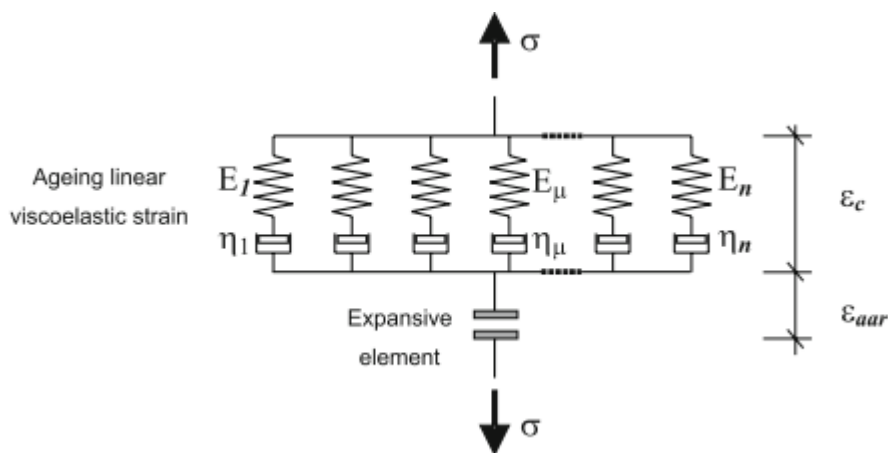


Figure 2.18 - Graphic Representation of Model (Herrador et. al. 2009)

In observance with the proportionality laws the parameters were expanded to include the compressive stress state, temperature, moisture and reactivity of the concrete taken into account:

$$\epsilon_{asr}^m = \beta^m(t) [F_C(\sigma_c, t) * F_T(t) * F_M(t) * F_R(t)]^m$$

Where  $F_C$  = Compressive stress state  
 $F_T$  = Temperature  
 $F_M$  = Moisture  
 $F_R$  = Reactivity  
 $\beta^m$  = Calibration factor for field observations

The expansion factors ( $F_C$ ,  $F_T$ ,  $F_M$  &  $F_R$ ) were normalised using the calibration factor to simulate the results from the field. It provided very accurate models for the deformation experienced in the dams (Figure 2.19) but does not take into account the physical mechanism of the reaction in doing so.

#### 2.4.4.2. Chemo-mechanical Coupling Model

This model assumed that the progress of ASR was accompanied by the degradation of the mechanical properties of the concrete. It operated under the framework of elastoplasticity and ignored the thermal and humidity aspects of the ASR development. It included temperature at a later stage to end up with an expansion rate that was controlled by the alkali content of the cement, the amount of confining stress and the temporal effects of the temperature (Pan et. al. 2012).

The model was very similar with field measurements and was later used to model the dynamic stability of the structure. A later variation was able to account for the swelling effects of ASR by assuming that the products of the reaction filled the surrounding pores and exerted a pressure.

### 3. Finite Element Modelling

Finite element analysis involves dividing a model into discrete shapes, called elements, which are joined at points called nodes. This system of elements and nodes is referred to as a mesh and is defined by boundary conditions and equations derived from relevant laws of physics. From this a system of linear equations can be constructed and unknown variables, such as nodal displacements, can be obtained. The element stresses and strains can then be derived from the nodal variables (Strand7).

There are various stages to consider when developing a finite element model:

- i. The mesh is designed based on the geometry of the physical system
- ii. The material properties must be appropriate and clearly defined
- iii. Boundary conditions must be carefully defined in terms of nodal restraints and externally applied loadings
- iv. The type of solver used must be appropriate to the problem.

There are several complicated mathematical models which focus on various elements but none which are easily replicated and useful in practical situations. A simplified finite element model developed for use in industry would therefore be of great use when investigating the effects of ASR on large pieces of infrastructure.

The main challenge presented in the project is that, even though it is quite capable of dealing with concrete as a material, Strand7 just not really built for a problem such as this. The mathematical models that deal with crack propagation are written to identify when a crack begins and allocate new nodes to the points where the elements have split apart. Strand7 does not do this and stops its calculations when the material begins to fail in such a manner.

The initial investigations into modelling using Finite element analysis resulted in..... This project was limited to:

The first stage was to build a simplified 2D model of the concrete to show the forces involved in concrete that is unaffected by ASR. Once this was achieved, methods of simulating the internal pressure created by the swelling action of the ASR need to be investigated and applied.

The second stage involves altering the model to simulate the presence of discrete cracks in the concrete

The third stage requires the same model to be done in 3D. This model will be a symmetric model based on a quarter of the column to save on computational time.

The fourth stage is designed to use the 3D model and apply the adhesive and carbon fibre to the surface of the cylinder to model the affects of the confining stresses

### **3.1.Element Types**

Finite element modelling breaks down a problem into discrete shapes which behave in definite ways. The difference between an accurate model that converges well and an inaccurate one is often the choice of what elements to use and where to use them.

In many cases involving stress and strain analysis in which Quad4 elements are used Strand7 will add a central node to the Quad4 element and redefines it as four Tri3 elements. The element matrices of the original Quad4 element are then calculated based on the four Tri3 elements (Strand7 2005).

This improved Quad4 element is not used for plain strain, plain stress or axisymmetric analysis involving:

- Nonlinear soil materials
- Nonlinear elasto-plastic materials
- Nonlinear elastic materials with the Max Stress yield criterion

Due to the difference between the standard Quad4 and the improved Quad4 a nonlinear material analysis would be different to a linear analysis even if the stress strain curve was linear.

If Quad8 or Quad 9 elements are used Strand7 offers an option of using a reduced integration scheme. A stiffness matrix calculated this way will have more 0 eigenvalues and if these are not properly restrained the global stiffness matrix will be singular. This system can have very good results as the extra zero eigenvalues can help to improve the performance of the element (Strand7 2005).

### **3.2.Boundary Conditions**

The boundary conditions are an important part of the finite element model as they help to define the area being investigated. Essential boundary conditions such as displacements and rotations directly affect the degrees of freedom at the nodes.

Support conditions are used to restrain structures against relative rigid body motions, they are also used to calculate the residual forces in the model. These are generally in the form of pins, rollers and fixed supports. In a two dimensional system there should be at least one translational restraint in the x axis, one restraint in the y and a restraint for rotation around the z axis (Felippa 2015)

### **3.3.Meshing**

The mesh size determines the accuracy of the model, the fineness of the mesh should be appropriate to the properties being modelled. The mesh should be fine when near cornering or sharply curved areas, if it is in the vicinity of point loads, cracks or areas of concentrated reactions or abrupt changes in material thickness or properties. For the remainder of the time a coarser mesh will do as using too much fine mesh in these areas will extend the amount of computing time and not contribute greatly to the results (Felippa 2015).

When modelling in two dimensions the opportunity to use a mesh of quadrilaterals should be taken over using triangles. In three dimensions bricks should be used over wedges and tetrahedral should be avoided.

The element aspect ratio describes the shape of the mesh sections. Mesh that is too elongated is doesn't necessarily provide bad results but it does tend to cause problems. As a rule of thumb an element aspect ratio of three should be treated with caution and an aspect ratio of 10 should be avoided (Logan 2007).

Physical interface, such as a change in two materials should be seen as an inter-elemental boundary and elements should not cross this. It should be represented as a line of nodes.

### 3.4.Aspect Ratio

Essentially this is the ratio of the longest side to the shortest side, as this ratio increases the accuracy of the model decreases. Due to the nature of FEM, this error will be carried on to the surrounding elements. The general rule for this is that compact regular shapes return the best results. If there is an element or shape that has a bad aspect ratio it is best practice to break it up into a series of regular shapes (Logan 2007).

### 3.5.Use of Symmetry

Symmetry refers to not only the shape of the model but also the material properties, loads and boundary conditions that it is subjected to. By utilising the existence of symmetry a model can be greatly simplified which will speed up the results or, alternatively it can allow for a more complex mesh formation in the model itself.

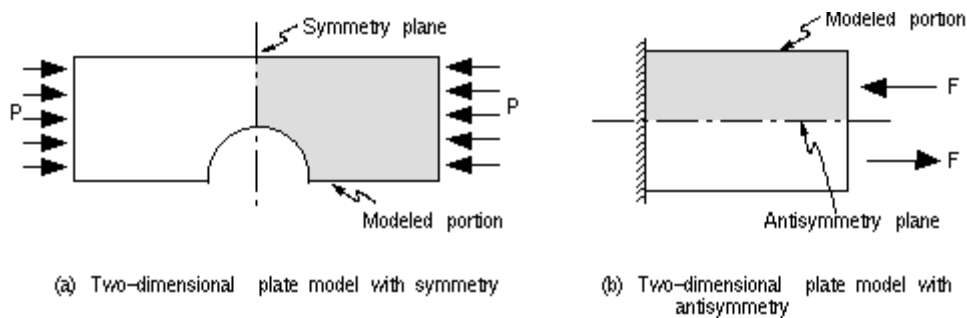


Figure 3.1 - Use of Symmetry ([http://www.ansys.stuba.sk/html/guide\\_55/graphics/GBAS21.gif](http://www.ansys.stuba.sk/html/guide_55/graphics/GBAS21.gif))

### 3.6. Natural Subdivisions at Discontinuities:

It is important to have a node present wherever there is an abrupt change in a condition or geometric shape, this represents a point where forces are concentrating and calculations should be made in the stiffness matrix to account for this. Examples of this can be at discontinuous udl's, sudden contractions in shape, point loads, re-entrant corners and at the surface of holes in members (Logan 2007).

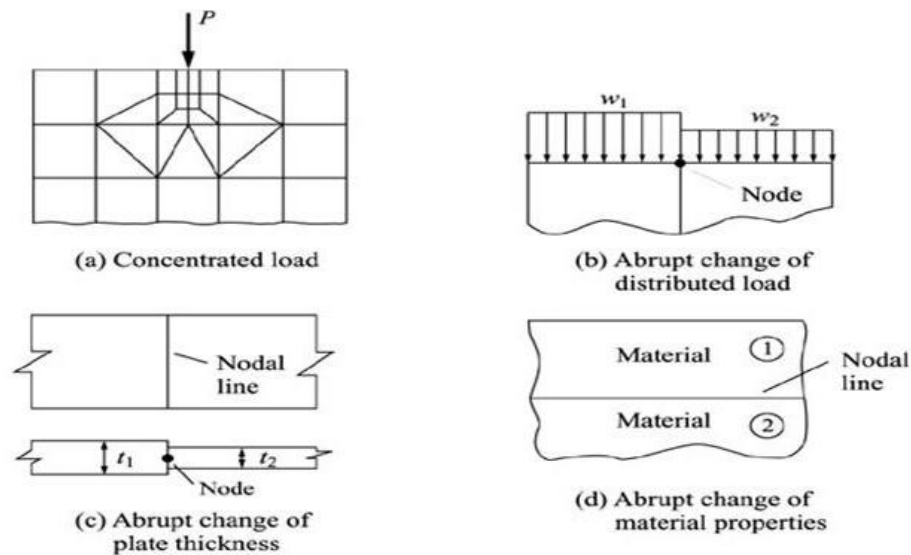


Figure 3.2 - Subdivisions at Continuities

### 3.7. Sizing of Elements – The *h* and *p* methods:

The aim of the operator is to create a model that will deliver as accurate results as possible. The *h* and *p* methods are automated processes that seek to spread the inaccuracy as evenly across the entire model as possible. This adaptive refinement depends on the geometry of the structure, the way in which the loads are applied and the boundary conditions (Logan 2007).

#### *h* Method:

This basically involves adapting the mesh to suit the conditions in the model. The operator will start off with a coarse mesh using appropriate element shapes which will return an acceptable degree of accuracy. These elements are then divided up into a series of regular, more uniform, compact shapes. It is also possible that part of the mesh can be enlarged in regions where stresses do not change very quickly.

#### *p* Method:

The *p* in this case stands for polynomial and means that the way the model is created adjusts the order of the polynomial used in the calculations. The degree of the polynomials are chosen to suit the boundary conditions, loadings and geometry of the model. A model will be run with a base polynomial and then run again with a higher order polynomial to compare results. Higher order polynomials usually achieve better results with the computer doing the iterations automatically.

*P* refinement can be done by increasing the degrees of freedom to existing nodes, adding internal degrees of freedom or by creating additional nodes on boundaries between elements.

### 3.8.Linear Static Vs Non-Linear Static Solver:

The linear static solver is the most widely used. It describes

The fundamental FEA equation relies heavily on the stiffness matrix [K] to define the behaviour of the model:

$$[f] = [K] * [d]$$

where: [F] = Known vector of nodal loads

[K]= Known stiffness matrix

[d] = Unknown vector of nodal displacements

The stiffness matrix [K] is calculated based on the geometry, material properties and the restraints. When a load is placed on a member and it begins to deform its stiffness can change in response to the changing geometry and the properties of the material change which are altered near the ultimate load.

Linear static analysis makes the following assumptions to simplify the process:

- i. All materials in the structure remain linearly elastic
- ii. The displacements/deflections observed are small
- iii. The boundary conditions do not change once the load is applied
- iv. The loading is slowly applied to avoid a dynamic or inertia effect

(Strand7 2005)

The principle of superposition applies to the linear static solver.

The nonlinear solver however deals with situations where the behaviour of the model is not a linear function of the applied loadings. Nonlinear behaviour can be evident in geometric nonlinearity, material nonlinearity or boundary condition nonlinearity, hence the first three of the above assumptions made in linear solver are not applicable to the nonlinear solver.

The equation that governs the nonlinear solver is:

$$f(u) = p$$

Where  $f(u)$  = Total element internal force vector  
 $u$  = Unknown nodal displacement vector  
 $p$  = Global equivalent load vector

The global stiffness matrix does not exist in this solver due to changing geometric and material properties but instead a tangential stiffness matrix is used through the iterative process until the equilibrium conditions are satisfied. The solution is said to have converged when the following conditions are satisfied:

i. Displacement Norm  $\frac{|\Delta u|}{|u|} < \epsilon_u$

Where  $\Delta u$  = Norm of incremental displacement vector  
 $u$  = Total displacement vector  
 $\epsilon_u$  = Convergence tolerance

ii. Residual Force Norm  $\frac{|r|}{|\Delta p|} < \varepsilon_r$

Where

$\Delta p$  = Norm of unbalanced force vector

$r$  = Current residual force vector

$\varepsilon_r$  = Convergence tolerance

(Strand7 2005)

## 4. Preliminary Finite Element Modelling

The aim of this thesis is to produce a simplified model of ASR using finite element analysis software which can be easily replicated in industry. Previous models such as the Parametric model (see sect 2.4.4.1) have sought to recreate the effects of ASR in finite element modelling software, but relied on extensive testing and complicated series of parameters. By simplifying this approach the model will be confined to simulating the reduction in characteristic strength only.

The first stage involves creating a model that accurately simulates a healthy concrete cylinder during the compression test. This is to be used as a control model against which the later models will be compared.

The next step will include recreating the internal expansive forces that are created by the alkali-silica reaction. The speed and intensity of the chemical reaction, the locations of the reactive sites and the initiation and propagation of cracks is beyond the scope of this thesis. Instead the internal pressures created by ASR will be done using temperature nodes. This simple mechanism acts by causing a highly localised temperature increase at the selected nodes and the expansive nature of the immediately surrounding concrete will simulate the expansion of the ASR. Ultimately the tensile forces in the concrete will cause microcracks which will lead to a loss of stiffness as can be seen in figure 4.1

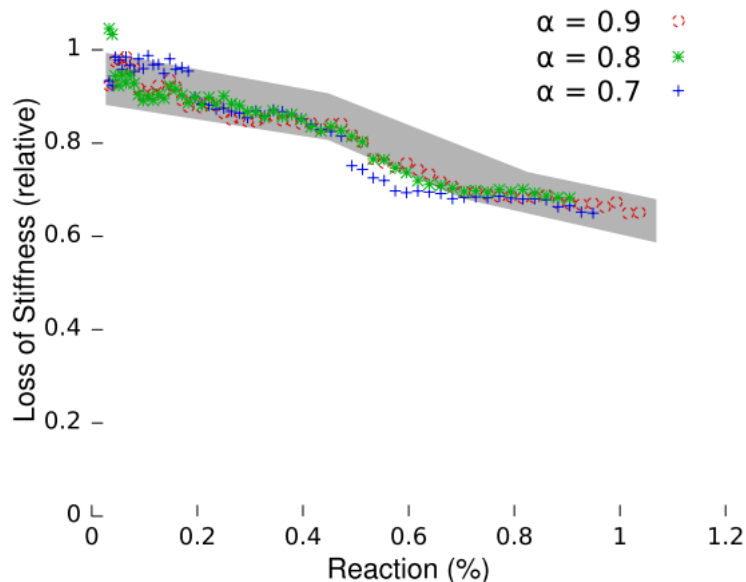


Figure 4.1 - Stiffness as the reaction progresses (Pan et. al. 2012)

## 4.1. Modelling of Concrete Cylinder Compression Test

The first step to creating this model is to recreate the mode of fracture of good quality concrete as a benchmark and test run it with the linear static solver. A concrete compression test involves a standard sized concrete cylinder subjected to an axial compression force. Of the three standardized sizes 50x100mm, 100x200mm and 150x300mm (Del Viso et. al. 2007) the largest was selected. This dimension is also consistent with the ratio used in the compression testing as per AS1012.9 - 2014. The variations of fracture patterns seen in figure 4.2 are due to the inexact interface between the concrete cylinder and the steel plates which are applying the force. Before the test the cylinders are cut and ground to ensure the most even force is applied.

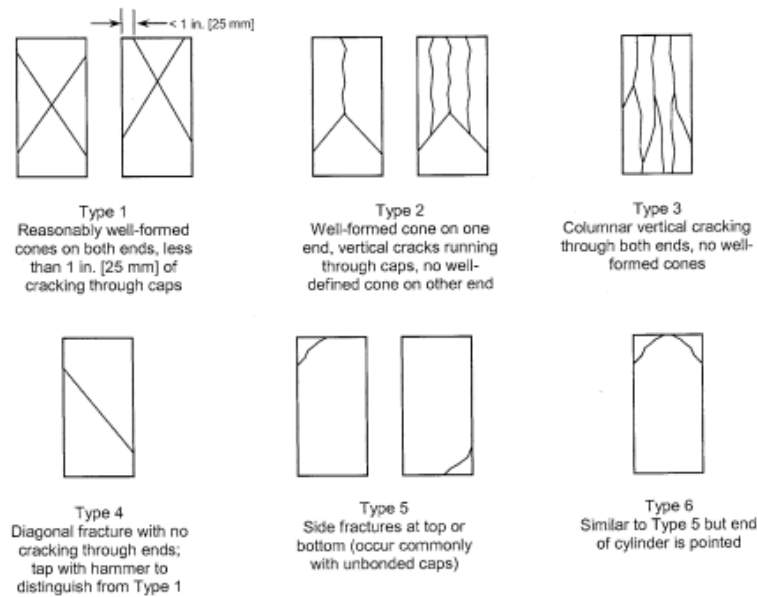


Figure 4.2 - Concrete Fracture Patterns (ASTM 39)

The model will be constructed and tested by using a linear solver with several different mesh sizes to determine which size gives the best results for the most economical mesh size. Once the mesh size is decided on the model will be run using a nonlinear solver to get the most accurate results.

## 4.2.Linear Static Model

For a concrete compression test different failure modes are associated with the restraining conditions at the end caps. Since friction is a function of the normal force the movement of the concrete ends in contact with the steel plate will reduce as the force increases. There is not an ideal interface between the concrete and the steel plate therefore the normal force is not evenly spread across the surface meaning differential movement across the ends. For this model it was assumed that there would be an ideal interface between the two and that the end caps are restrained to prevent movement in the transverse direction. The following are the typical fracture patterns which are dependent on the confinement of the ends (Murray et. al. 2007).

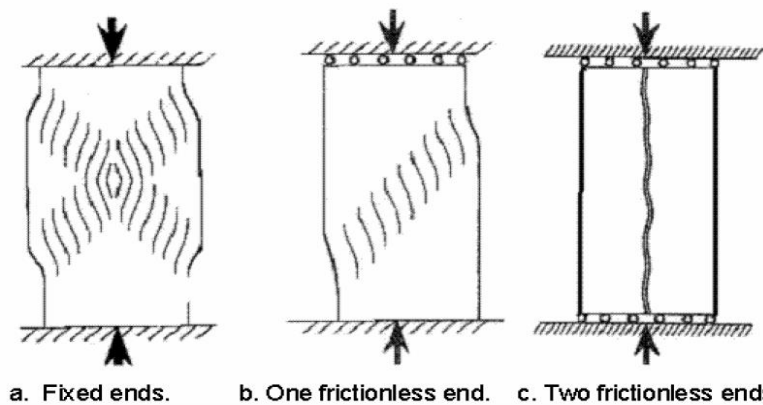


Figure 4.3 - Failure modes determined by boundary conditions (Murray et. al. 2007).

### 4.2.1.Axisymmetric Model

It was decided that, due to the symmetry of both the cylinder and loading, the most efficient method would be to use the axisymmetric model. This takes a three dimensional problem and reduces it down to two dimensions by treating the 2D strain plane revolving 360° around the central z axis (Logan 2012).

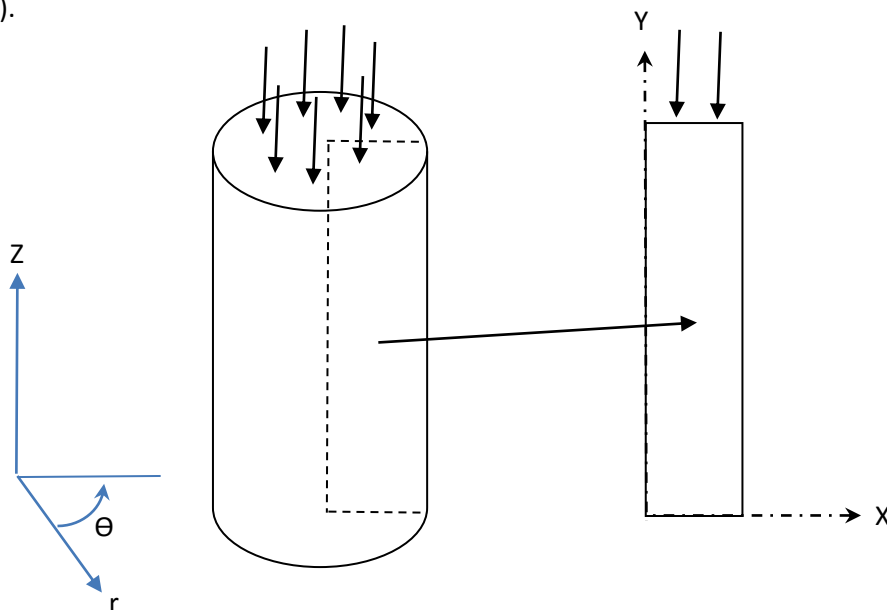


Figure 4.4 - Transform a 3D image to 2D

Due to the confinement experienced by the theta co-ordinate, the resultant model was a cross section which radiated out from the origin on the Zr plane. For simplified use in the model the Z and r axis were substituted with the X and Y axis. In axisymmetric models the stresses are largely independent of the theta direction but are evident in circumferential strains due to the radial displacements. The shear strains  $[\gamma_{z\theta}, \gamma_{\theta z}]$  are zero and the remaining strains  $[\epsilon_r, \epsilon_\theta, \epsilon_z, \gamma_{rz}]$  in the XY plane are used to calculate the stresses  $[\sigma_r, \sigma_\theta, \sigma_z \text{ and } \tau_{rz}]$  (Strand7 2005).

Plates are used in this model due to its two dimensional nature and an external pressure is therefore applied via an edge load. It is important to note that point forces are applied per radian around the model so later when nodal forces are introduced a node on the XY plane but this will in fact be expressing a thermal load of x degrees per radian around the entire  $2\pi$  of the model. As a result the amount of force that is being imposed on the model will be a radial ring with a total force of  $x \cdot 2\pi$ . This is not a consideration when dealing with edge pressures due to the way a pressure works, a 3MPa pressure is going to be 3MPa all the way around.

#### 4.2.2. Plates and Meshing

The subject of the model was to be a 150mm x 300mm cylinder (Del Viso et. al. 2007), which converted to a rectangle 75mm wide and 300mm tall. I maintained an aspect ratio as close to 1 when subdividing the rectangle so that the results would be as accurate as possible. The mesh consisted of four node quadrilaterals as they are dimensionally stable and avoid issues with stress found with the triangular shapes.

#### Boundary conditions

The axisymmetric model is based on the shape rotating around the origin with the model in the x+ and Y+ axis. It is important to supply a sufficient number of restraints in order to avoid rigid body motions. It is advised when creating a solid axisymmetric model to supply restraints in the X direction along the Y axis, the effect of not doing so can potentially allow spurious “voids” to form in the structure.

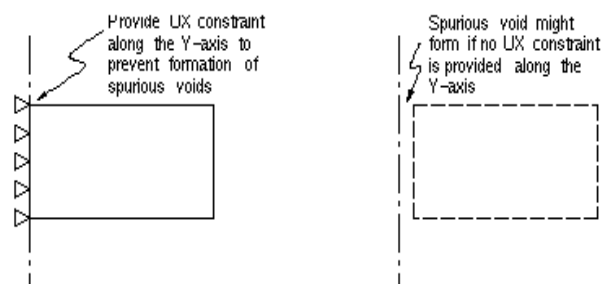


Figure 4.5 - Constraints for Solid Axisymmetric Structure ([http://mostreal.sk/html/guide\\_55/g-bas/GBAS2.htm](http://mostreal.sk/html/guide_55/g-bas/GBAS2.htm))

The nodes along the bottom face were fully restrained in the X and Y-direction, in accordance with the end cap restraints described by the (Murray et. al. 2007) while the nodes along the top were restrained in the X-direction only. Finally a pressure load was placed along the top edge of the plates.

The material was set as isotropic and the properties such as Poissons ratio and Young's Modulus were chosen according to the AS3600 properties for 40MPA concrete.

The outcome of the first stage of the model was encouraging. The stresses in the primary 11 direction are shown on the left side of figure 4.6 shows that the top and bottom in compression while the majority of the middle section is experiencing degrees of tension, which is to be expected. On the right side of figure 4.6 the displacement of the elements suggests a failure of the concrete cylinder in the same fashion as Type 1 in figure 4.3.

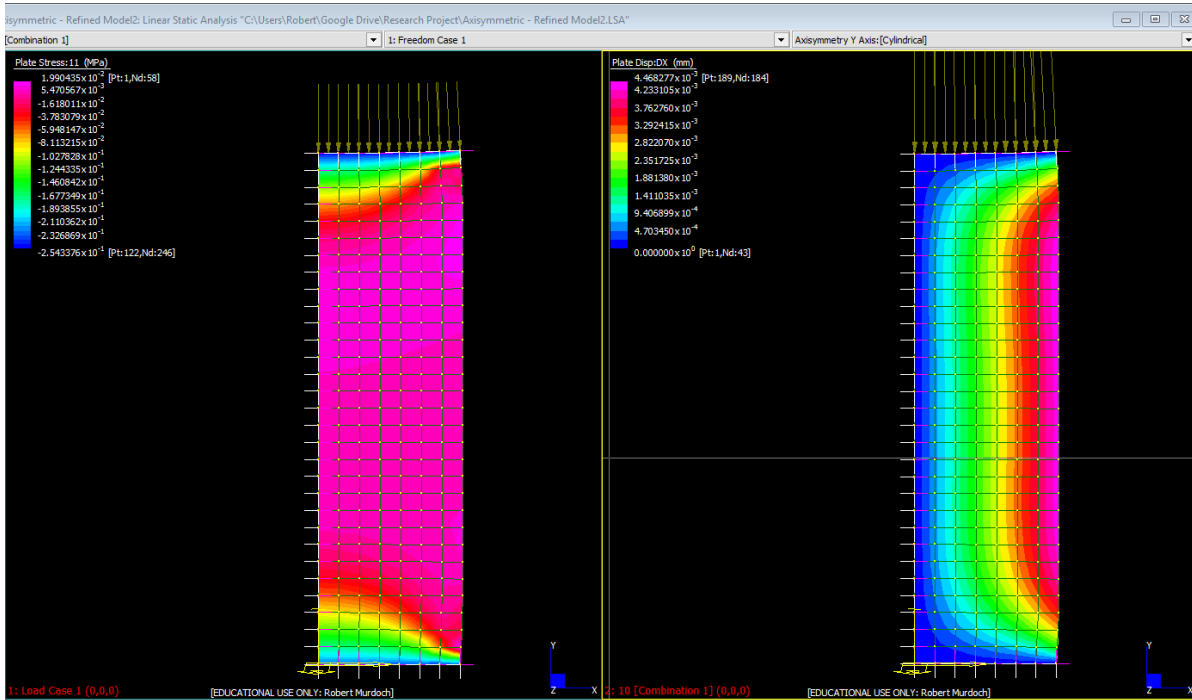


Figure 4.6 - Standard Compression Test, (Left) Stress in 11, (Right) Displacement in X Direction

### 4.3. Convergence Study

The purpose of doing a convergence study is to ascertain how fine a mesh needs to be to give an accurate result. The trade off is that a finer mesh will require more time and computing power to run but will return a more accurate result. The size meshes considered were (Table 4.1) and the models were made so that there was as little variance in the meshes used as possible. The material properties and boundary conditions were consistent for all models used and the same external loading was also placed on all five models.

Table 4.1 - Mesh Sizes and Results

Square Element Dimension	Number of Elements	DX (mm)
25	36	1.85E-02
15	100	1.84E-02
5	900	1.83E-02
3	2500	1.83E-02
2	5700	1.83E-02
1	22500	1.83E-02

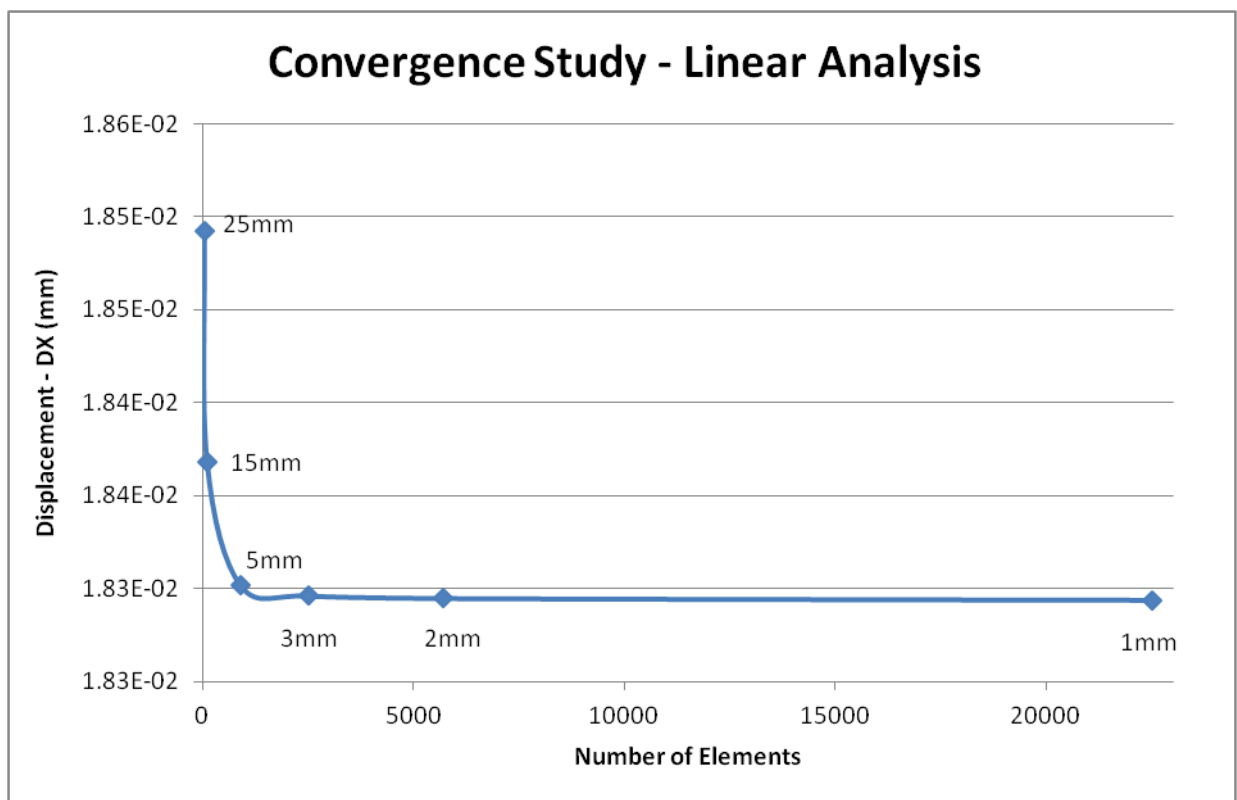


Figure 4.7 - Convergence study on the linear model

From the results in figure 4.7 it can be seen that initially the gains in accuracy were quite large when going from a 25mm to a 15mm mesh size but this trend slowed and eventually there is was little gain in using a mesh finer than 5mm. The difference in the number of elements between the 5mm mesh and the 3mm mesh ultimately decided that the 3mm mesh was too fine and would slow the process down for very little return. Therefore a 5mm mesh was decided on when running the nonlinear static solver.

#### 4.4. Nonlinear Static Model

The nonlinear static model required a great deal more thought and research into how to set it up and what tables and failure criterion to use to make it work properly. This is an analysis based on the nonlinearity of the material, which is described as elastic and therefore accommodates a nonlinear relationship between the stress and strain and it is assumed that there is no plastic deformation.

##### 4.4.1. Yield Criterion

The yield criterion is a law which dictates the behaviour of a nonlinear material. It defines the elastic behaviour under any combination of  $\sigma_1$ ,  $\sigma_2$  and  $\sigma_3$ . Depending on what level of behaviour is focused on will determine how we choose to make the concrete perform. Concrete, even though it is technically quasi-brittle in nature (see sect. 2.1.2 Fracture Mechanics), displays some ductile properties. It has an initial elastic phase and displays a significant amount of plastic deformation during its softening phase before ultimately failing. This is not a true ductility as the strains observed are due to an incremental deformation due to the formation of microcracks (Carpinteri & Ingrassia 2012).

The stress-strain curve in this case had to be capable of defining both the compressive strength and the tensile strength of the concrete as the model was intended to show the tensile failure of the concrete due to internal expansive forces.

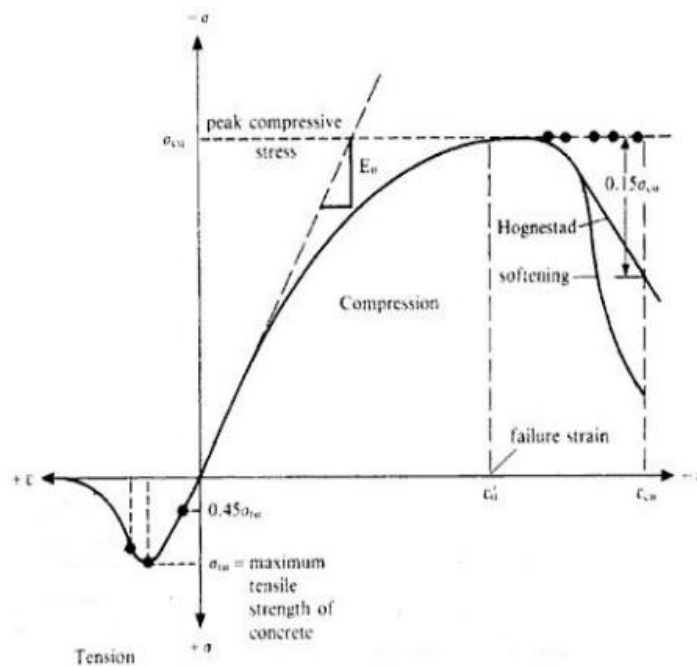


Figure 4.8 - Tensile and Compressive Stress-strain Curve of Concrete (Bajracharya 2010)

In many models concrete can be idealized as an elasto-plastic material and hence the Mohr-Coulomb or Druker-Prager failure criterion are favoured. The Mohr-Coloumb failure criteria is based on the premise that these materials fail predominantly in shear and hence the main factors controlling this are the internal angle of friction and the cohesive strength. Typical values for concrete have the internal angle is usually between 33 and 42 deg. and the cohesive strength around 5.

This is not useful in this application as the internal forces which induce cracking that are of primary interest. For this model the tensile forces need to be tracked which means that other models of failure had to be investigated. Initially the von Mises failure criterion was utilised for this model. Von Mises is usually used with ductile materials and the failure criterion is based on the maximum distortion energy theory for ductile materials which states that a material will fail when the Von

Mises stress (Eq. 4.1) reaches the yield point of the material (See figure 4.9).

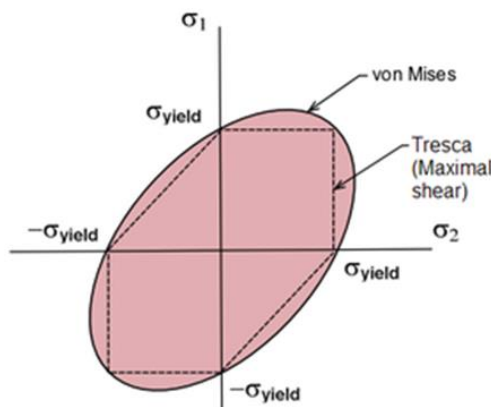


Figure 4.9 - Von Mises Failure Critereon

**Equation 4.1 - Von Mises Yield Criterion**

$$\sigma_{vm} = \frac{1}{\sqrt{2}} \sqrt{(\sigma_1 - \sigma_2)^2 + (\sigma_2 - \sigma_3)^2 + (\sigma_3 - \sigma_1)^2}$$

Where  $\sigma_1, \sigma_2, \sigma_3$  are principle stresses

It was soon discovered that the Strand7 program did not allow for the Von Mises criterion to be used when the material displayed a different failure limit in compression than in tension. In Strand7 the Von Mises solver only refers to the first quadrant (+,+) of the Cartesian graph which only gives the results for the tensile qualities and assumes that these are replicated for the compression characteristics. The compressive strength, which is detailed in the third quadrant (-x,-y) is therefore not incorporated into the solution.

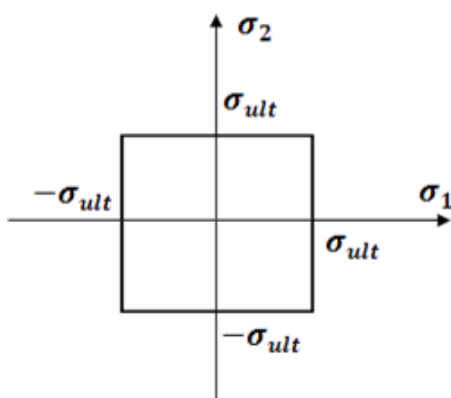


Figure 4.10 - Max Strain Failure Criterion

The only solver that considered information from both the first and third quadrant was the Max Stress solver which is suggested by the program for materials such as concrete. The maximum normal stress criterion is based on the Maximum normal stress theory which states that a material will fail when the maximum principle stress exceeds the ultimate strength for that orientation. This is mostly applied to brittle materials and generally deals with, but is not limited to, tensile stresses.

The general idea is that when subjected to a tensile force the strength of a material is affected more as cracks will contribute to the overall reduction in strength of the material. The opposite is not true with compression as the cracks will simply be compressed and close together.

This theory operates on the assumption that the material is the same in tension as it is in compression and is generally used with brittle materials. For this criterion it is not advised to use the yield strength to define the limit stress since brittle materials have no clearly defined yield point.

The prediction mechanism therefore works by:

**Equation 4.2 - Max Stress Yield Criterion**

$$f = |\sigma_1|, |\sigma_2|, |\sigma_3| = 0$$

**4.4.2. Stress Strain Table**

A stress strain table was created to define the tensile and compressional strength of concrete.

The conditions that the curve had to meet were:

- 1) Point of origin;  $f=0, \epsilon=0$
- 2) Point of maximum compressive stress;  $f = -f_o, \epsilon = -\epsilon_o$
- 3) Slope of curve equal to  $\frac{df}{d\epsilon} = E_c$  for region  $0 < \epsilon < 0.45f_c$

Two idealised curves were proposed by Ali et. al. (1990)

$$1) \frac{f}{f_o} = 2.1 \left(\frac{\epsilon}{\epsilon_o}\right) - 1.33 \left(\frac{\epsilon}{\epsilon_o}\right)^2 + 0.2 \left(\frac{\epsilon}{\epsilon_o}\right)^3$$

$$2) \frac{f}{f_o} = \frac{1.9\left(\frac{\epsilon}{\epsilon_o}\right)}{1+0.9\left(\frac{\epsilon}{\epsilon_o}\right)^{2.1}}$$

Where:

- $f$  = Flexural Strength
- $f_o$  = Flexural Strength at Failure
- $\epsilon$  = Strain
- $\epsilon_o$  = Strain at failure

The Ultimate Strain was found using the equation:

$$\epsilon_u = \frac{0.0078}{(f_o)^{0.25}}$$

(Ali et. al. 1990)

The Ultimate Tensile Strength is generally about 1/10 to 1/7<sup>th</sup> of the compressive strength, so for this set of curves it taken as 1/10 as it is the more conservative.

Ali et. al. found that the second equation was the best universal fit for most applications and strength characteristics so it was adopted for this model.

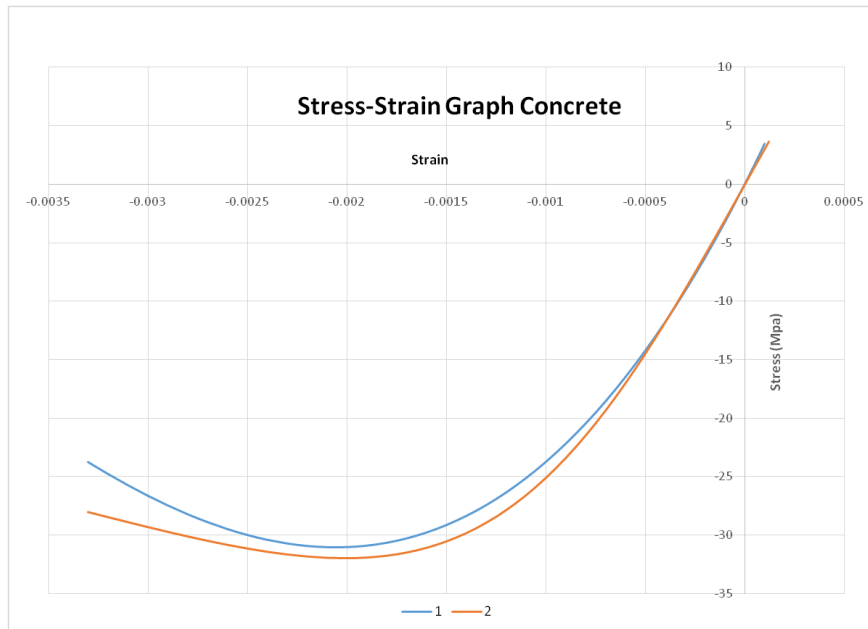


Figure 4.11 - Stress-Strain Curves

### 4.4.3. Results

For quite some time I was struggling to get results for any of my nonlinear models. There are large sections of this report that are based on the linear models as there were no nonlinear results to write about. By the time the nonlinear versions started to work there was not enough time to go back and do them properly.

At first I thought there might be something wrong with placing an axial loading on an axisymmetric model as I couldn't find any examples of this being done in any of the literature. During the course of the investigation, after checking boundary conditions, meshing and values I decided to try a few different types of loadings as well. I found the program ran perfectly when the loading was placed on the side (representing a hoop stress) but continued to break up from the beginning if I tried to place the load axially.

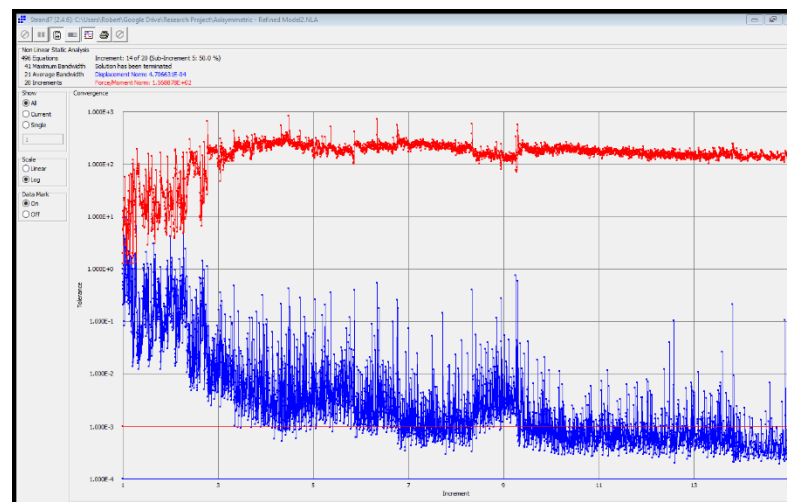


Figure 4.12 - Initial Nonlinear Results

The axisymmetric model ran for quite a long time but still broke up on the first iteration. The lack of convergence of the residual forces vector invited the idea that there were boundary condition issues.

The residual forces vector describes the difference between the loadings and the reaction forces from the material, if there are rigid body movements then there would be unbalanced forces and movement would result. I tried using the log file to check the summation of the forces on both the elements and in the global load vector but had trouble understanding what the parts of the readout were referring to and how to relate it back to the applied forces.

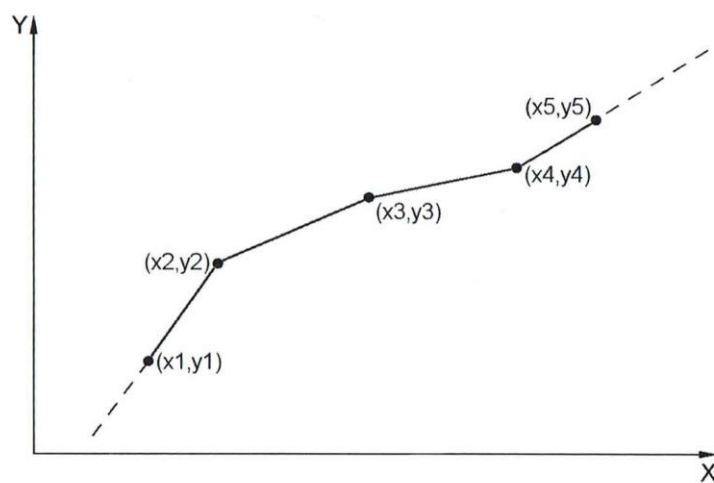
One problem with the axisymmetric model involves the differences in the way Quad4 plates are used between linear and nonlinear models. In a linear model the Quad4 plate is broken up into 4 Tri3 elements and the stiffness matrix calculated based on these. The nature of CST elements limits the effectiveness of nonlinear solving techniques as the entire area bounded by the element is considered to be a uniform strain. This simplification may contribute to the difference between the two types of models.

The progress of this dissertation was stymied by the lack of effective models in the initial stages. Subsequently, there has been a lot of time and energy put into investigating why the models will not work. In order to be thorough I decided to go back to the start and revisit the fundamental principles of creating a finite element model:

- i. The Mesh – To begin with I checked that it was an appropriate size and shape. It was suitably fine for the application and the quadrilateral elements had an aspect of 1. Initially the mesh in the axisymmetric model changed from one size to another to accommodate regions where the nodes would be but it proved too difficult to carry through to the 3D models in the final stages. Since the models in the primary stages were not at all complex varying the grading was eventually abandoned to avoid any conflicts and stress localisations.

The elements themselves are appropriate for this type of use. There was an option of using Quad8 or 9 elements which would have been very accurate and better for the outside curved surface, there is also a facility in the solver to simplify the integration of these two elements, but unless applied in exactly the right conditions they have a habit of returning erratic data.

- ii. The Material Properties – The key to this section is recognising the nonlinear nature of the concrete. A lot of investigation went into finding a suitable stress-strain curve. At one stage the error message said that the curve had intersected the horizontal axis. After some investigation it was found that Strand7 extrapolates a curve by maintaining the last known gradient (Figure 14.13). To stop this error message the curve was adjusted slightly so that the final gradients at both ends were zero (figure 14.14)



F  
Figure 4.13 - Table Extended By Maintaining Gradient (Strand7)

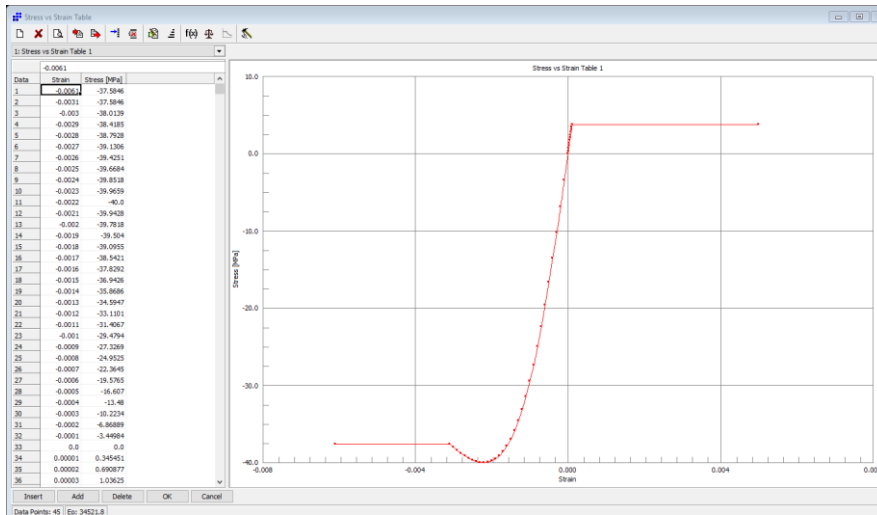


Figure 4.14 - Revised Table With Zero Gradient Ends

- iii. Boundary Conditions – While checking the boundary conditions I discovered that on the axisymmetric model I had to lock the node for the x direction at all points where  $x=0$ . If this is not included it may assume that there is an infinitely small hole along the axis and can sometimes result in spurious behaviour at nodes at these points.
- iv. The type of solver used must be appropriate to the problem. There was a choice between the nonlinear static and the Quasi-static solver. The major difference being that in the nonlinear static the load is applied in increasing increments whereas the quasi-static solver applies the incrementally as well as taking the speed of the loadings into account. Nonlinear static was chosen for this application as the loading appears over a long period of time. The step size of load increments has a great impact on convergence, these were reduced greatly to make sure the solution was not breaking up due to the steps being too large. The automatic load stepper was also employed, this regulates the size of the incremental substeps and reduces them if certain conditions are met. Finally the bandwidth was checked and the nodes reordered to speed up the solution process. This really didn't do much as the model was so small.

The turning point in the process came when I realised that when I was dividing the loadings into substeps I had only been dividing the load case and not the freedom case as well. This accounted for the red line in figure 4.12 (which is the geometric conditions) not converging while the blue line (which relates to the loadings) was converging well. Once this was corrected the program converged the way it was expected to (Figure 4.15).

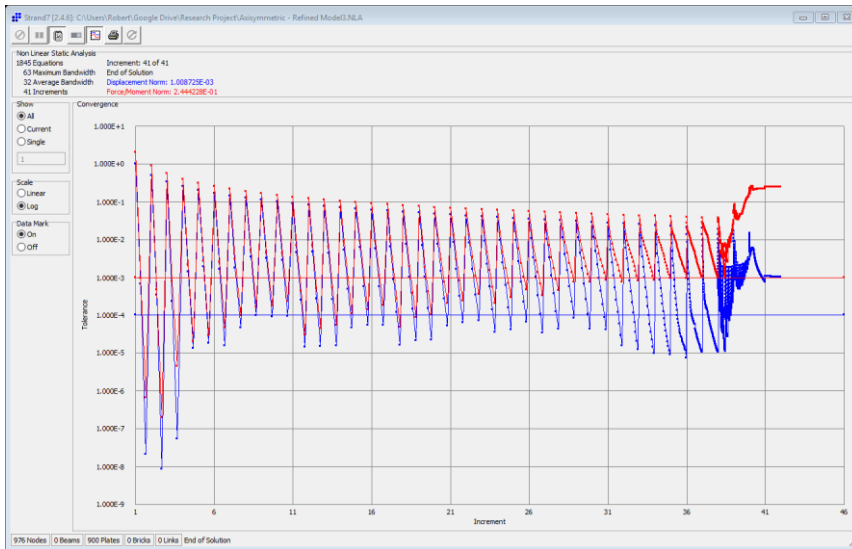


Figure 4.15 - Graph Showing Model Converging

At 1MPa increments the model converges well for the majority of the program and then starts to break up at around iteration #38. In order to allow the model to run the full length I tried to correct this by using a finer scaling to the iterations (0.5 MPa steps and again 0.1MPa steps) but this failed to have any real impact.

Below (figure 4.16) is the model in the last iteration before it stopped converging. The model displays the same characteristics as the linear static model.

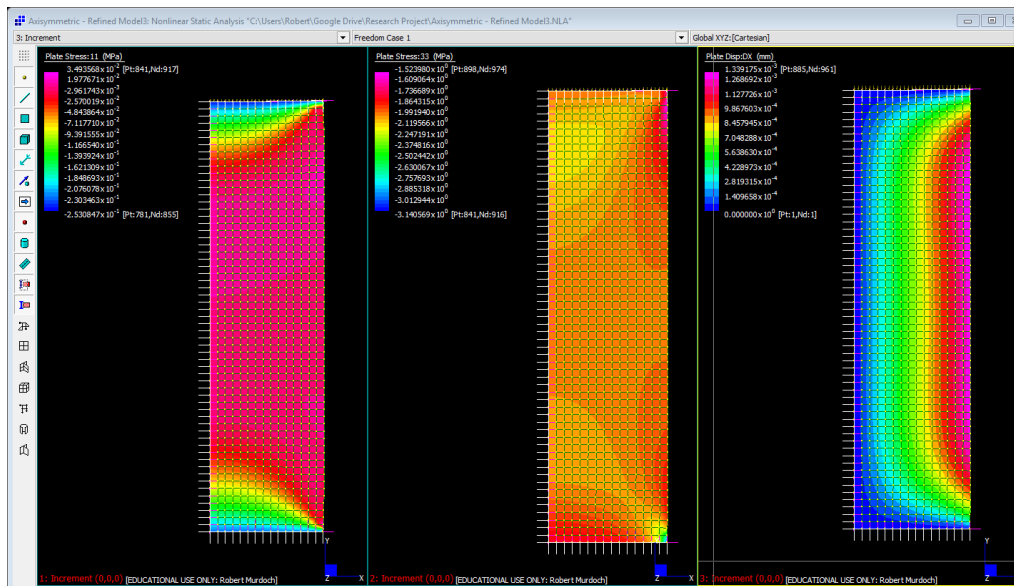


Figure 4.16 - Model Results at 37MPa (Stress 11, Stress 33, Disp. DX)

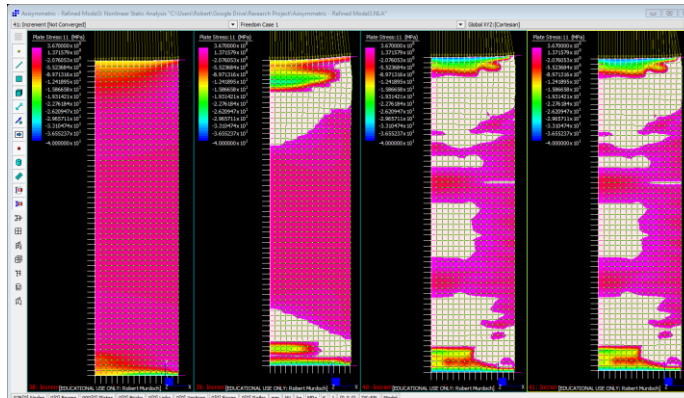


Figure 4.17 - Stress 11 Results at 38 - 41 MPa

Figure 4.17 and 4.18 are the stress in the 11 and 33 orientations from step 38 through to 42. By manipulating the legend so it only showed colour within the range [-40, 3.67] which makes the white zones show mode the failure is in. In the 11 and 22 directions the failure is in tension while the failure in the 33 direction is in compression had expected this type of behaviour at the final step, 41MPa, or possibly at 40MPa but not this early in the process.

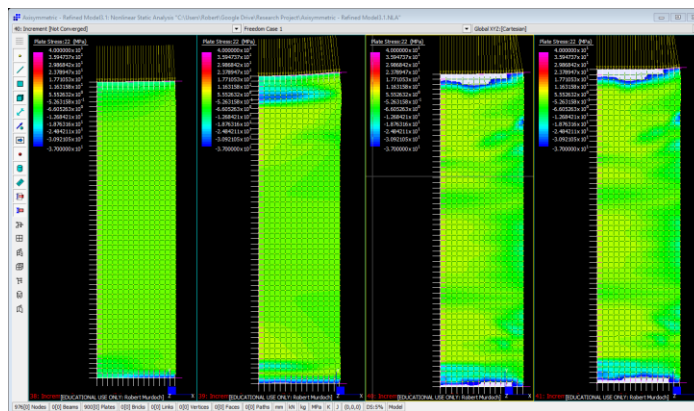


Figure 4.18 - Stress 22 at 38 to 41 MPa

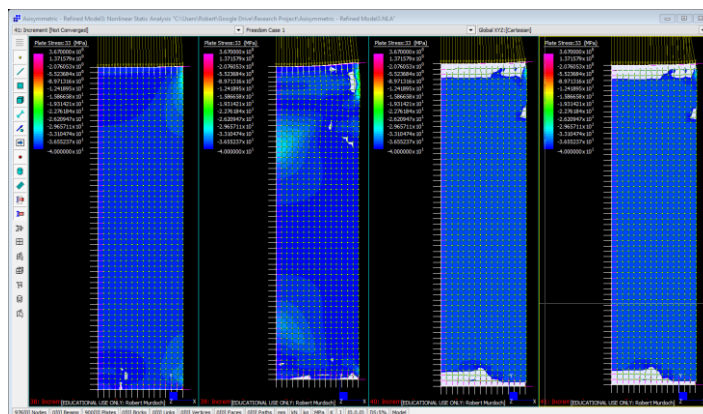


Figure 4.19 - Stress 33 at 38 to 41 MPa

This model was run under several loading increments to ensure that the final stages had the chance to converge but each time it ended with the 37.5MPa loading being the last increment to converge properly.

There are two stress-strain curves to consider when analysing these diagrams. The ultimate failure appears to follow the part of the compression stress-strain curve where it reaches a maximum and the slope approaches zero

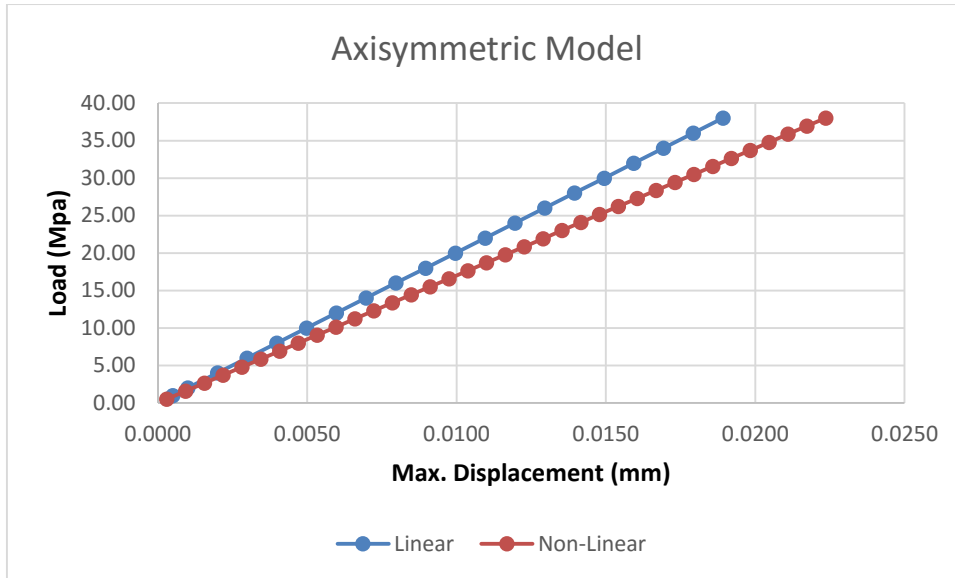


Figure 4.20 - Comparison of Linear to Nonlinear Model

Finally, figure 4.20 shows the degree of difference between the linear and the nonlinear performance in this test. The nonlinear is showing a marginally larger displacement for a given loading.

## 5. Refined Model

The next stage in the process involved introducing the effects of ASR to the concrete cylinder.

### 5.1. Results From Previous Thesis Concrete Cylinder Compression Test

Last year two students were able to replicate the deleterious nature of ASR in mortar bars by immersing them in a NaOH solution (Fig. 5.1). The aim was to encourage the formation of ASR and hence create a 0.2% expansion within 16 days as per ASTM C1260. Below are the pictures of the specimens which are subject to extensive map cracking.



*Figure 4.1 – ASR replication, cracking after 7 weeks.*



*Figure 4.2 – ASR replication, cracking after 11 weeks.*



*Figure 4.3 – ASR replication, cracking after 16 weeks.*

**Figure 5.1 - Results From Tracy Knight's Experiments (Knight 2014)**

The following graph shows the effect it had on the compressive strength of the concrete cylinders.

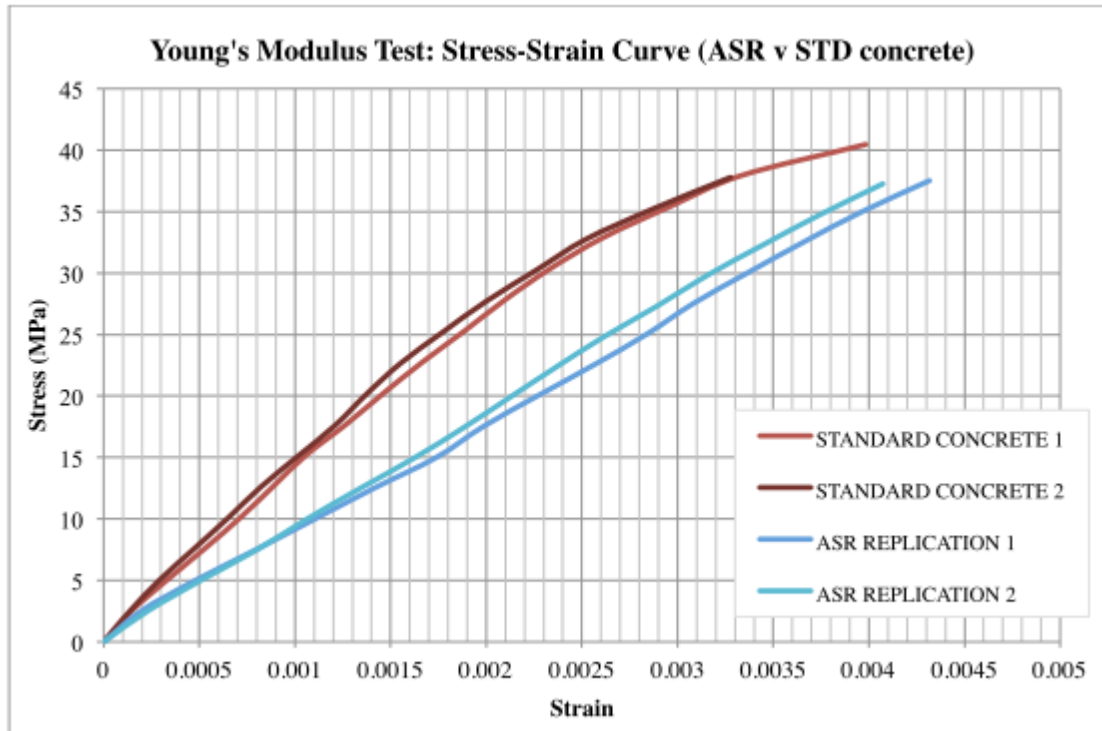


Figure 5.2 - ASR effect on characteristic strength (Knight 2014)

When subjected to a compression test the specimens affected by ASR showed a 37% reduction in the modulus of elasticity. The cracking is a response of the quasi-brittle nature the concrete possesses, as the process continues the microcracks join up into larger crack networks and there is a significant reduction in the stiffness. The ultimate compressive strength was reduced from the control specimens. Sample set two showed a 47% reduction in compressive strength.

### 5.2.How to simulate the ASR Testing

ASR can be present in a sample but exhibit no adverse effect until the right conditions are met, the deleterious effects are seen when the ASR begins to expand. ASTM C1260 defines deleterious expansion as greater than 0.2% of the specimen therefore this model must be designed to reflect the cracking caused by the internal expansion which brings about the softening of the concrete and characteristic loss of compressive strength. The effects of the reinforcement will not be present in this model.

Internal pressure, designed to simulate the swelling ASR, will be introduced to the concrete by way of increasing the temperature at various nodes to encourage thermal expansion by the surrounding concrete. This approach has been done before by Shin (Shin 2009) where a paste was introduced to the concrete matrix and assigned a fictitious thermal expansion factor then the temperature was increased and the ASR was replicated by the swelling pressure created.

Initially this will be done without the compressive load imposed on the first model to ensure that the results we are observing are happening due to the internal pressure and not the external load being

applied. This internal pressure should be just enough to exceed the tensile strength of the concrete and be seen on the surface as cracking.

The cracking observed in affected samples is at the surface where the internal pressures generated encounter the outer layers which lack the containing pressure. Several models will have to be made to compare the effects of the depth with which the ASR reaction is taking place. For example, if the cracking in the sample cylinders (figure 4.3) was 4mm how far toward the centre do the expansive nodes need to start? The rate of thermal expansion of the concrete will determine how quickly it expands but what temperature and what type of placement do the nodes need to be to reflect this pressure? Do they all need to be the same or alter as they get to the surface? In the case of the testing the presence of water and ionic compounds closer to the surface would imply the reaction is greater with proximity to the surface.

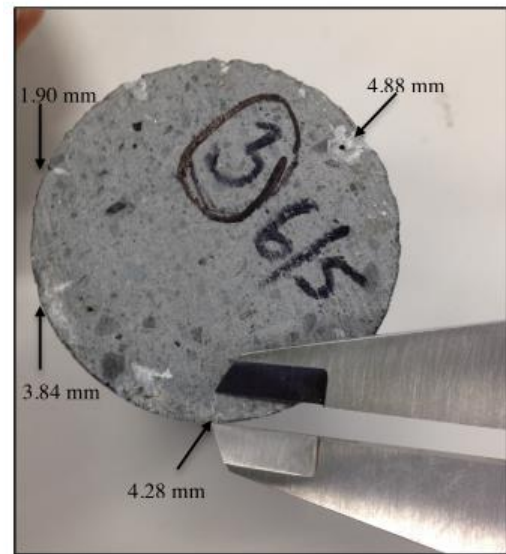


Figure 5.3 - Cracking in Cylinders (Knight 2014)

The expansive nature of the concrete due to the influx of temperature can be controlled via two different mechanisms. The first is a simple numerical value assigned as the rate of thermal expansion in the linear properties section, the other involves creating a table of thermal expansion vs temperature which will allow the rate of expansion to increase at different rates within the same model. The important thing to note at this point is that the temperature is not a factor in the failure of the concrete but merely a vehicle to create localised internal stresses intended to simulate the development of the ASR.

To counter any possible reduction in strength from the increase in temperature a Modulus Vs Temperature table was created that maintained a factor of one from the reference temperature to temperatures well above the scope of the experiments. This effectively mitigated against any nonlinear behaviour due to temperature changes.

Strand7 operates by assigning a temperature at which no stress is experienced and then the effects are based on the difference between the residual temperature and the applied temperatures. This is defined in the global loading conditions section. The temperature of the particular nodes of interest were then assigned values above this and the linear static analysis run to see the effects. In all of the tests the residual temperature was set at 25C°.

### 5.3.Application of Temperature Nodes in Models

The mesh was refined for this task to get a more accurate idea of how the material will react to the internal forces that will be applied. The cracking is a highly localised effect so the model has to be able to reflect this. In addition to this, a transition zone had to be established where the newly refined mesh meets the original larger mesh. If the mesh was not stepped from one size to the other stress points would concentrate where out of place nodes exist.

Initially I set out by applying random nodal temperatures in single nodes in models and running the program to see the results. This produced erratic results, depending on the temperature applied and where they were placed gave results varying from expansion to contraction as well as wildly distorted elements.

The next configuration I experimented with was horizontal regions where temperature loads were assigned across a line of nodes. I was looking for a combination of the expansive effect of the nodes combined with the failure on the surface.

I experimented with the spacing between lines of nodes, if they were immediately next to each other or if there was a different effect if they were spaced farther apart. It was also important to note the depth of the lines from the surface and whether the surface itself was failing from the influx in pressure.

The same methodology was applied to vertical configurations and finally a mix.

#### 5.3.1. Linear Analysis of Temp Load

The first thing I found out when running this linear analysis was that thermal loads are not treated the same way in post processing as external loads. Previously I had simply used progressively larger factors in the loading combinations in order to use the same model to simulate incrementally larger loads. When I attempted this for the thermal loads the program advised me that it cannot calculate the combined strain energy density and these combinations had to be set up as primary load cases.

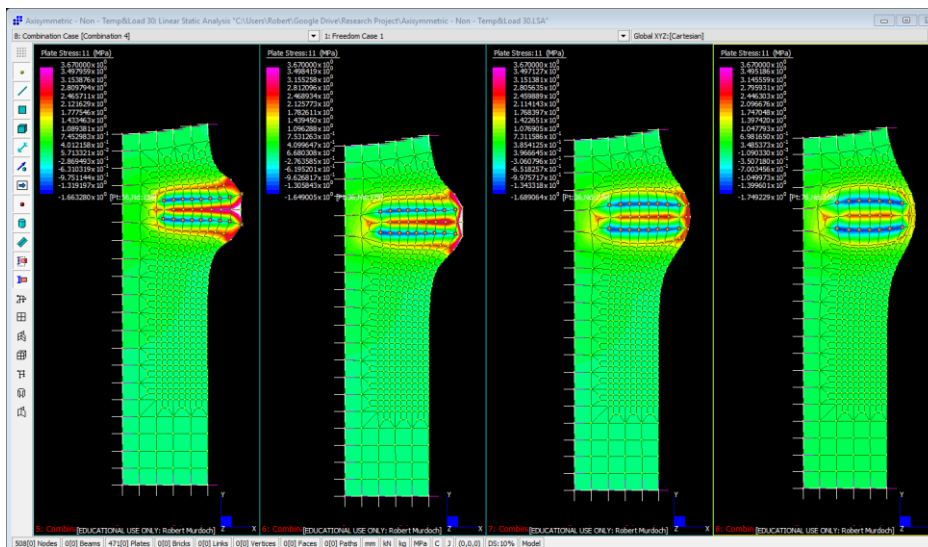


Figure 5.4 - Linear Analysis Horizontal Temp Nodes @ 40 Degrees

## Horizontal Case Loads

Figure 5.4 shows two horizontal rows of nodes with a space between them all at a temperature of 40°C. The model shows the stress in the 11 plane and the legend is set so that the model does not display any colour higher than the tensile yield point, this is an easy method which shows any area that has yielded as white.

It is important to note that once the nodes get to a certain distance away from the surface the internal pressure generated does not eventuate as surface cracking.

The temperature was increased to 46°C to see the direction the cracking would propagate. Fig 5.5 shows that the next area to fail is around the nodes themselves.

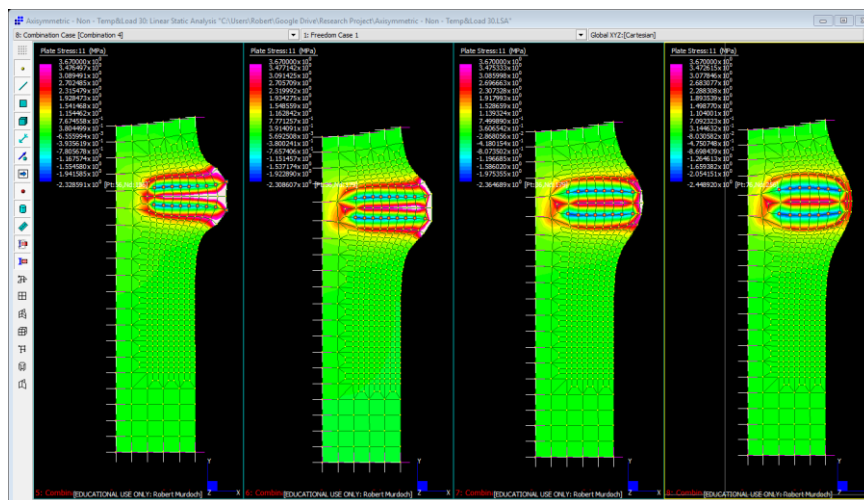


Figure 5.5 - Linear Analysis Horizontal Temp Nodes Yielding @ 46 Degrees

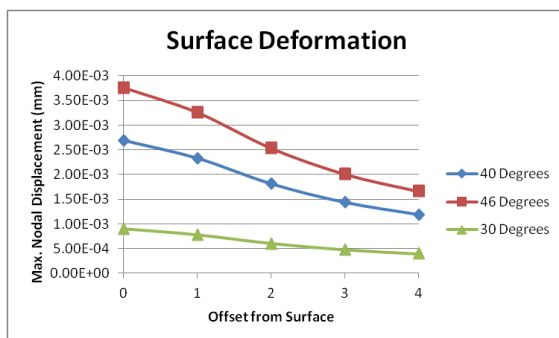


Figure 5.7 - Results Increasing Distance From Surface

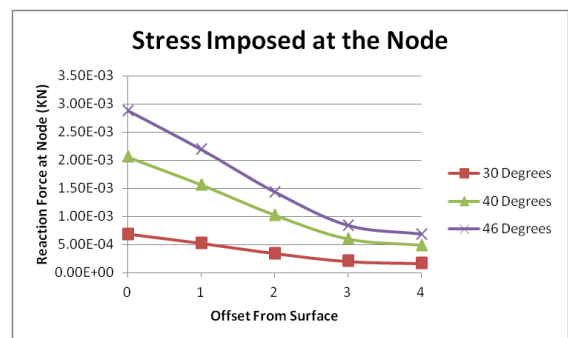


Figure 5.6 - Stress on Nodes

Figure 5.6 and 5.7 show the expansion of the cylinder and the stress imposed at the nodes with the increasing temperatures and the change in the alignment of the nodes. These are not perfectly linear relationships and the final result will not be able to be established until the external loading is modelled concurrently with the internal forces.

Another trial was to increase the number of nodes in the same pattern to see how it affected the stress and displacement in the cylinder. In the previous model failure was evident at the surface nodes at 40 degrees but with the new configuration it can be seen in Fig. 5.9 that there is no cracking at the same temperature when the number of nodes affected has increased. The 46 degree model showed that the failure remained the same and simply took an effect over a larger area.

The shape of the deformation extends to align itself with the affected nodes.

### Vertical Case Loads

The horizontal lines of nodes went deep into the heart of the sample however in the empirical testing the concrete cylinder was submersed in an acidic solution and the cracking was only around 4mm from the surface. As stated by Knight (2014) there are many examples of structures that are affected by ASR which have shown satisfactory load tests, in these cases it is the durability of the structures in question where map cracking has occurred on the surface exposing the reinforcement to water. Therefore it was decided to experiment with nodes in vertical lines closer to the surface to compare the results against each other.

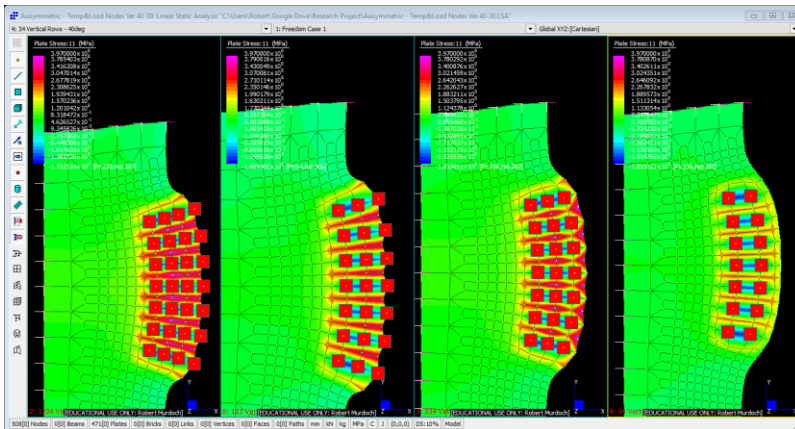


Figure 5.8 - Vertical Nodes at 40 Degrees

The same relationship applied as with the horizontally placed nodes where a distance away from the surface exists where they stop inducing a tensile failure at the surface.

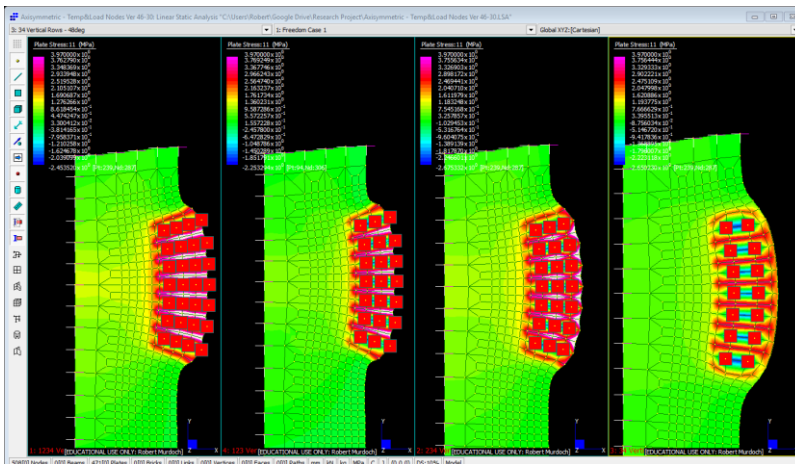


Figure 5.9 - Vertical Nodes at 46 Degrees

### 5.3.2. Nonlinear Analysis of Temp Load

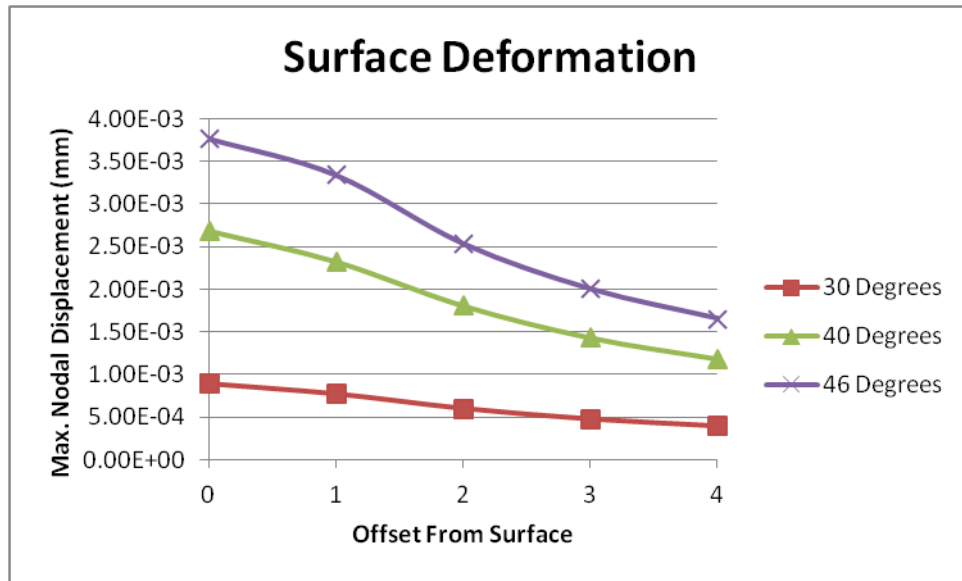


Figure 5.10 - Deformation of Nonlinear Model

The results of the surface deformation on the nonlinear model are shown in figure 5.10. This is a case where the cylinder showed signs of fatigue at 46 degrees. There is very little difference between this and the linear model and the effects of the temperature nodes are very apparent.

### 5.4. Combined Temperature and External Loading

At this point in the process I was faced with the problem of how to apply the loadings. The sample in the testing done in last year's dissertation was exposed to the expansive effect of ASR first and then subject to a compressive load. To model this would mean that I would apply the full temperature loading incrementally and then apply the external loading incrementally. However this model is to be used for concrete in the field which would be subjected to the compressive load well before the expansive effect of ASR became a problem. In this case it would make sense to apply the full compressive load incrementally and then apply the full temperature loading incrementally. The intermediate case would involve incrementally applying alternative loadings.

#### 5.4.1. Linear Analysis

This would not present itself as a major problem while using the linear solver as it ignores materials, geometry and boundary conditions. These will have an effect though on the way the shape deforms as elements will deform in a path determined by the previous iteration. I decided that the best way to investigate this was to run a few scenarios side by side and compare the effects of the loadings as they varied.

In order to do this I had to set up an axisymmetric model that had the load steps as primary loading cases as the linear solver would not combine the external loading and temperature loadings as a load case combination. For each node temperature three different external loadings (20, 25 and 30MPa) were given to observe the combined effects.

The linear results showed that for a given external load as the node temperature increased the displacement in the x direction also increased. This is expected as the temperature is creating an expansion in the concrete and the poisons factor would determine how the element would elongate horizontally when a force was placed on it vertically..

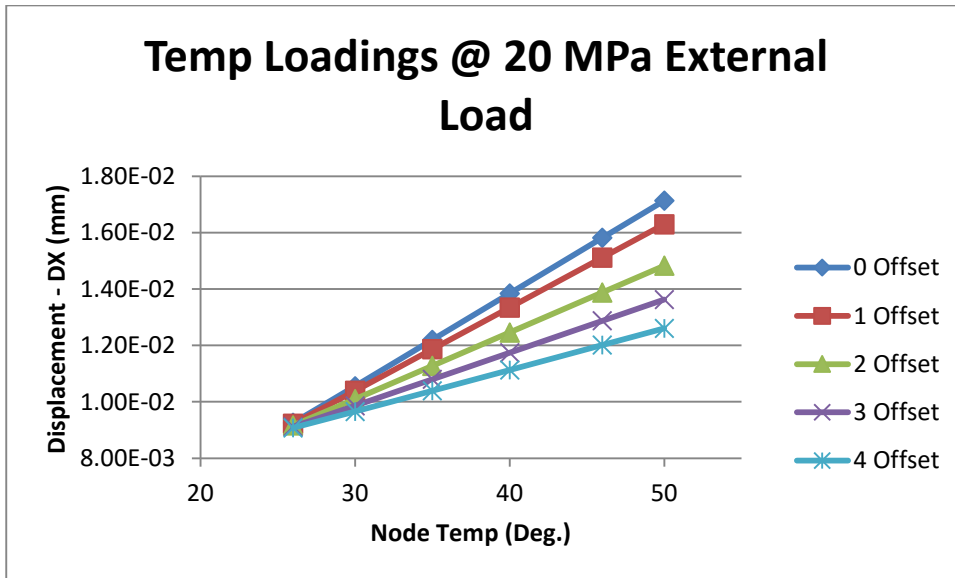


Figure 5.11 - Effect of Temperatures at Nodes

A better observation of the behaviour happened when the nonlinear solver was run due to the difference in the way the solver worked.

### 5.4.2. Nonlinear Analysis

The solver for the nonlinear analysis of the model allowed separate external loadings and nodal temperatures to be combined through the use of factors in the solver itself. This was distinctly unlike the linear analysis which only allowed one primary loading which meant that if the loading was factored up both the nodes and the external load would be factored up equally. The result was that a nodal temperature for a given arrangement could effectively be analysed for all loadings, conversely a particular loading could be analysed for a range of temperature nodes. The issue of loading orders is addressed in Section 7.1.

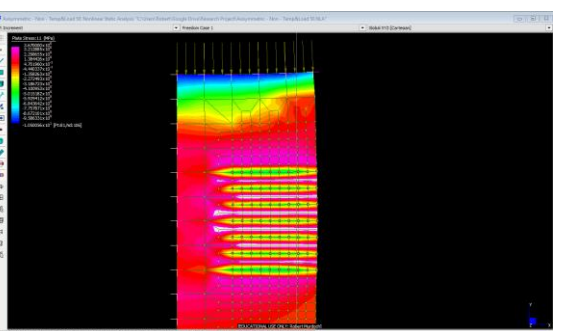
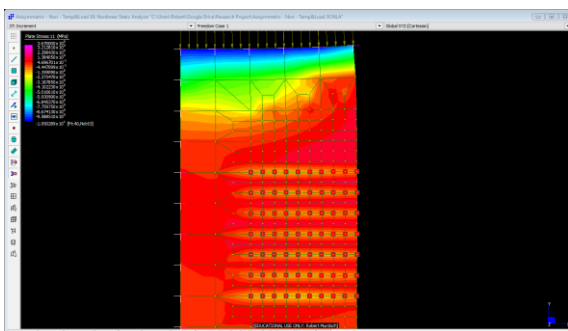
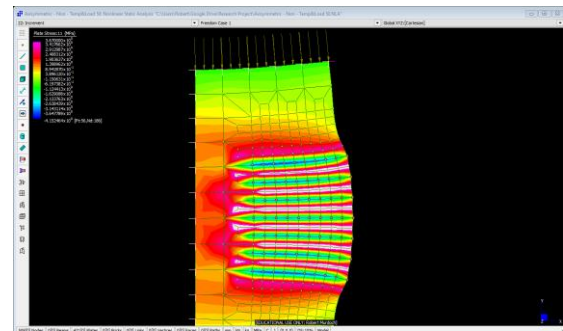
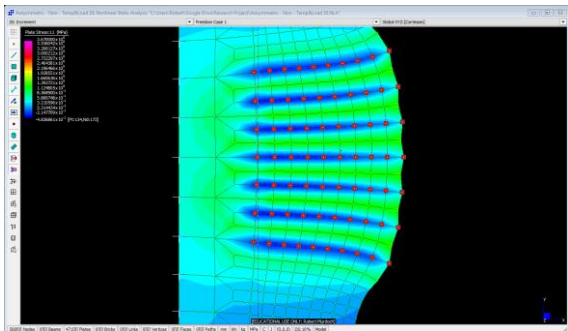
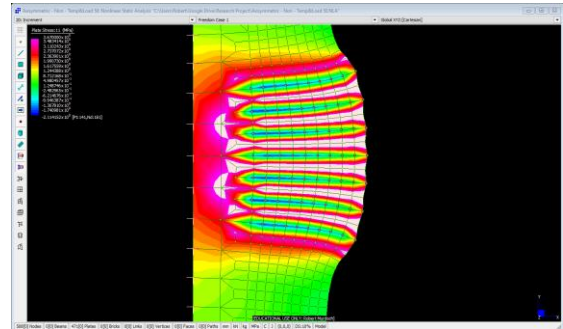
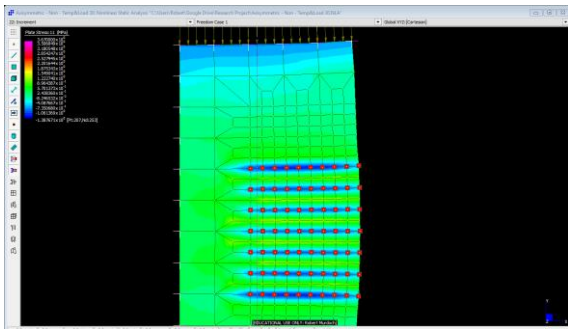


Figure 5.13 - 30 Deg. Nodes Step 20, 22 & 37

Figure 5.12 – 50 Deg. Nodes Step 20, 22 & 37

For both of the above loadings (Fig. 5.12 and 5.13) the nodes were first brought to full temperature (steps 1-20) and then the loading was gradually applied (steps 21-41). This process allowed me to observe the expansion due to the temperature and the tensile cracking which results and then the effect of the compression force allows for a stress strain curve to be produced. The counteraction of the expansive forces mentioned in the Parametric model (refer Section 2.4.4.2) is showed here where there is a reduction in the displacement in the Y direction as soon as the compressive force is applied.

As can be seen on the chart below (Fig. 5.14) the Stress-Strain curve is unaffected by the temperature nodes even though their effect on the concrete through tensile failure can clearly be noted in figures 5.12 and 5.13. The two curves fit perfectly on top of one another which means that the Strand7 program is unable to use temperature nodes to recreate the depletion in the modulus.

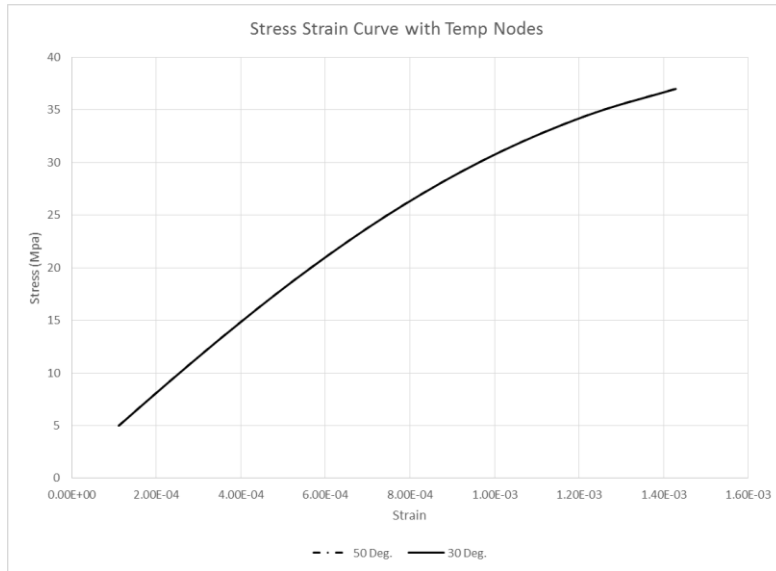


Figure 5.14 - Stress-Strain Graph with Temperature Nodes

The depletion of the concrete will be observed using the max stress failure criterion rather than the modulus. The difference between this model and the actual process lies in the fracture mechanics where, in a quasi-brittle material, the surrounding stress is relieved when the crack is formed however that process is not at play here and no softening can be observed.

Finally Fig. 515 shows the results of a 40MPa concrete cylinder that has been subjected to a load of 30MPa and is failing in tension due to the temperature nodes (48deg). This constitutes a 25% reduction in strength based on the Max Stress criterion.

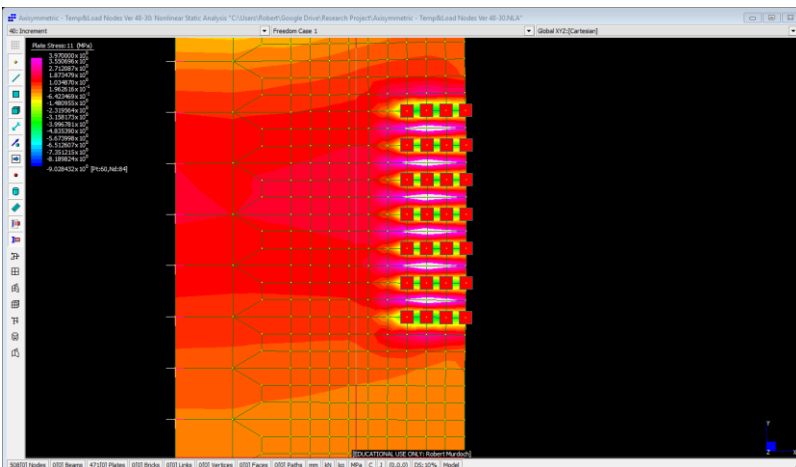


Figure 5.15 - 40MPa Concrete Subjected to 30MPa Load With Temp Nodes

## 6. Three Dimensional Model

The three dimensional model is required to provide a comparison and add legitimacy to the simplified two dimensional model.

The first step was to decide on the most appropriate type of three dimensional model to develop.

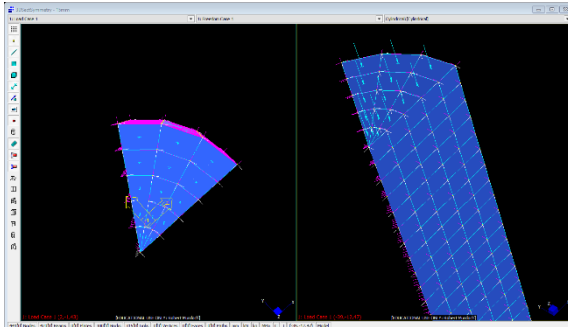


Figure 6.1- Single Radian Sector Symmetric Model

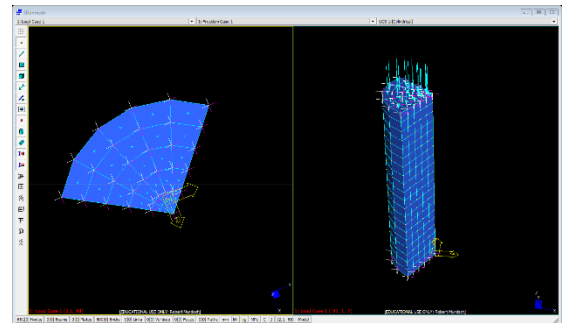


Figure 6.2 - 90 Symmetric Model

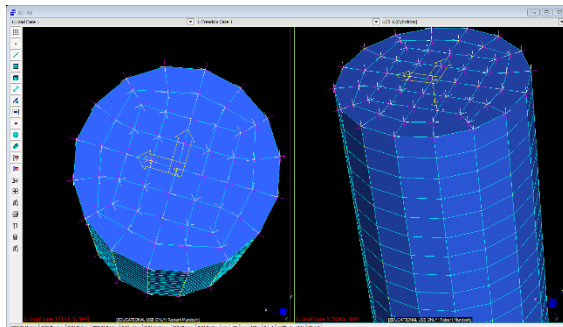


Figure 6.4 - Complete Cylinder (US Dept Roads Mesh)

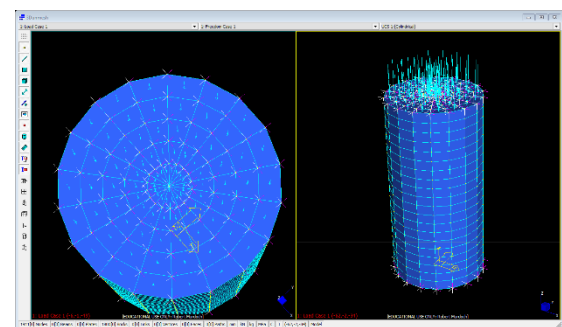


Figure 6.3 - Complete Cylinder (Sector Meshing)

If the 3 dimensional version were to be done as a symmetric model it would make sense to do it as a single radian sector symmetric model (figure 6.1) as opposed to the 90 degree section in figure 6.2. This choice would make the comparison to the original as simple as possible as the axisymmetric model calculates its results for a one radian section. However, due to the small and uncomplicated nature of the model it was decided it could simply be built as a complete cylinder. By doing it this way the results will have to be multiplied by  $2\pi$ .

The next issue is the type of meshing used on the model. When the US Department of Transport created a FE model of a concrete cylinder they used the meshing shown in figure 6.3. Different meshing are going to give different results, but again it seems that the choice is driven by the compatibility with the axisymmetric model. The Dept. Of Transport's method would be a good approach if it were not for the fact that it will not be able to provide a ring of nodes equidistant from the central axis to simulate the axisymmetric model. Therefore it would be a better option to create a mesh that was similar to the axisymmetric model (figure 6.4) and extruded radially to give a banded appearance.

It is important to continue the use of the same charts and tables as well as other basic material properties.

After significant time was spent trying to replicate the varying mesh sizes developed for the axisymmetric model it was decided that the mesh would be even throughout. What was a simple application in two dimensions was beyond my skill to replicate in three dimensions.

## 6.1. Linear Static Analysis

The linear static model of the compression showed very positive results.

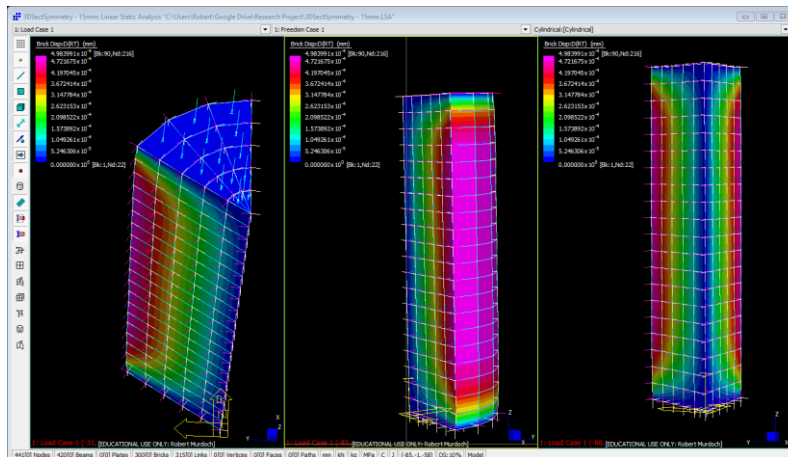


Figure 6.6 - Linear Results 3D Sector Symmetric Model

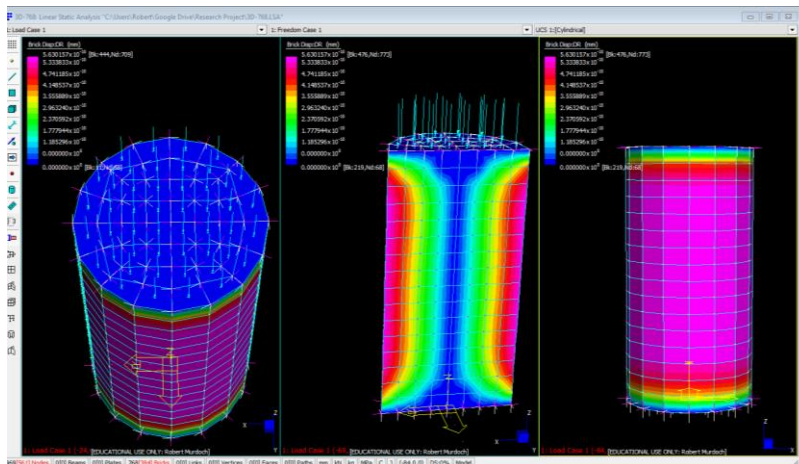


Figure 6.5 - Linear Results 3D Cylinder (US Dept. Transport Mesh)

The sector symmetry model was able to produce a diagram very similar to the axisymmetric model. It was decided though that it would be simple enough to develop the model as an intact cylinder and run the test for the axisymmetric model from that. Consideration when using this model was required as the results for the temperature nodes would be  $2\pi$  greater than the axisymmetric model.

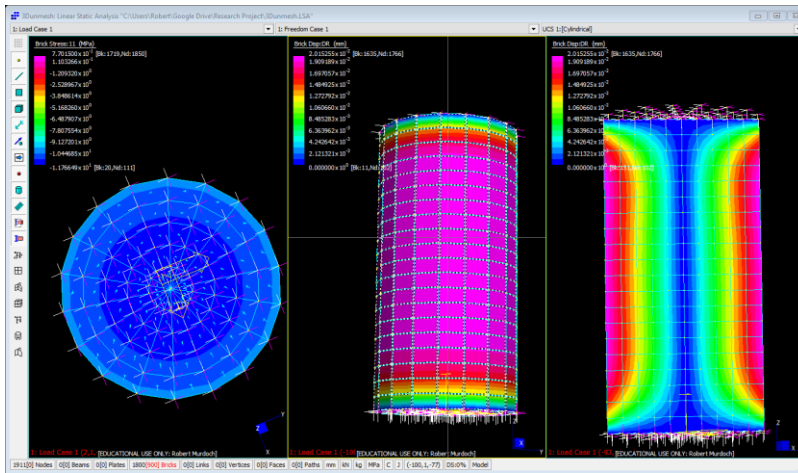


Figure 6.7 - Linear Results 3D Cylinder (Radial Mesh)

A convergence study, as was done in Part 4.3, was then done to determine how fine the mesh in the 3 dimensional model needed to return accurate results. The brick sizes considered were 25mm, 15mm, 12.5mm, 7.5mm, 5mm and 3mm. These values are true for the r and Z orientations of the bricks but the outer and inner sides are determined by the theta and are always going to be longer on the outer edge. To decide how many theta divisions were going to be used for each model a ring halfway between the centre and the outer edge was calculated and divided by the length of the mesh size. This way the mesh size was correct for the centre line and diverged evenly either side of it.

Table 6.1 - Brick Size and Displacement

Brick Size (r & Z)	Number of Bricks	DY
25	234	-0.00874448
15	1500	-0.00874723
12.5	2592	-0.00874773
7.5	12320	-0.00874858
5	42300	-0.00874894
3	180000	-0.00874916

The run time of the linear 3mm mesh model was over three hours without a great improvement over the 7.5mm mesh which took one hour.

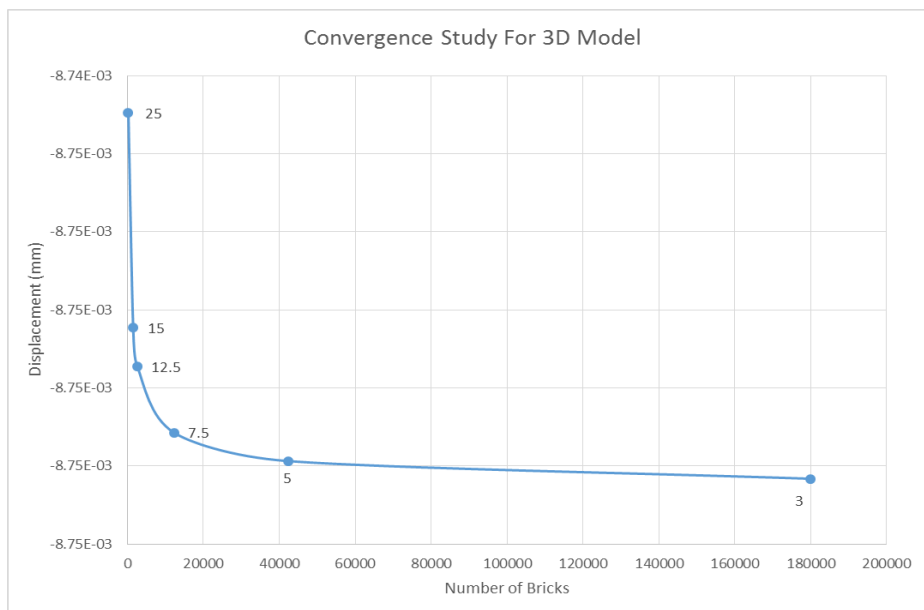


Figure 6.8 - Convergence Study for 3 Dimensional Model

## 6.2. Nonlinear Static Analysis

The idea of using the complete cylinder was abandoned once the nonlinear solver was started on the 7.5mm mesh model. After four hours it was still going and it was apparent that an alternative was needed. The 7.5mm one radian sector symmetry model had 2000 bricks as opposed to the 7.5mm full cylinder which had 12000. It had showed good results in the linear analysis and is the easiest to apply to the axisymmetric model.

Following is a comparison between the axisymmetric model, the full three dimensional model and the sector symmetric model. All have been allocated a simplified 7.5mm mesh throughout to make the comparison accurate. It shows that the three models are all behaving the same way under the same conditions.

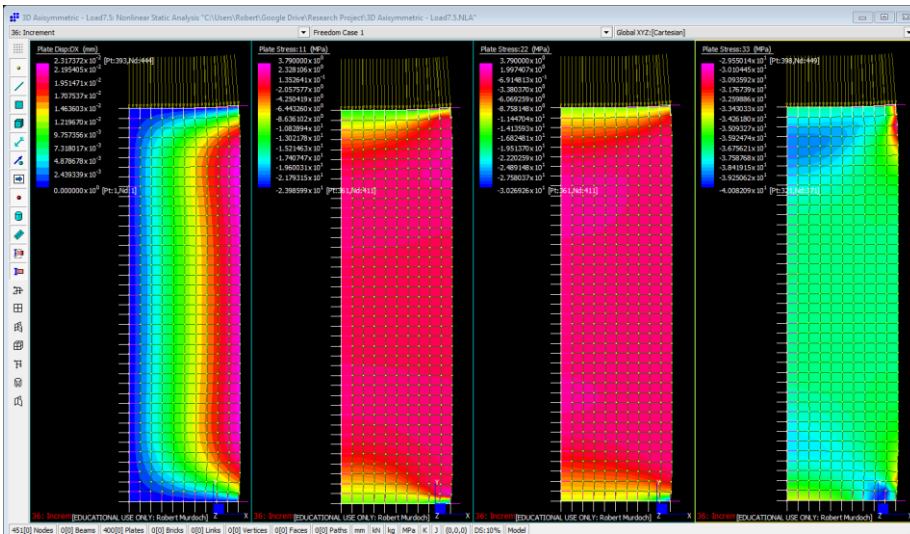


Figure 6.9 - 7.5mm Axisymmetric Model

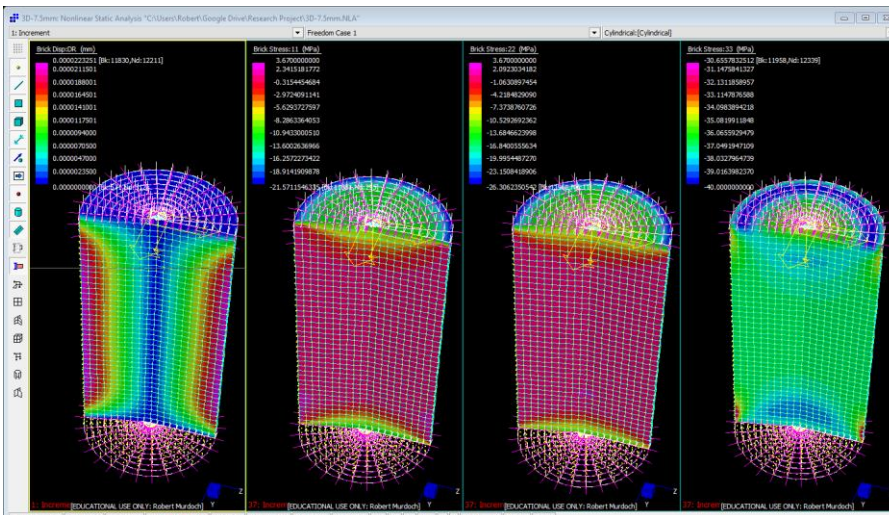


Figure 6.10 - 7.5mm Full 3D Cylinder Model

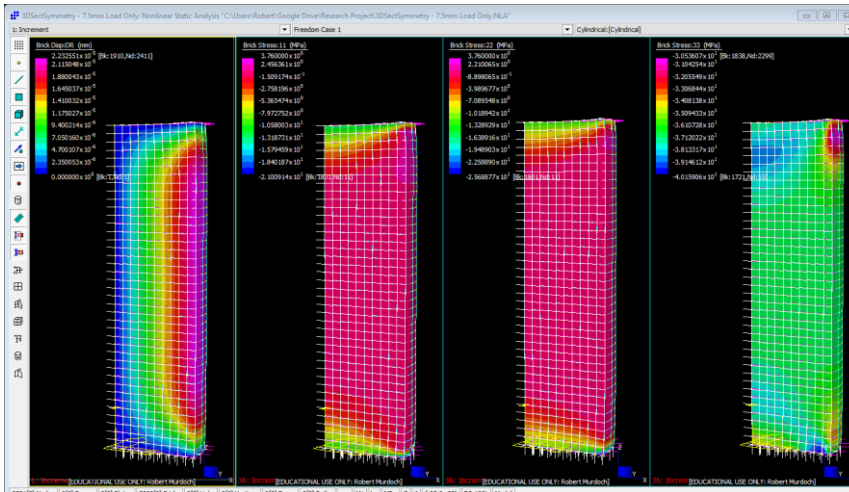


Figure 6.11 - 7.5mm One Radian Sector Symmetric Model

To test for similarities measurements of expansion in the X/R and Y/Z directions were made. The graphs of the results can be seen below as Fig. 6.12 and 6.13.

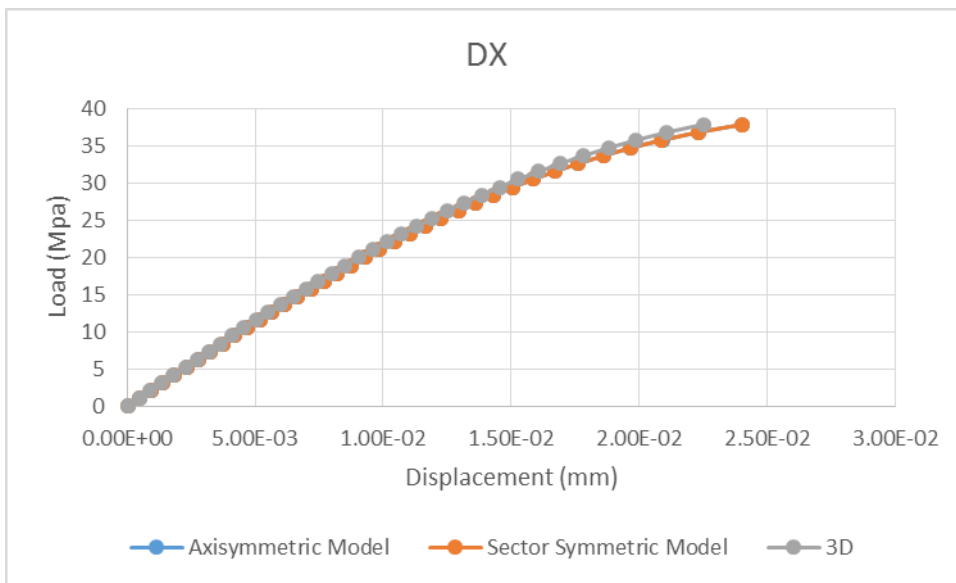
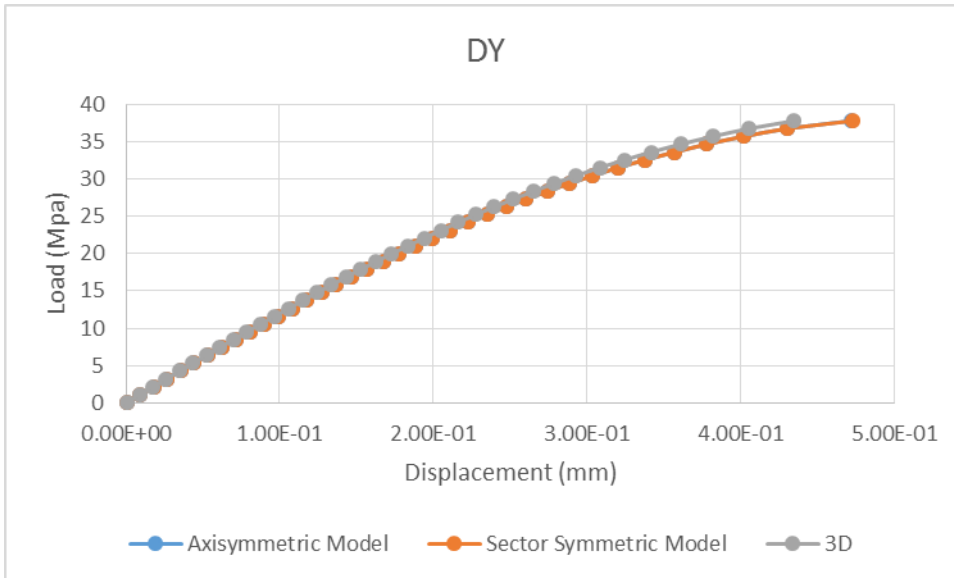


Figure 6.12 - Comparison of Three 7.5mm Models in DX

Fig. 6.12 shows that the axisymmetric and the sector symmetric behave very similarly through the course of the loading. The variation in the three dimensional model may have been due to an oversight when defining the freedom load increments in such a way that they did not match the other two models.



**Figure 6.13 - Comparison of Three Models in DY**

Again the axisymmetric and the sector symmetric showed very close results.

The results on all three models had to be reduced to 38 increments rather than 40 due to spurious results from unconverged final iterations.

### 6.3.Addition of Temp Nodes

The nodes which are on the axisymmetric model represent the temperature which is spread through the one radian section, therefore care must be taken when allotting temperatures to nodes in the sector symmetric model to ensure the same amount of energy is dispersed over the one radian section.

Increase in Temp	$46-25=21$
Divided by Number of Nodes	$21/5=4.2$
Temp of Each Node	$25+4.2=29.2$
Factor Required in Solver	$29.2/26=1.123$

Figure 6.14 and 6.15 show the sector symmetry model response compared to the axisymmetric response to the same loading. They are shown with the same progression across the diagram but the axisymmetric development happened slightly quicker, a slight error in the calculation of the temperature nodes in the sector symmetric diagram can be attributed to this. Overall the effect is very similar and the failure in fatigue is quite apparent.

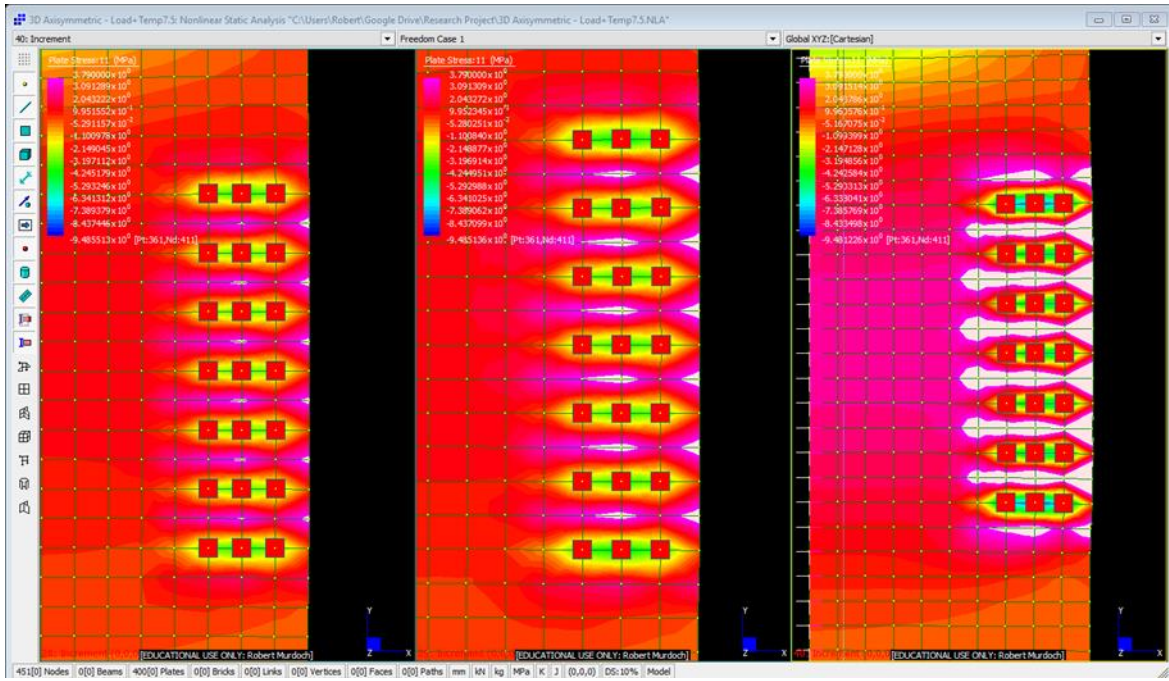


Figure 6.14 - Stress Development in Axisymmetric Model

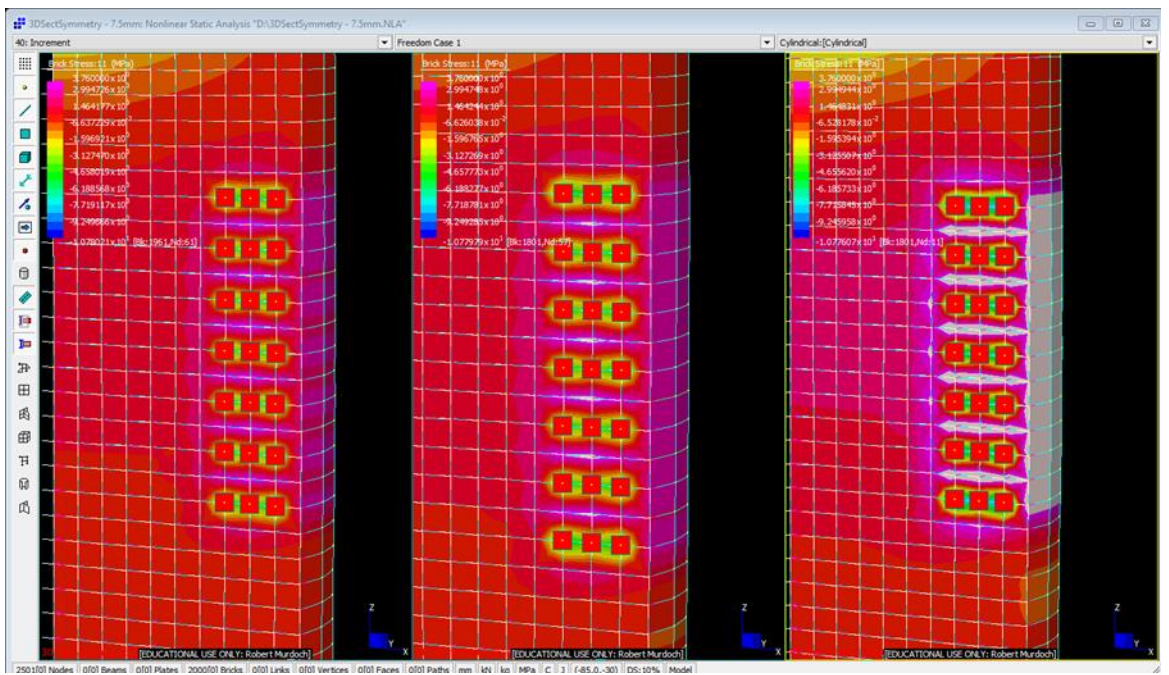


Figure 6.15 - Stress Development in Sector Symmetric Model

The graph (figure 6.16) shows the stress at the nodes between the top two rows of temperature nodes. From left to right the nodes are very similar until the fourth node which was located on the outer surface. The reason for the discrepancy is most likely due to the slight variation in the degrees of freedom between the two models. The axisymmetric model is fixed against rotation in the z axis whereas the three dimensional model is not fixed for rotation in any direction. This constraint, especially at the edge where only one side is confined, could add to the stress in the two dimensional model. Other nodal constraints for the sector symmetric model could have contributed to this as well.

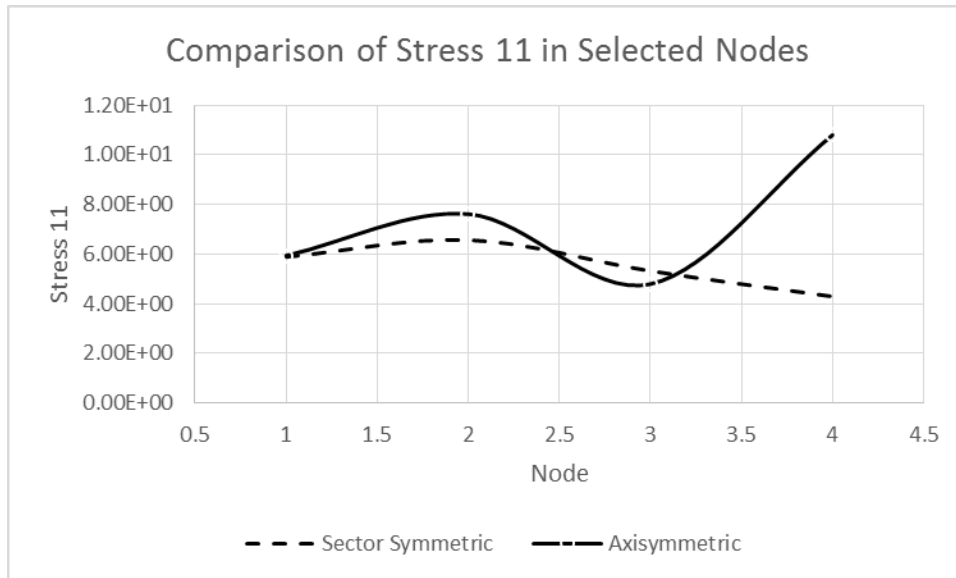


Figure 6.16 - Comparison of Stress Development Between Two Models

## 7. Discussion

### 7.1. Order of Loadings

During the modelling it was noticed that the order the loadings were imposed affected the integrity of the structure itself. If a significant amount of temperature was applied to the nodes before any loading was imposed there was tensile failure around the nodes due to the expansion not being constrained. However if the loading was imposed first and the temperature was applied second there were times when no tensile failure occurred at all.

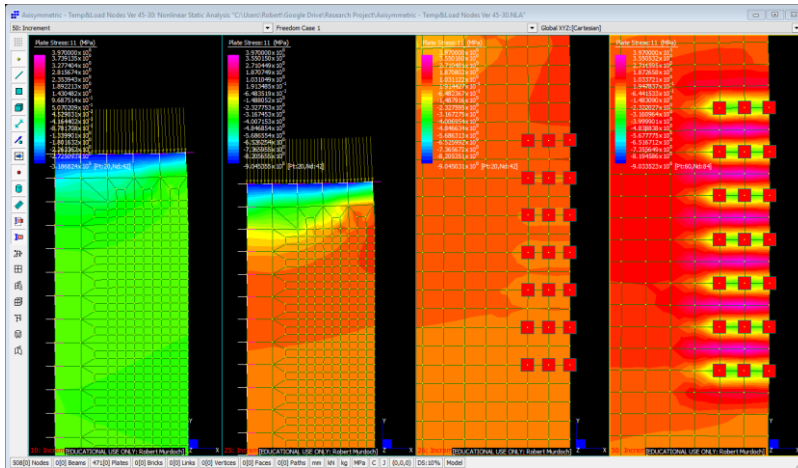


Figure 7.1 - External Load Applied Followed By Node Temperatures

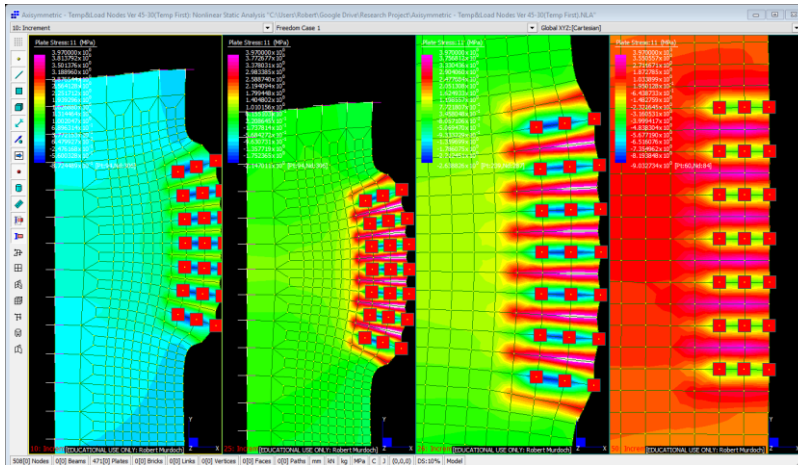


Figure 7.2 - Node Temperatures Applied Followed By External Load

Cracking isn't a parameter that this program involves but once the cracking has occurred in a quasi-brittle material the properties change accordingly. As shown in the progression the crack would close once the external load is applied but the inherent strength that was there is no longer there because the bond has been broken.



**Figure 7.3 - Comparison of Load Deflection Curve For Both Combinations**

In terms of Knight’s study her samples were created and exposed to chemicals to induce the ASR but all of this was done while the specimen was unconfined. This would have meant that the amount of ASR required to induce cracking would have been significantly less than if they were under load at the time. This is reminiscent of Richardson (2002) who observed that several structures had developed significant ASR but not experienced any softening related activity.

This isn’t so much a problem for studies such as Knight’s where the cracking is needed in order to perform the test. It does however pose a problem when trying to create an accurate model of the cylinder when it is subject to confinement or when a structure where the concrete will be under load for a considerable period of time before the reaction even starts.

This particular characteristic has made the parametric study for this dissertation particularly difficult. For the loading case where the temperature is applied first, for a given concrete strength, the failure in tension occurs quicker as the temperatures present at the nodes increase. However if there is an external loading applied first it is highly dependent on the size of the external loading as to how high the nodal temperature needs to be to induce tensile failure; it is simply a case of action-reaction.

## 7.2. Conclusions

The purpose of this dissertation was to develop a simplified model of the alkali-silica reaction for use with FEA software. The constraints of the software are that it does not have any facility to create and propagate cracks which itself is a significant part of the behaviour of concrete. To circumvent this shortcoming temperature nodes were employed to create expansion and induce premature tensile failure in the concrete thus replicating the reduced strength.

Due to the way that a simplified model works it will only replicate certain characteristics of the system it is modelling. In this case the reduction in the overall strength of the concrete is not seen as a change of slope in the stress-strain curve but rather a hastening of the concrete to fail in tension. This has been proven in the body of this dissertation where stress-strain graphs do not alter with the introduction of temperature nodes but the tensile failure happens at a lower external loading.

The temperature characteristics of the axisymmetric model were tested against a sector symmetric model due to the runtime the full cylinder would take. The results were mostly comparable with the outer face showing dissimilarity. This was put down to a problem with the freedom conditions of the models themselves.

Problems were encountered when trying to plan how this would be mainly due to the way the temperature nodes work to induce tensile stress. The simple loading procedure where the temperature load is applied first and the external loading second is fine for the primary strength test done by Knight but the confinement stage will present issues.

This thesis came short of its intended goals, not due to poor planning but rather the requirement of learning a new piece of software. Several months were lost trying to find the reason the nonlinear models would not converge but this ultimately led to a much greater understanding of how the process works.

## 7.3. Recommendations

This thesis was able to meet the initial objectives but fell short of the ultimate goal to model the confined concrete and replicate the results found by Knight in 2014. Therefore the recommendations for continuing research would be:

1. The next stage would be to apply the confinement to the axisymmetric model and test to see if the confining stress reinstates the concrete strength in a similar fashion to Knight's results.
2. The next step would be to repeat this test with a three dimensional concrete cylinder. The results should be the same as the axisymmetric model and similar to Knight's.
3. Further investigation into the parametric study is warranted. This is where the practical application will eventuate from. The eventual aim would be to create a series of comprehensive tables or develop the equations required to consistently recreate these results.
4. Possibly examine this model with the function for creep as well considering that this is a reaction that occurs over a significant period of time. Other models (see parametric model Sect. 2.4.4.1) have used the creep function to alter the stresses imposed on the nodes over time.

## References:

Ali, AM, Farid, BJ & Al-janabi 1990, *Stress-Strain Relationship for Concrete in Compression Madel of Local Materials*, Eng. Sci., Vol. 2, pp. 183-194, College of Engineering, University of Basrah, Iraq. Viewed 10 July 2015, < [https://www.kau.edu.sa/Files/135/Researches/54136\\_24603.pdf](https://www.kau.edu.sa/Files/135/Researches/54136_24603.pdf)>

Carpinteri A & Ingrassia AR 2012, *Fracture Mechanics of Concrete: Material Characterization and Testing*, Springer Science & Business Media, viewed 4 June 2015, <[https://books.google.com.au/books?id=39LyCAAQBAJ&pg=PA200&lpg=PA200&dq=concrete+micro+cracking+primary+secondary&source=bl&ots=urpbcS7OE\\_&sig=XReyePmEtSy7dA8oVX7pTmeeNVk&hl=en&sa=X&ved=0CC4Q6AEwA2oVChMI3eG30NTDxwIVZSimCh3mqgVA#v=onepage&q=concrete%20micro%20cracking%20primary%20secondary&f=false](https://books.google.com.au/books?id=39LyCAAQBAJ&pg=PA200&lpg=PA200&dq=concrete+micro+cracking+primary+secondary&source=bl&ots=urpbcS7OE_&sig=XReyePmEtSy7dA8oVX7pTmeeNVk&hl=en&sa=X&ved=0CC4Q6AEwA2oVChMI3eG30NTDxwIVZSimCh3mqgVA#v=onepage&q=concrete%20micro%20cracking%20primary%20secondary&f=false)>

Chung, D 2010, *Composite Materials: Science and Applications*, Springer, Manchester

Del Viso JR, Carmona JR, Ruiz G 2007, Size and Shape Effects on the Compressive Strength of High Strength Concrete, 6th International Conference on Fracture Mechanics of Concrete and Concrete Structures, p. 1297-1304, viewed 5 July 2015 <<http://framcos.org/FraMCoS-6/193.pdf>>

Farny, JA & Kerkhoff, B 2007, *Diagnosis and Control of Alkali-Aggregate Reactions in Concrete*, Web Document, Portland Cement Association, Illinois, viewed 8 January 2015, < [http://www.cement.org/docs/default-source/fc\\_concrete\\_technology/is413-02---diagnosis-and-control-of-alkali-aggregate-reactions-in-concrete.pdf](http://www.cement.org/docs/default-source/fc_concrete_technology/is413-02---diagnosis-and-control-of-alkali-aggregate-reactions-in-concrete.pdf)>.

Felippa CA 2015, Chapter 7 - Finite Element Modeling: Mesh, Loads, BCs., Course material, University of Colorado, viewed on 7 May 2015, <<http://www.colorado.edu/engineering/cas/courses.d/IFEM.d/IFEM.Ch07.d/IFEM.Ch07.pdf>>

Ferraris, CF 1995, 'Alkali-Silica Reaction and High Performance Concrete', Report NISTIR 5742, National Institute of Standards and Technology, Gaithersburg, MD, 1995, pp. 1 – 20, viewed 12 December 2014, <<http://fire.nist.gov/bfrlpubs/build95/PDF/b95004.pdf>>.

Fernandes, I, Broekmans, M 2013, 'Alkali-Silica Reactions: An Overview. Part 1', *Metallography Microstructure Annual*, vol. 2, p. 257-267, viewed 10 December 2014, <[link.springer.com.ezproxy.usq.edu.au/article/10.1007%2Fs13632-013-0085-5](http://link.springer.com.ezproxy.usq.edu.au/article/10.1007%2Fs13632-013-0085-5)>.

Fournier, B, Ideker, JH, Folliard, KJ, Thomas MDA, Nkinamubanzi, PC, & Chevrier, R 2009, 'Effect of Environmental Conditions on Expansion in Concrete Due to Alkali-Silica Reaction (ASR)', *Materials Characterization*, vol. 60, pp. 669-679, viewed on 10 January 2015, <<http://www.sciencedirect.com.ezproxy.usq.edu.au/science/article/pii/S1044580308003513>>.

Giaccio, F, Zerbino, R, Ponce, JM & Batic, OR 2008, 'Mechanical Behaviour of Concretes Damaged by Alkali-Silica Reaction', *Cement and Concrete Research*, Vol. 28, pp.993-1004, viewed 15 January 2015, <<http://www.sciencedirect.com.ezproxy.usq.edu.au/science/article/pii/S0008884608000537>>.

Gurit 2015, *Gurit: Guide to Composites*, Gurit, as viewed 28 January 2015, <<http://www.gurit.com/guide-to-composites.aspx>>

Helmuth, R, Stark, D, Diamond, S & Moranville-Regourd, M 1993, *Alkali-Silica Reactivity: An Overview of Research*, Strategic Highway Research Program Contract, viewed 15 January 2015, <<http://onlinepubs.trb.org/Onlinepubs/shrp/SHRP-C-342.pdf>>.

Herrador, MF, Mertinez-Abella, F, & Fernandez-Gago, R 2009, *Mechanical behaviour model for ASR-affected dam concrete under service load: formulation and verification*, *Materials and Structures*, Vol 42, P201 – 212, viewed on 3 August, <<http://download.springer.com.ezproxy.usq.edu.au/static/pdf/710/art%253A10.1617%252Fs11527-008-9378-6.pdf>>

Hobbs, D 1988, *Alkali-Silica Reaction in Concrete*, Thomas Telford, London.

Ichikawa, T & Miura, M 2007, 'Modified Model of Alkali-Silica Reaction', *Cement and Concrete Research*, Vol. 37, pp.1291–1297, viewed 20 January 2015, <<http://www.sciencedirect.com.ezproxy.usq.edu.au/science/article/pii/S0008884607001329>>.

Lee, S 1989, *Dictionary of Composite Materials Technology*, Technomic Publishing Company, viewed 22 January 2015 < <http://composite.about.com/od/referencematerials/l/blpreface.htm> >

Logan DL 2007, *A first course in the finite element method*, Thomson, Toronto

Lowes L.N 2000, *Finite Element Modeling of Reinforced Concrete Beam-Column Bredige Connections*, Dissertation Doctorate of Philisophy in Civil Engineering, University of California, Berkeley, as seen 2 August 2015, <<http://faculty.washington.edu/lowes/dissertation/dissertation/>>

Mahmoud, ZI 1997, *Bond Characteristics of Fibre Reinforced Polymers Prestressing Reinforcement*, Thesis submitted to Faculty of Engineering , Alexandria University, Egypt, viewed 1 July 2015, < [http://www.ce.ncsu.edu/srizkal/linked\\_files/Bond\\_Characteristics\\_of\\_Fiber\\_Reinforced\\_Polymers.pdf](http://www.ce.ncsu.edu/srizkal/linked_files/Bond_Characteristics_of_Fiber_Reinforced_Polymers.pdf) >

Mor Dr & Associates 2015, *Concrete Forensics and Litigation Support*, Webpage Q&A, Marina Del Ray, California, viewed 2 June 2015, < <http://www.drmor.com/qa/pgs/QA404.html>>

Murray, YD, Abu-Odeh A & Bligh R 2007, *Evaluation of the LS-Dyna Concrete Material Model 159*, US Dept. Transport, Mclean VA. Viewed 28 August 2015, < US Dept Transport <https://www.fhwa.dot.gov/publications/research/infrastructure/structures/05063/index.cfm>>

Pan, JW, Feng, YT, Wang, JT, Sun, QC, Zhang, CH & Owen, DRJ 2012, *Modeling of alkali-silica reaction in concrete: a review* , State Key Laboratory of Hydrosience and Engineering, Tsinghua University, Beijing viewed on 3 May 2015 < <http://link.springer.com.ezproxy.usq.edu.au/article/10.1007%2Fs11709-012-0141-2> >

Richardson, MG 2002, *Fundamentals of Durable Reinforced Concrete*, Spoon Press, London, pp.133-159, viewed on 13 January 2015, <<http://www.scribd.com/doc/72676667/Fundamentals-of-Durable-Reinforced-Concrete-2002-Mark-G-Richardson#scribd>>.

Schlangen, E & Copuroglu, O 2010, *Modeling of Expansion and Cracking Due to ASR with a 3D Lattice Model*, *Fracture Mechanics of Concrete and Concrete Structures - Assessment, Durability, Monitoring*

and Retrofitting of Concrete Structures, Korea Concrete Institute, Seoul, viewed on 5 May 2015, <<http://framcos.org/FraMCoS-7/08-06.pdf>>

Scott Bader 2005, *Crystic Composites Handbook*, Scott Bader, as viewed 11 January 2015, <[http://www.scottbader.com/uploads/files/3381\\_crystic-handbook-dec-05.pdf](http://www.scottbader.com/uploads/files/3381_crystic-handbook-dec-05.pdf)>.

Service, T 2002, Finite Element Modelling in Failure Analysis, *Failure Analysis and Prevention*, Vol 11, *ASM Handbook*, ASM International, p 380–389, viewed on 18 March 2015, <[http://products.asminternational.org.ezproxy.usq.edu.au/hbk/do/section/content/V11\\_2002/D04/A07/s0090260.htm?highlight=false](http://products.asminternational.org.ezproxy.usq.edu.au/hbk/do/section/content/V11_2002/D04/A07/s0090260.htm?highlight=false)>

Shah, SP, Swartz, SE, Ouyang, C 1995, *Fracture Mechanics of Concrete: Applications of Fracture Mechanics to Concrete, Rock and Other Quasi-Brittle Materials*, John Wiley & Sons, Brisbane.

Shi, X, Xie, N, Fortune, K, Gong, J 2012, 'Durability of Steel Reinforced Concrete in Chloride Environments: An Overview', *Construction and Building Materials*, v 30, p 125-138, viewed 15 January 2015, <<http://www.sciencedirect.com.ezproxy.usq.edu.au/science/article/pii/S095006181100715X>>.

Shin J h. 2009, Modeling alkali-silica reaction using image analysis and finite element analysis. Dissertation Tip, University of Illinois at Urbana-Champaign, viewed 4 May 2015 <<http://www.sciencedirect.com.ezproxy.usq.edu.au/science/article/pii/S000888461200051>>

Standards Australia 1996, *Alkali Aggregate Reaction: Guidelines on Minimising the Risk of Damage to Concrete Structures in Australia*, SAA HB79-1996, Standards Australia and Cement and Concrete Association of Australia, Sydney, viewed 15 January 2015, <<http://www.saiglobal.com/online/autologin.asp>>.

Standards Australia 2002, *Guide to concrete construction 2nd ed.*, Standards Australia and Cement and Concrete Association of Australia, North Sydney.

Strand7 2005, *Strand7 Theoretical Manual*, Strand7, Sydney

Swamy, RN 1992, *The Alkali-Silica Reaction in Concrete*, Van Nostrand Reinhold, Glasgow, viewed 9 January 2015, <[http://reader.eblib.com.au.ezproxy.usq.edu.au/\(S\(xz4dofd10bhewg5ccfznhph5\)\)/Reader.aspx](http://reader.eblib.com.au.ezproxy.usq.edu.au/(S(xz4dofd10bhewg5ccfznhph5))/Reader.aspx)>.

Transportation Research Board 2003, Bonded Repair and Retrofit of Concrete Structures Using FRP Composites, National Cooperative Highway Research Program Report 514, viewed 17 February 2015, <<http://www.trb.org/main/blurbs/153775.aspx>>.

US Dept. of Defence 1997, *Composite Materials Handbook, Volume 3. Polymer Matrix Composites Materials Usage, Design and Analysis*, Handbook, as viewed 11 January 2015

<<http://www.lib.ucdavis.edu/dept/pse/resources/fulltext/HDBK17-3F.pdf>>

Wang, X 2010, *Analysis of Climate Change Impacts on the Deterioration of concrete Infrastructure Part 1: Mechanisms, Practices, Modelling and Simulations – A Review*, Online Document, CSIRO, viewed 15 January 2015, <<http://www.csiro.au/Portals/Publications/Research--Reports/concrete-durability-report-part-1.aspx>>.

## Appendix A: Project Specification

UNIVERSITY OF SOUTHERN QUEENSLAND

FACULTY OF HEALTH, ENGINEERING & SCIENCES  
SCHOOL OF CIVIL ENGINEERING & SURVEYING

### ENG4111/2 Research Project PROJECT SPECIFICATION

FOR: Robert Murdoch  
TOPIC: Structural Modelling of an ASR Affected Column Using Finite Element Method.  
SUPERVISOR: A/Prof. Yan Zhuge (School of Civil Eng. USQ)  
PROJECT AIM: To create a finite element model of an ASR affected concrete column using Strand7 software. The empirical results reported in previous USQ student's thesis on ASR affected concrete columns and FRP retrofitting, which was done in conjunction with the TMR, will be used to verify the Finite Element model developed by this project.  
PROGRAMME: Issue A: 17th March 2015

1. Using Strand7 to create a two dimensional model to represent the outer layer of the concrete column. Once this is created we will use the temperature load functions of the software to simulate the ASR pressure in the unconfined concrete.
2. Reuse this model from part 1 and generate discrete cracks by creating a line of nodes which allow for small spaces between the cracking.
3. Create a three dimensional model, assume that the cracking is symmetrical, use one quarter of the model and apply the moulding.
4. Retrofit the three dimensional model with a layer of adhesive and a layer of carbon fibre composite material around the moulding.

AGREED: (Student)  (Date) 20/3/2015  
(Supervisor)  (Date) 19/3/2015

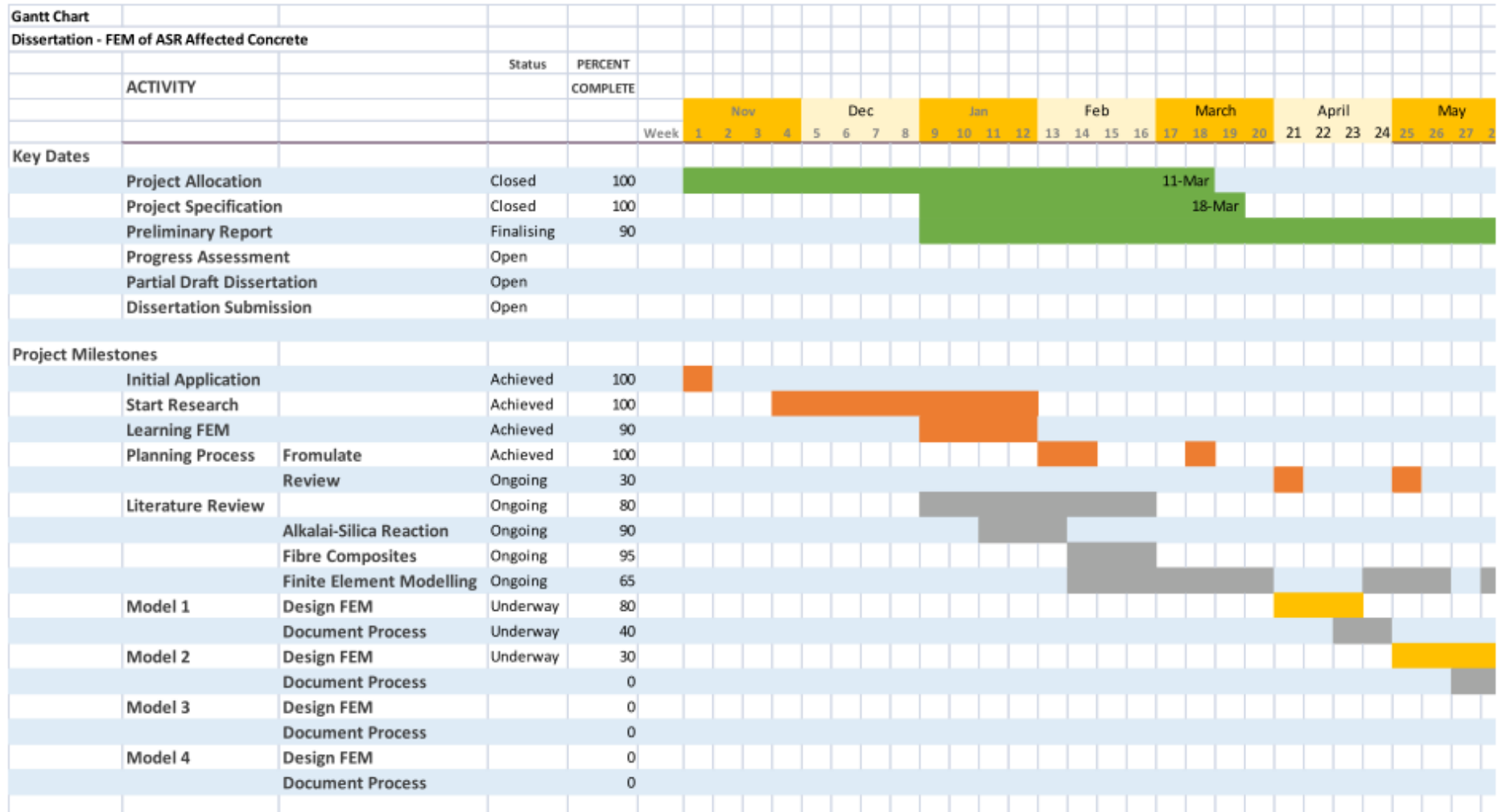
## Appendix B: Risk Assessment

Risk Assessment for Thesis/General Officework							
Carried out by Robert Murdoch - 28/02/2015							
What are the hazards?	Who might be harmed and how?	Residual Risk Rating	What are you already doing?	Do you need to do anything else to control this risk?	Action by who?	Action by when?	Done
Psychosocial Problems with Officework	Student May Feeling Overwhelmed and Succumb to Stress	Medium	Maintain good communication with supervisor	Organise for one on one meetings as well as email	Student	From now on	1/12/2014
			Well defined task, clearly defined aims and objectives		Student / Supervisor		28/02/2015
			Establish timeline for completion of milestones	Review dates and identify when dates not met	Student		15/03/2015
			Identify students who are doing similar topics		Student	xx/xx/xx	15/02/2015
			Seek Specialist Training		Student		20/05/2015
Office Environment	Student health may deteriorate from poor surroundings	Low	Appropriate Lighting for Long Term Exposure	Try to work near window when possible	Student		1/02/2015
			Noise Controlled to Limit Discomfort		Student	Ongoing	1/02/2015
			Thermal Comfort		Student		1/02/2015
			Air Quality		Student		1/02/2015
Workspace Layout	Student Health at Risk from Poor Equipment	Low	Desk Suitable for Student To Work on Both Computer and Written Tasks		Student		1/02/2015
			Chair is Adjustable and Appropriate for Task	Make sure it is adjusted	Student		1/02/2015
			Adequate Lighting		Student		1/02/2015
			Adequate Storage Facilities	Make sure workspace clean and free from trip hazards	Student		1/02/2015

Working With Computers	Student can be physically afflicted	Low	Screen Type Reduces Radiation	Use of LED and LCD screens only	Student		1/02/2015
			Position of Screen For Posture	Raised to appropriate level	Student		1/02/2015
			Eye Strain Minimised	Good Lighting, use glasses	Student		1/02/2015
			Comfortable Use of mouse		Student		1/02/2015
			Schedule Regular Breaks		Student	Ongoing	1/02/2015

		Potential Consequences					
		L6	L5	L4	L3	L2	
		Minor injuries or discomfort. No medical treatment or measureable physical effects.	Injuries or illness requiring medical treatment. Temporary impairment.	Injuries or illness requiring hospital admission.	Injury or illness resulting in permanent impairment.	Fatality	
		Not Significant	Minor	Moderate	Major	Severe	
Likelihood	Expected to occur regularly under normal circumstances	Almost Certain	Medium	High	Very High	Very High	Very High
	Expected to occur at some time	Likely	Medium	High	High	Very High	Very High
	May occur at some time	Possible	Low	Medium	High	High	Very High
	Not likely to occur in normal circumstances	Unlikely	Low	Low	Medium	Medium	High
	Could happen, but probably never will	Rare	Low	Low	Low	Low	Medium

## Appendix C: Gantt Chart





## Appendix D: Stress Strain Table

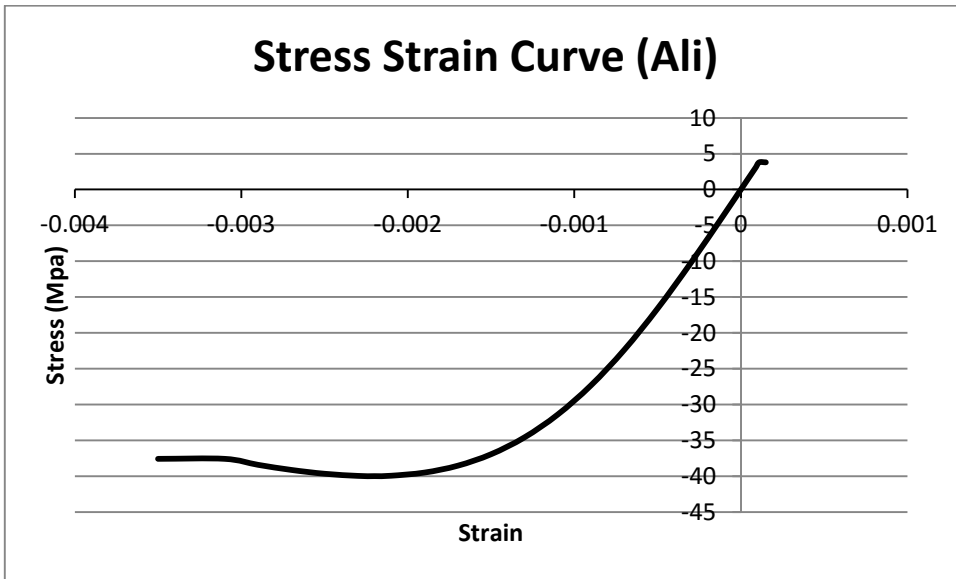


Fig. 4.11

Strain	Compressional Stress	Strain	Tensile Stress
-0.0035	-37.58459202	0	0
-0.0031	-37.58459202	0.00001	0.345451
-0.0029	-38.41847493	0.00003	1.036251
-0.0027	-39.13060125	0.00005	1.726723
-0.0025	-39.66835043	0.00007	2.416622
-0.0023	-39.96586817	0.00009	3.105693
-0.0022	-40	0.00011	3.793674
-0.0021	-39.94276106	0.00015	3.793674
-0.0019	-39.50400647		
-0.0017	-38.54208419		
-0.0015	-36.9425995		
-0.0013	-34.59466521		
-0.0011	-31.4067127		
-0.0009	-27.32687065		
-0.0007	-22.36454263		
-0.0005	-16.60701956		
-0.0003	-10.22344961		
-0.0001	-3.449836187		
0	0		

## Appendix E: Graphs and Data

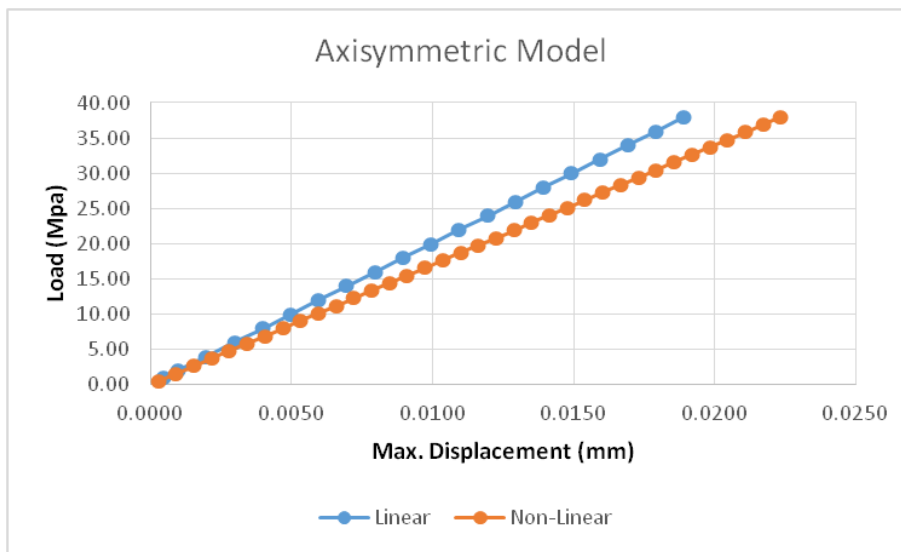


Fig. 4.20

Axisymmetric Model					
Linear		Nonlinear			
Mpa	MaxDisp	Mpa	MaxDisp	Mpa	MaxDisp
1	4.98E-04	0.5	2.94E-04	21.92857	0.012896
2	9.96E-04	1.571429	9.23E-04	23	0.013527
4	1.99E-03	2.642857	1.55E-03	24.07143	0.014157
6	2.99E-03	3.714286	2.18E-03	25.14286	0.014788
8	3.98E-03	4.785714	2.81E-03	26.21429	0.015419
10	4.98E-03	5.857143	3.44E-03	27.28571	0.01605
12	5.98E-03	6.928571	4.07E-03	28.35714	0.016681
14	6.97E-03	8	4.70E-03	29.42857	0.017312
16	7.97E-03	9.071429	5.33E-03	30.5	0.017943
18	8.96E-03	10.14286	5.96E-03	31.57143	0.018574
20	9.96E-03	11.21429	6.59E-03	32.64286	0.019205
22	1.10E-02	12.28571	7.22E-03	33.71429	0.019836
24	1.20E-02	13.35714	7.85E-03	34.78571	0.020467
26	1.29E-02	14.42857	8.48E-03	35.85714	0.021099
28	1.39E-02	15.5	9.11E-03	36.92857	0.02173
30	1.49E-02	16.57143	9.74E-03	38	0.022361
32	1.59E-02	17.64286	1.04E-02		
34	1.69E-02	18.71429	1.10E-02		
36	1.79E-02	19.78571	1.16E-02		
38	1.89E-02	20.85714	1.23E-02		

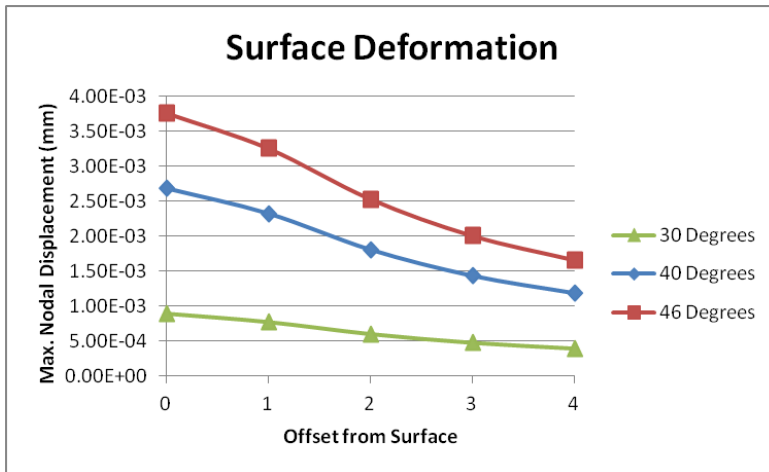


Fig. 5.7

Displacement (mm)			
Offset	30	40	46
0	8.95E-04	2.69E-03	3.76E-03
1	7.75E-04	2.33E-03	3.26E-03
2	6.03E-04	1.81E-03	2.53E-03
3	4.78E-04	1.43E-03	2.01E-03
4	3.95E-04	1.18E-03	1.66E-03

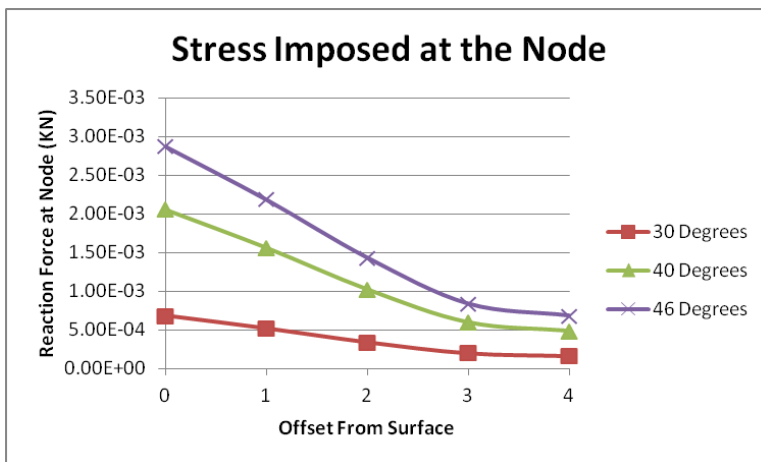


Fig. 5.6

Reaction Force at Node (KN)			
Offset	30	40	46
0	6.85E-04	2.06E-03	2.88E-03
1	5.21E-04	1.56E-03	2.19E-03
2	3.42E-04	1.03E-03	1.44E-03
3	2.00E-04	5.99E-04	8.38E-04
4	1.63E-04	4.88E-04	6.83E-04

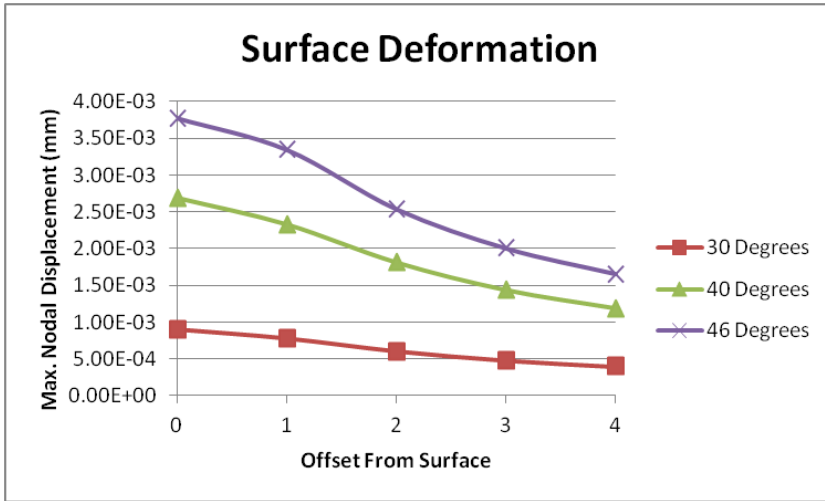


Fig. 5.10

Nonlinear Displacement			
Offset	30	40	46
0	8.95E-04	2.69E-03	3.77E-03
1	7.75E-04	2.33E-03	3.34E-03
2	6.03E-04	1.81E-03	2.54E-03
3	4.78E-04	1.43E-03	2.00E-03
4	3.95E-04	1.18E-03	1.65E-03

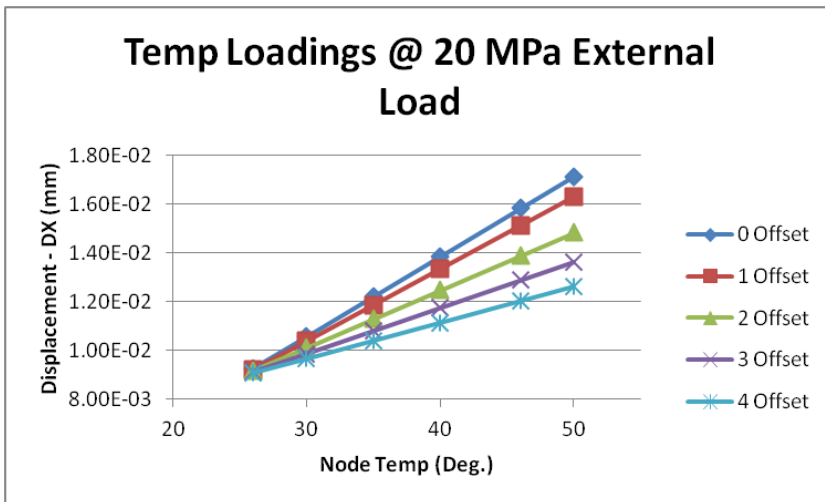


Fig. 5.11

Node Temp	Node Offset From Edge				
	0	1	2	3	4
26	9.26E-03	9.22E-03	9.17E-03	9.12E-03	9.08E-03
30	1.06E-02	1.04E-02	1.01E-02	9.86E-03	9.66E-03
35	1.22E-02	1.19E-02	1.13E-02	1.08E-02	1.04E-02
40	1.38E-02	1.33E-02	1.25E-02	1.17E-02	1.11E-02
46	1.58E-02	1.51E-02	1.39E-02	1.29E-02	1.20E-02
50	1.71E-02	1.63E-02	1.48E-02	1.36E-02	1.26E-02

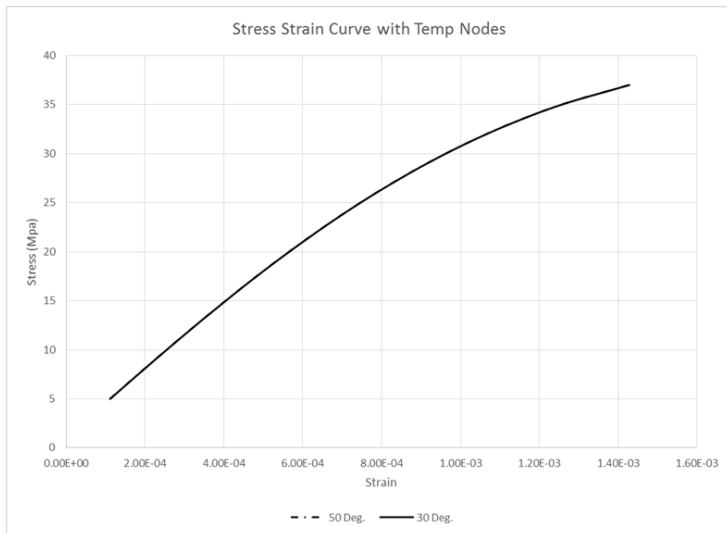


Fig. 5.14

Stress	Strain	
	50 Deg.	30 Deg.
0	2.85E-05	2.85E-05
1	5.18E-07	5.18E-07
3	5.55E-05	5.55E-05
5	1.12E-04	1.12E-04
7	1.69E-04	1.69E-04
9	2.26E-04	2.26E-04
11	2.84E-04	2.84E-04
13	3.44E-04	3.44E-04
15	4.05E-04	4.05E-04
17	4.67E-04	4.67E-04
19	5.32E-04	5.32E-04
21	6.00E-04	6.00E-04
23	6.71E-04	6.71E-04
25	7.46E-04	7.46E-04
27	8.27E-04	8.27E-04
29	9.15E-04	9.15E-04
31	1.01E-03	1.01E-03
33	1.12E-03	1.12E-03
35	1.26E-03	1.26E-03
37	1.43E-03	1.43E-03
39	1.73E-03	1.80E-03
41	6.65E-03	5.45E-02

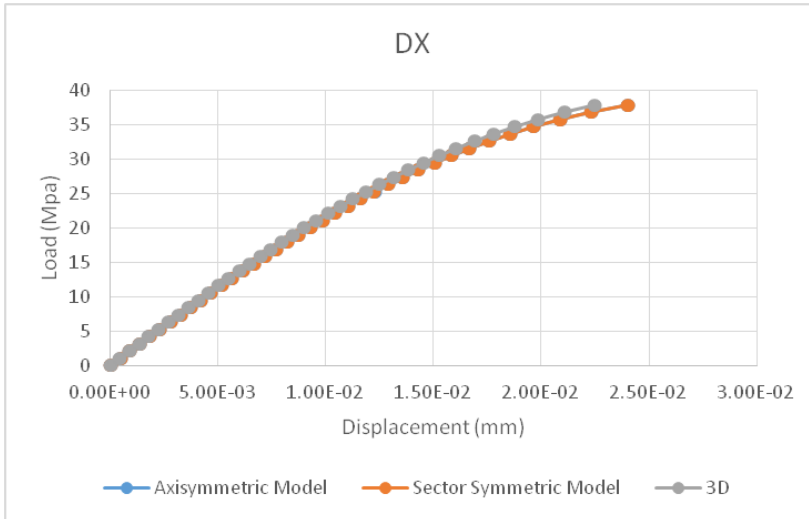


Fig. 6.12

		DX							
Load		Axi	3D	Sect Sym	Load	Axi	3D	Sect Sym	
0.05		2.2E-05	2.2E-05	2.19E-05	21.05	0.009874	0.009873	0.009579	
1.1		0.000483	0.000483	0.000471	22.1	0.010441	0.01044	0.010134	
2.15		0.000945	0.000945	0.00092	23.15	0.011039	0.011038	0.010694	
3.2		0.001406	0.001406	0.001369	24.2	0.01165	0.011648	0.01129	
4.25		0.001871	0.00187	0.001821	25.25	0.012273	0.012271	0.011885	
5.3		0.002336	0.002336	0.002274	26.3	0.012937	0.012935	0.012515	
6.35		0.002802	0.002801	0.002727	27.35	0.013601	0.013599	0.013164	
7.4		0.003271	0.00327	0.003182	28.4	0.01433	0.014328	0.013834	
8.45		0.003745	0.003745	0.003644	29.45	0.01506	0.015058	0.014549	
9.5		0.00422	0.004219	0.004105	30.5	0.01587	0.015869	0.015282	
10.55		0.004697	0.004696	0.004567	31.55	0.016695	0.016693	0.016079	
11.6		0.005185	0.005184	0.005042	32.6	0.017615	0.017614	0.016912	
12.65		0.005674	0.005673	0.005518	33.65	0.0186	0.018598	0.017812	
13.7		0.006165	0.006164	0.005993	34.7	0.019666	0.019665	0.018805	
14.75		0.006672	0.006671	0.006484	35.75	0.020891	0.020889	0.019879	
15.8		0.007181	0.007179	0.006979	36.8	0.022312	0.022312	0.021083	
16.85		0.007693	0.007691	0.007473	37.85	0.024031	0.024031	0.022498	
17.9		0.008227	0.008225	0.007989	38.9	0.026158	0.026171	0.024244	
18.95		0.008761	0.008759	0.008509	39.95	0.084057	2.116653	0.026632	
20		0.009306	0.009305	0.009029	41	1.303127	2.146347	0.031394	

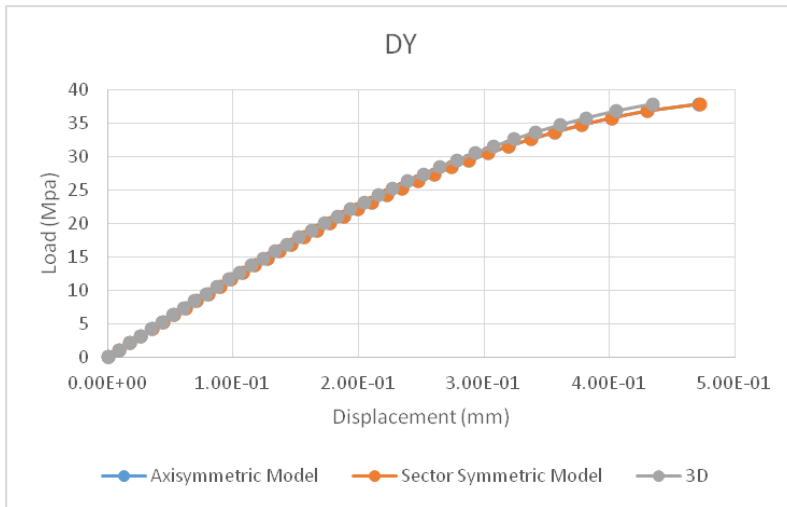


Fig. 6.13

DY							
Load	Axi	3D	Sect Sym	Load	Axi	3D	Sect Sym
0.05	-4.19E-04	-4.19E-04	0.000419	21.05	-1.89E-01	-1.89E-01	0.183354
1.1	-9.22E-03	-9.22E-03	0.009007	22.1	-2.00E-01	-2.00E-01	0.193965
2.15	-1.80E-02	-1.80E-02	0.017594	23.15	-2.11E-01	-2.11E-01	0.204802
3.2	-2.68E-02	-2.68E-02	0.026181	24.2	-2.23E-01	-2.23E-01	0.216141
4.25	-3.57E-02	-3.57E-02	0.034819	25.25	-2.35E-01	-2.35E-01	0.227626
5.3	-4.46E-02	-4.46E-02	0.043484	26.3	-2.47E-01	-2.47E-01	0.239699
6.35	-5.34E-02	-5.34E-02	0.052149	27.35	-2.60E-01	-2.60E-01	0.252127
7.4	-6.24E-02	-6.24E-02	0.060868	28.4	-2.74E-01	-2.74E-01	0.265092
8.45	-7.15E-02	-7.15E-02	0.069695	29.45	-2.89E-01	-2.89E-01	0.278739
9.5	-8.05E-02	-8.05E-02	0.078527	30.5	-3.04E-01	-3.04E-01	0.292968
10.55	-8.96E-02	-8.97E-02	0.087388	31.55	-3.20E-01	-3.20E-01	0.308207
11.6	-9.90E-02	-9.90E-02	0.096459	32.6	-3.38E-01	-3.38E-01	0.324345
12.65	-1.08E-01	-1.08E-01	0.105553	33.65	-3.57E-01	-3.57E-01	0.341725
13.7	-1.18E-01	-1.18E-01	0.114672	34.7	-3.78E-01	-3.78E-01	0.360834
14.75	-1.27E-01	-1.27E-01	0.124063	35.75	-4.02E-01	-4.02E-01	0.381819
15.8	-1.37E-01	-1.37E-01	0.133529	36.8	-4.31E-01	-4.31E-01	0.405656
16.85	-1.47E-01	-1.47E-01	0.143031	37.85	-4.72E-01	-4.73E-01	0.434509
17.9	-1.57E-01	-1.57E-01	0.152872	38.9	-6.03E-01	-6.06E-01	0.475408
18.95	-1.67E-01	-1.67E-01	0.162832	39.95	-3.64E+00	-4.29E+01	0.536544
20	-1.78E-01	-1.78E-01	0.172866	41	-2.70E+01	-4.35E+01	0.707445

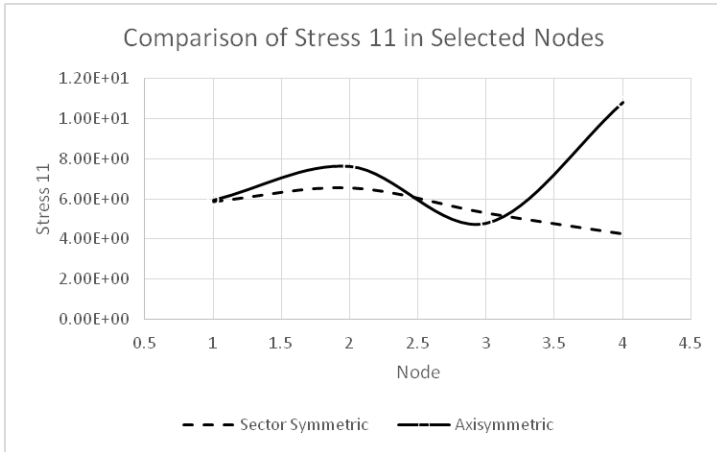


Fig. 6.16

		x	y(Ave)	Y (Min)	Y (Max)
Sector Symmetric	40	1	5.87E+00	5.18E+00	6.74E+00
		2	6.54E+00	6.12E+00	6.89E+00
		3	5.30E+00	4.00E+00	6.74E+00
		4	4.27E+00	4.18E+00	4.37E+00
Axisymmetric	40	1	5.94E+00	3.43E+00	8.35E+00
		2	7.61E+00	6.91E+00	8.09E+00
		3	4.79E+00	2.27E+00	7.36E+00
		4	1.08E+01	1.05E+01	1.11E+01